The Behaviour of Thin Film Magnetic Recording Heads and their Application to the Study of Micromagnetics

by

Ian Ross Walker

BSc. (Honours), University of British Columbia, 1984

A THESIS SUBMITTED IN PARTIAL FULFILLMENT

OF THE REQUIREMENTS FOR THE DEGREE OF

MASTER OF SCIENCE

in the Department

of

Physics

SIMON FRASER UNIVERSITY

September 1987

Approval

Name: Ian Ross Walker

Degree: Master of Science

Title of Thesis: The Behaviour of Thin Film Magnetic Recording Heads and their Application to the Study of Micromagnetics

Examining Committee:

Chairman: David. H. Boal

Anthony S. Arrott
Senior Supervisor

Richard H. Enns

Bretislav Heinrich

E. Daryl Crozier
Examiner
Professor, Department of Physics

Date Approved: September 11, 1987

PARTIAL COPYRIGHT LICENSE

I hereby grant to Simon Fraser University the right to lend my thesis, project or extended essay (the title of which is shown below) to users of the Simon Fraser University Library, and to make partial or single copies only for such users or in response to a request from the library of any other university, or other educational institution, on its own behalf or for one of its users. I further agree that permission for multiple copying of this work for scholarly purposes may be granted by me or the Dean of Graduate Studies. It is understood that copying or publication of this work for financial gain shall not be allowed without my written permission.

Title of Thesis/Project/Extended Essay

The Behaviour of Thin Film Magnetic Recording Heads and their Application to the Study of Micromagnetics

Author: _____
(signature)

Ian Ross WALKER
(name)

22/9/1987
(date)

Abstract

The size scale of most interest in the study of the technical aspects of ferromagnetism is from 10 nm to 10 μm, for these are distances over which substantial changes in the direction of magnetization occur. This scale is the domain of the study of micromagnetics. The magnetic recording industry has pursued ever smaller devices to store and retrieve information on magnetic disks at ever higher densities. Thin film heads are the most recent advance. The dimensions of their active pole faces are about 2 x 20 μm. This enters the range of interest in micromagnetics. The purpose of the research reported here was to explore the possibilities of using commercially produced thin film magnetic recording heads for the study of micromagnetics. The thin film heads were obtained through the courtesy of the Cybernex Corporation and IBM Canada.

The thin film heads were studied by measuring their response to one another and to specially fabricated arrays of fine current carrying wires. Phase sensitive detection and signal averaging techniques were employed to extract the low level signals in these experiments. Optical interferometry was used to measure the position of the heads.

The ability of the heads to resolve small magnetic structures, the linearity and the frequency dependence of the response, the efficiency of flux transport and the effects of externally applied magnetic fields were among the subjects investigated. It was found that heads are able to resolve isolated magnetic structures with dimensions of a few microns. The second and third harmonic responses are both down by 50 dB, indicating high linearity. If the heads are exposed to large external fields, 10-500 G, at various angles, permanent rearrangement of their internal domain structure occurs. For small fields, 0.1 to 10 G, movement of domain walls in the head material can result in responses similiar to Barkhausen noise, found in irregular wall motion in typical ferromagnetic materials. The ac response then becomes a function of the applied dc fields. The heads function at frequencies as high as 50 MHz, although large phase shifts (approaching $\pi/2$) may appear at just a few MHz. The efficiency of a Cybernex head measured at 10 kHz is about 70%. The frequency response measurements indicate that this value remains constant up to several MHz.

The experiments demonstrate possible uses of thin film heads in the study of micromagnetics. The most promising application is for the measurement of dynamic susceptibility of small regions of ferromagnetic materials. The heads can produce fields of up to 1 kG at frequencies from dc to 50 MHz. At the same time they can detect the response to those fields of test material in the vicinity of the pole faces. A pair of heads could be used as a sender and a receiver through a test material. The ability of heads to talk to one another has been demonstrated in this work.

To my grandmother:

Mary Boyd Ross

Acknowledgements

To begin with, I would like to thank Anthony Arrott for the wisdom and guidance he has given me in his capacity as senior supervisor. I appreciate especially the freedom he gave me to use my own judgement during the course of the research.

Bret Heinrich made useful comments on the properties of real magnetic materials (and educated me in many other ways). For this, I am grateful.

I would like to thank the inimitable Andre Van Schyndel, whose earlier work on the use of thin film heads in micromagnetics studies prompted this investigation.

The assistance of Albert Curzon, Onkar Rajora and Doug Wilson in the scanning electron microscopy and x-ray fluorescence spectroscopy studies is greatly appreciated. So too is the consent given by Daryl Crozier for the use of his electron beam evaporator. Ken Urquhart provided useful information concerning the use of the computing system at SFU, and also procured my laser.

I wish to thank Maurice LeNoble, for his assistance in the use of the computer aided drafting system at TRIUMF, and Ray Bula, for wire bonding some of my field sources. For allowing me to use their probe station, and for wire bonding field sources, I would like to thank Albert Leung and Gary Houghton of the Engineering Science School at SFU. Len Wohlgemuth, Henry Sudermann, and Werner Grundmann of Microtel Pacific Research respectively carried out the field source lithography, made surface profile measurements, and donated chip carriers. Their assistance is greatly appreciated. I would also like to thank IBM Canada for providing the 3380E thin film heads.

I wish to thank the members of the Faculty of Science machine shop and electronics shop for their patience and consideration during my numerous sojourns in search of materials and components. The assistance provided by the members of the instructional media center in the preparation of the figures was helpful. I would especially like to thank Bill Schuss and Bob Birtch for their superlative rendition of the apparatus in Figs 9 and 10.

Finally, the conversation and companionship shared with me by my fellow graduate students have made my stay at SFU a pleasure. I would like to thank in particular Jeff Rudd, Don Hunter, Stephen Purcell, Rudolf Bauchspieß, and Saravanamuthu Maheswaran for many hours of delight.

Table of Contents

List of Tables

List of Figures

Chapter 1. Introduction

The main purpose of the work described in this thesis is to understand of the properties of thin film recording heads. This has been done with the view of applying these heads to the study of the micromagnetic properties of ferromagnetic materials. In order to explain the motivation behind this work, the following chapter will: 1) Survey the methods available to the experimentalist for conducting micromagnetics studies, 2) Introduce thin film recording heads, discuss their history and their known properties, and 3) Describe the initial attempts which were made to apply these heads to the study of magnetic domain structures. In the second chapter, apparatus which was constructed to investigate the heads, and methods which were used during the experiments, are described. The third chapter discusses models which were developed to describe the behaviour of small wire arrays (used to determine the response of heads to known magnetic fields), magnetic discs, and the thin film heads. In the fourth chapter, the experimental results are described. The final chapter summarizes the results of the work and places them in the context of micromagnetics investigations .

1.1) Methods Available for Micromagnetics Studies

Perhaps the oldest method available for the study of magnetic domain configurations is the Bitter pattern technique. A ferromagnetic fluid is applied to the surface of the material under study. This consists of a colloidal suspension of small ferromagnetic particles (around 100 Å in diameter) in a liquid carrier. Because the particles are so small, thermal agitation prevents them from settling. Although hydrocarbon fluids were originally used as carriers, other liquids, such as water, silicones, and fluorocarbons, are now also used for this purpose. If the particles are in the presence of a magnetic field gradient, they will move in the direction of that gradient. As a result, the fluid will tend to collect around domain walls, and structures (such as crossties) associated with walls. Thus, magnetic domain structures can be visualized by observing where the fluid collects.

According to Bozorth[1] this method was first tried by Francis Bitter in 1931, but the results were complicated by the presence of surface domains[2]. A successful application of the technique was made in 1949 by Williams, Bozorth, and Shockley[3]. They observed domains in a highly polished sample of bulk material. The method can also be applied to the observation of domain patterns in thin film samples. An example of such an experiment is one performed by Huber, Smith, and Goodenough in 1958[4]. The Bitter pattern technique has the advantage of being fairly

simple, and the disadvantage of being rather qualitative in the sense that it does not provide information about magnetic field strengths. It is also incapable of providing information in a situation where the domains are moving around rapidly.

There exist devices in the world of micromagnetic analysis which can be best classified as miniature Gaussmeters. These are tiny Hall[5] and magnetoresistive[6] probes which are small enough (with characteristic dimensions on the order of several μm) to move directly against the sample under study. If an appropriate mechanism is provided to facilitate their movement, they are capable of resolving domain structures and delivering an accurate indication of the magnetic field distribution. The choice of a Hall probe or a magnetoresistive probe depends on how much effort the researcher is willing to spend and what his requirements are. Hall probes are more difficult to fabricate than magnetoresistive probes, but are more directional. For some purposes directionality is not a requirement, and magnetoresistive probes can be used. Both devices are usually fabricated on glass substrates using photolithographic techniques. Standard x-y motor translators have been used to control the lateral position of these sensors, which is monitored either interferometrically, or with a microscope. Such devices as piezoelectric transducers and pneumatic positioners have been used to control the vertical position. This is often monitored by observing the interference bands formed between the glass substrate and the sample.

Miniature probes of this type have had some popularity with researchers interested in determining the fields produced by magnetic recording heads. They have been less popular with those interested in micromagnetics. The main reason for this is probably the existence of Kerr effect imaging methods, which allows magnetic domain movement to be viewed in real time. Although it should be possible to create an arrangement which would allow a limited amount of real time imaging to take place using small probes, such apparatus would be much more complicated than the equivalent Kerr arrangement. Another disadvantage of small probe analysis methods is the need to position the glass plate supporting the device accurately next to the sample. This can be awkward, especially for oddly shaped samples. Because of its complexity and cost, and considering its limited flexibility, the use of miniature magnetic probes will probably remain of secondary importance in the field of micromagnetic analysis.

The Kerr effect methods just mentioned involve the use of the magneto-optic Kerr effect[7]. A beam of light, usually from a laser, is polarized and sent through a beamsplitter into the eyepiece of a microscope. The light emerges from the objective lens, reflects from the target, and retraces its path through the microscope. After emerging from the eyepiece, it reflects off the beamsplitter, and passes through a polarization analyzer to strike a detector. The detector can have a single element, if information from only a single spot on the target is needed, or it can have an array of elements if an image is desired. The crucial aspect of the arrangement is the fact

that a beam of plane polarized light, upon reflection from a magnetized target, will have its plane of polarization rotated in a direction and to a degree which depends on the orientation and intensity of the magnetization. This is the magneto-optic Kerr effect.

The usefulness of this method in the study of micromagnetics is due to three facts. Firstly, it is relatively simple to set up, although not nearly so simple as the use of Bitter patterns. Secondly, it is a quantitative technique, since it provides information about the direction and magnitude of magnetic fields. Finally, it is capable of providing information in situations where the magnetization is changing rapidly. It has the drawback of being incapable of providing information in situations where magnetization features are much smaller than the wavelength of light. There are many circumstances in which this is not a consideration, such as the micromagnetic analysis of thin film recording heads, and in these cases the technique is widely used.

A method of micromagnetic analysis based on electron microscopy, called Lorentz microscopy, has been available for many years[8]. It relies on the focusing and defocusing of a beam of electrons in the presence of the field produced by a sample, arising from the Lorentz (qv **x B**) force. This technique is often employed in the analysis of thin films in a transmission electron microscope. It can also be used with scanning electron microscopy, which means that domain structure in bulk materials can be studied. Lorentz microscopy, unlike Kerr effect methods, has the ability to resolve structures which are far smaller than the wavelength of light. It is also capable of producing images very rapidly.

The most serious disadvantage of Lorentz microscopy is its insensitivity to small magnetic fields distributed over small areas. This is due to the fact that the amount of refocusing which an electron beam will undergo (which determines the contrast) is determined by the amount of flux which is enclosed by adjacent parts of that beam. The lower limit on the amount of flux which neighboring parts of the beam must enclose if there is to be any refocusing is set by the flux quantum ($\Phi_0 = hc/e = 4 \times 10^{-7}$ G cm^2). In practice, this means that very small magnetic structures which produce weak fields may be difficult to observe[9].

Recently, a modification of Lorentz microscopy called electron beam tomography has been proposed[10]. This technique has the capability of producing three dimensional information on the direction and magnitude of stray magnetic fields (conventional Lorentz microscopy is capable of giving only two dimensional information). The method uses the same approach as many of the tomographies which are now in widespread use, such as x-ray tomography, positron emission tomography, etc. In this case, a fanned electron beam carries out a scan in the region above the sample, while the sample itself rotates about an axis which is perpendicular to the plane spanned by the beam. Some form of imaging detector, such as a microchannel photomultiplier, is used to

sense the electrons which have passed the sample. The discrete version of a particular integral transform is then applied to the resulting data to obtain a map of the fields. It turns out that symmetries present in the electromagnetic field can allow a great reduction in the amount of computation needed over that required for other kinds of tomography. Consequently, electron beam tomography may not be much more expensive than Lorentz microscopy, since a microcomputer could carry out the analysis.

Some rather sophisticated (and very powerful) methods of micromagnetic analysis have appeared in recent years. They allow one to obtain quantitative information about the magnetic state of materials almost down to an atomic scale, and to observe rapid changes of state as they occur. One such method, which was recently developed by Yoshida et. al. at Hitachi[11], makes use of the wave nature of electrons. Referred to as "electron beam holography", the technique starts with the production of monoenergetic electrons using a field emission source. The resulting beam is split into two parts, of which one is sent through the sample. These beams are then recombined on a screen to form an interference pattern, which is magnified, and recorded on photographic film. The interferogram produced in this way must then be reconstructed optically in order to produce an image which can reveal the micromagnetic structure of the sample. The procedure is entirely analogous to ordinary holography, except that the experiment takes place under vacuum in a modified transmission electron microscope. The important aspect of this experiment is the fact that the phase of the electron wavefunction can be modified in the presence of a magnetic field by:

$$\Delta\phi = \frac{2\pi e}{hc}\int \mathbf{A}\cdot d\mathbf{x}$$

Where ϕ is the phase of the electron wavefunction, $\mathbf{A}$ is the magnetic vector potential, and $d\mathbf{x}$ is an element of length. Consider two possible paths from the electron gun to the detector. The phase of the wavefunction corresponding to one path will be shifted with respect to that of the other path by:

$$\Delta\phi = \frac{e}{\hbar c}\oint \mathbf{A}\cdot d\mathbf{x} = \frac{e}{\hbar c}\iint \nabla \times \mathbf{A}\cdot d\mathbf{S} = \frac{e}{\hbar c}\iint \mathbf{B}\cdot d\mathbf{S} = \left(\frac{e}{\hbar c}\right)\Phi$$

Where $d\mathbf{S}$ is an element of area, $\mathbf{B}$ is the magnetic field in the region between the two paths, and Φ is the flux enclosed by the path. Consequently, it can be seen that the interferogram resulting from the contributions of many such paths will form a record of the magnetic state of the sample.

Since the wavelength of the electrons used to make the interferogram can be very small, the size of the structures which can be examined using this technique approaches atomic dimensions.

There is no reason, in principle, why images of moving magnetic structures could not be made using this method, although I am not aware of such an experiment. Unfortunately, electron beam holography has two major drawbacks. It requires the use of a specially modified transmission electron microscope, which is an expensive piece of apparatus. Its use is also restricted to those specimens which can be penetrated by 200 keV electrons without excessive scattering. This means that only thin films and flakes of thickness less than about 1000 Å may be used. Samples of material with this order of thickness are of growing importance, however, so the widespread use of this technique is to be expected.

Recently, Pierce et. al. at the National Bureau of Standards have developed techniques for the efficient production and detection of spin polarized electrons[12]. This has permitted the development of a number of very powerful surface analytical methods which make use of the ability of materials to preferentially absorb and emit electrons in different spin states. One of these methods, of special interest to those interested in micromagnetics, is known as scanning electron microscopy with polarization analysis, or SEMPA. In normal scanning electron microscopy a beam of electrons is moved across a sample. Electrons which are ejected from the sample are collected by a detector, the output of which is used to modulate a cathode ray tube synchronized with the scanning beam. The image appearing on the cathode ray tube is a representation of the topography of the object being scanned. In SEMPA, the conventional electron multiplier detector is replaced by one which is capable of measuring polarization as well as electron beam intensity . This results in the production of an image which depends on magnetic structure as well as surface structure. The reason for the sensitivity of SEMPA to micromagnetic structure is the exchange interaction. Electrons which impinge on the surface under study interact with the atomic electrons, and scatter with a cross section which depends on the relative orientation of the two spins.

The major advance made by the group at the NBS has been the development of a detector which is capable of measuring the polarization state of a significant number of incident electrons. The latest detectors rely on low energy diffuse backscattering from thick polycrystalline gold films followed by channel plate electron multiplication. The basic idea behind this detector is to use the spin-orbit interaction to transform a distribution of electron spins into a spatial distribution of scattered electrons. Unfortunately, this detector adds to the complexity of an already complicated instrument. To make matters worse, since only those electrons which scatter from the top 50 Å of sample can escape, the surface of the sample must be free of nonmagnetic contaminants. This means that only an ultrahigh vacuum scanning electron microscope or a scanning Auger microscope can be used as the basis for a SEMPA machine. In addition to the pumps required to maintain the ultrahigh vacuum (about 10^{-10} Torr), an ion sputtering gun is

normally required to remove surface contaminants. Offsetting the problem of cost is the unique ability of SEMPA to study magnetization down to the lower resolution limits of scanning electron microscopy (about 60 Å) in both thin films and bulk materials. Furthermore, one can use the ordinary SEM capabilities of SEMPA to determine whether surface topography is affecting magnetic structure. If scanning Auger microscopy is being used, the composition of the sample may be determined as well.

The last item in this list of micromagnetic analysis tools is somewhat speculative, since it does not yet exist. The instruments on which it would be based do exist, however, so it is reasonable to discuss what its capabilities might be. This tool is the magnetic version of the scanning tunneling microscope (STM), the device developed by Heinrich Rohrer and Gerd Binnig in the early 1980's[13]. The chief virtues of the STM are its ability to image individual atoms, and its simplicity. In essence, the instrument consists of a very sharp tungsten needle which is raster scanned over the object of interest using piezoelectric transducers. The needle is moved close enough to the substrate that a tunneling current can be set up. As the needle is scanned, its height above the substrate is adjusted to maintain a constant current. Since the tunneling current has an exponential dependence on the distance between the needle and the substrate, the voltage required to adjust the needle is a very sensitive measure of the gap distance. In fact, the vertical resolution of the scanning tunnelling microscope is about 0.01 Å. The lateral resolution of the microscope is substantially less than this (about 1 Å), but is sufficient to allow individual atoms to be distinguished.

A modification to the STM has been proposed[14] which might make it possible to create magnetization images in which the spin states of individual atoms would be discernible. In this microscope, the tungsten needle would be replaced by one consisting of magnetic atoms. If such a needle were scanned over a magnetic sample, the probability of an electron tunnelling from the sample into the needle would depend not only on the usual geometrical and electronic considerations which apply to ordinary STM's, but also on the relative spin states of the atoms in the substrate and the tip. The tunnelling current would consequently be an indication of the micromagnetic state of the surface of the sample, and would presumably permit the same resolution which is achievable with ordinary STM's.

The STM is a much cheaper and simpler device than an electron microscope, even when one takes into account the scanning and detection electronics. It is also much smaller than an electron microscope, which means that it can be readily incorporated into larger instruments, such as an electron microscope, or an MBE machine. It seems reasonable to suppose that a scanning tunneling magnetic microscope, if and when it is developed, could be a tool of great value in the study of the epitaxial growth of magnetic materials. This would be especially true if it could do

double duty as a scanning tunneling microscope. The STM is presently capable of operating quickly enough to produce images in real time, so that the motion of atoms can be watched as they occur. If a scanning magnetic microscope were developed, it should have similar capabilities. Consequently, it ought to be possible to observe the formation and propagation of magnetic domains on an atomic level.

1.2) Thin Film Recording Heads

Magnetic recording heads, the devices which have been used for many years to record and retrieve information stored in the form of magnetic structure in suitable media, have recently been getting very small. These devices have traditionally taken the form of rings of ferromagnetic or ferrimagnetic material with coils of wire on one side and a small gap on the other (see Fig. 1). When recording takes place, current passing through the wire magnetizes the ring and produces a magnetic field in the gap. Fringing fields from this gap produce magnetic patterns in the medium

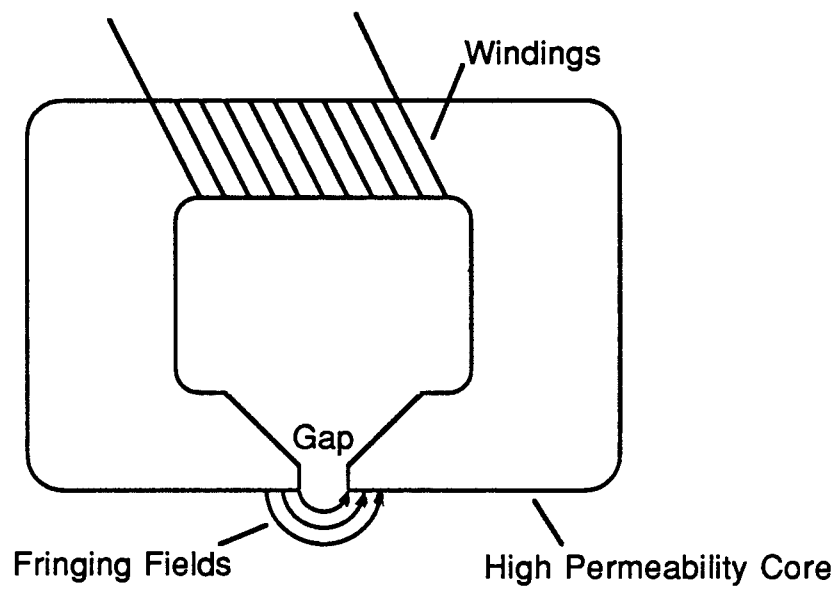

Fig. 1. Schematic diagram of a magnetic recording head.

passing underneath. During retrieval, the magnetized medium moves under the gap and magnetizes the ring. Faraday induction produces a voltage in the coils. In that branch of magnetic recording which is concerned with the storage of digital information on rapidly rotating rigid discs, the conventional heads have become so minute that it is now necessary to assemble

them under a microscope. This has made it very difficult for the manufacturers of disc drives to maintain consistency and keep down the cost of production.

The solution to this problem has come from the microelectronics industry in the form of photolithographic fabrication techniques. These have made possible the construction of much smaller heads with a much higher degree of control than is possible using traditional methods. They have also made it possible to use materials which retain their permeability at very high frequencies (allowing the use of high read and write rates), and which exhibit low eddy current losses (resulting in improved head efficiency). Heads which are produced using photolithography are made up of layers of thin films (see Figs. 2 & 3). This means that the part of the ring which contains the gap can be very narrow, so that these heads can have rather high resolution compared with heads made out of bulk material. Owing to their structure, the new devices have come to be known as "thin film heads".

According to Valstyn and Shew[15], the idea of using lithographic processes to fabricate recording heads dates back to the early 1960's[16]. It wasn't until 1969, however, that the first experimental work on the fabrication of thin film heads was carried out. These investigations, carried out by Watanabe, Matsumoto, and Najima[17], involved constructing heads by electroplating nickel-iron films on a single turn sensing wire. The film was patterned using photolithography and chemically etched to produce the gap. This head was not used to record or retrieve data, but to measure mechanical displacement. In 1970, Romankiw, Croll, and Hatzakis[18] described a head which was produced entirely using lithographic and film deposition methods. This head also had a single turn winding, and was actually used to record information (although not to retrieve it). The first thin film head to read information was fabricated in 1971 by Kaske et. al.[19]. It basically consisted of a wire with a loop of permalloy deposited around it and having a gap on the lower surface. The first multiturn thin film head was constructed in 1970 by Lazzari and Melnick[20]. It had a five turn coil, in which the conductors were separated by SiO_2, and had a core which consisted of laminations of Ni-Fe-Cr and SiO_2 films. The latter structure was used in order to reduce eddy current effects which could limit the frequency response of the head. In 1973, Valstyn and Shew and Lazzari[21] described single turn thin film heads which could both read and write information. In the same year, Burroughs introduced the first commercially available thin film head in its 5N disc drive. This was a relatively primitive machine, however, which could be used only as a secondary or tertiary mass storage device. By 1979, thin film head technology had progressed to the point where such heads could be profitably installed in commercial primary mass storage systems. In that year, IBM incorporated thin film heads in its new 3370 disc drives.

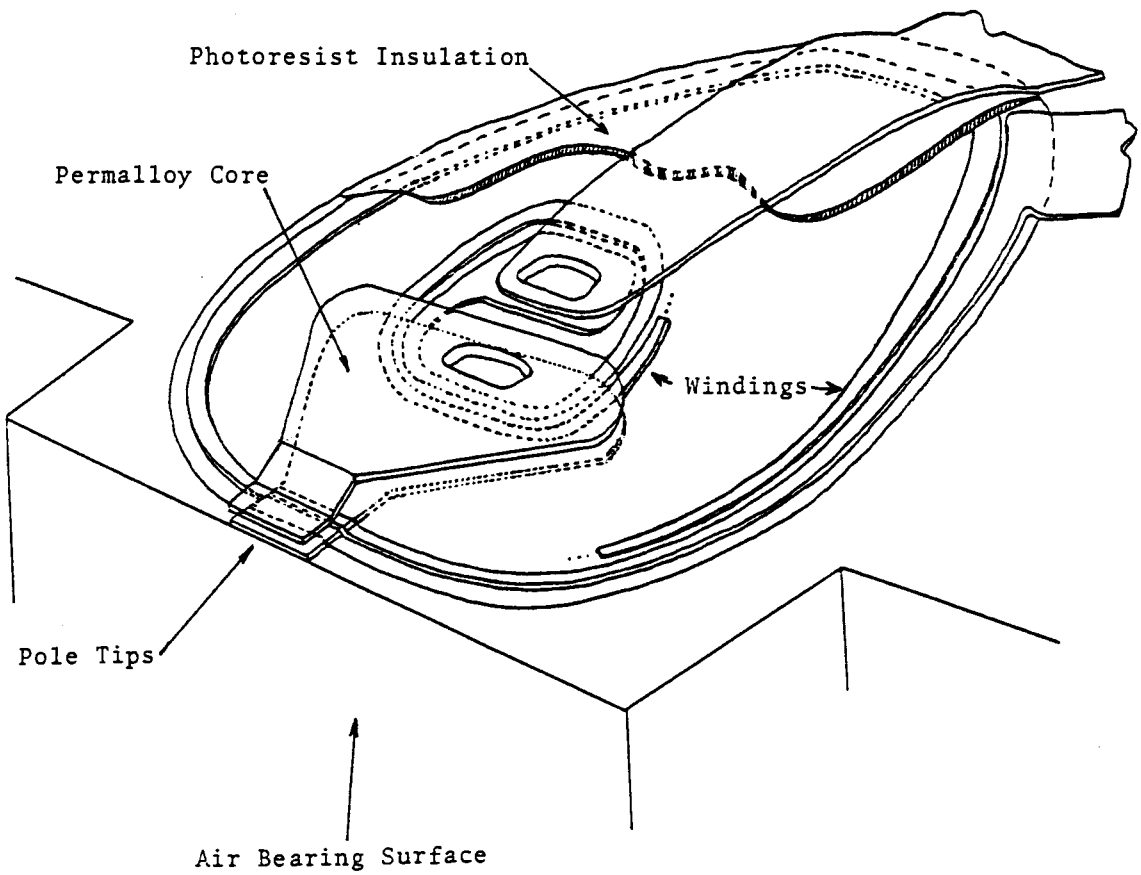

Fig. 2. Schematic diagram of an IBM 3370 thin film head (after Robert E. Jones, Jr and Walther Nystrom, "Thin Film Inductive Transducer", U.S. Patent 4,190,872, February 26, 1980 (Filed December 21, 1978)). See also the lower photograph in Fig. 3 (the IBM 3370 and IBM 3380E heads are very similar).

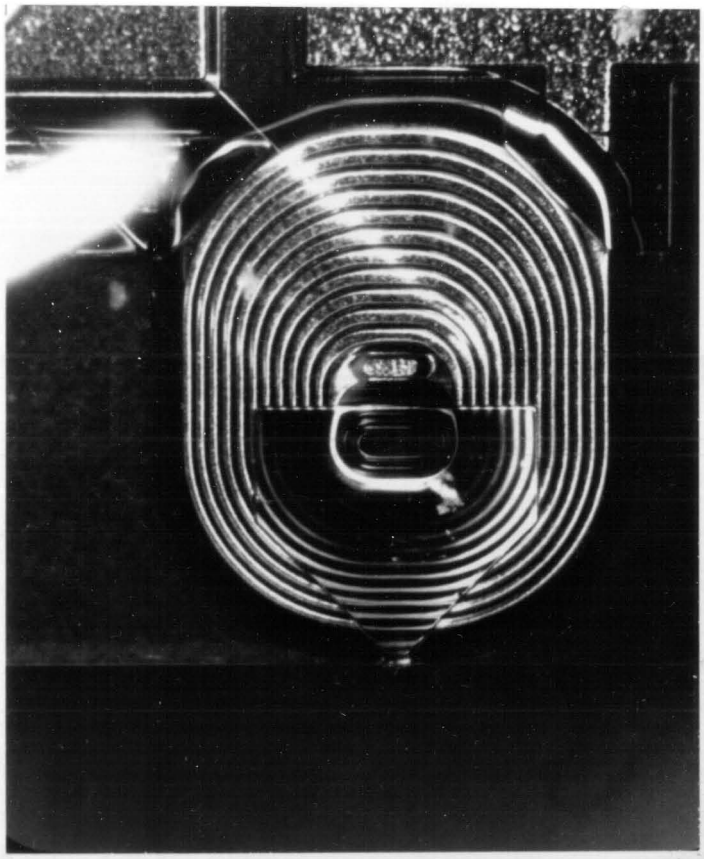

Cybernex Head

500 μm

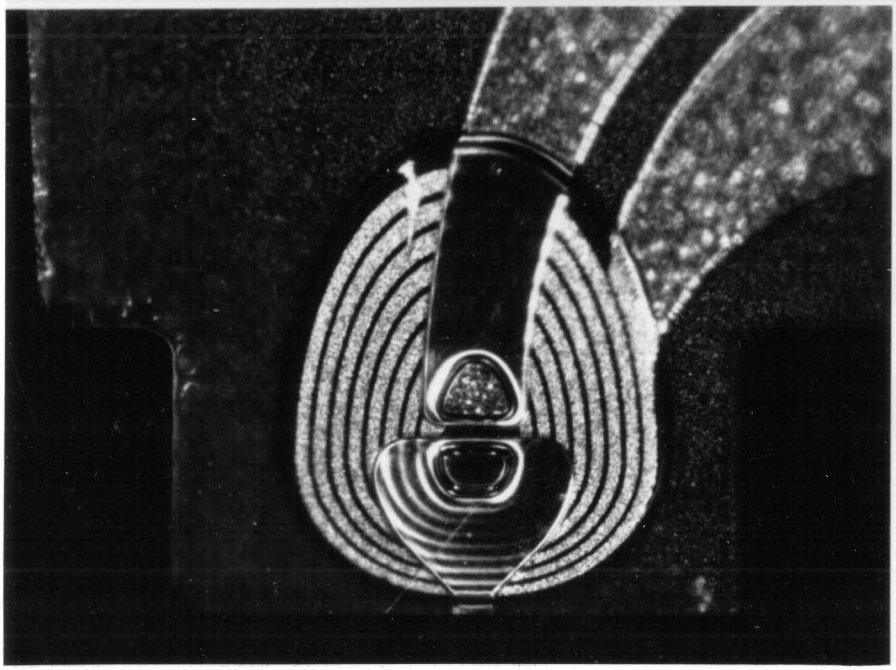

IBM 3380E Head

Fig. 3. Photomicrographs of Cybernex and IBM heads. The Cybernex heads each had a 24 turn, 18 Ω coil which was equipped with a centertap. The first and second pole tips were respectively about 1.6 μm and 2.8 μm wide, and approximately 21 μm and 17 μm long. The gap was about 0.7 μm. The IBM heads each had a 8 turn, 8 Ω coil with no centertap. The first and second pole tips were resepectively about 1.6 μm and 2.2 μm wide, and approximately 31 μm and 27 μm long. The gap was about 0.6 μm.

Research into the processes involved in magnetic recording have reached the stage where it is now fairly well known what one must do to make a good thin film head. Much of the knowledge which goes into the fabrication of these heads is proprietary, but the general principles involved are available in the open literature[22,23]. The core material is a form of permalloy, containing 81% iron and 19% nickel, which is either sputtered or electroplated onto the substrate. The reason for choosing permalloy is because it is magnetically soft, and because it has a high permeability (about 2500). The reason for choosing this particular composition is because its magnetostriction constant is nearly zero. If it were possible for a significant amount of magnetostriction to take place, those parts of the permalloy film which turn corners would be subjected to some strain. This could reduce the effective permeability of the permalloy in these places by a factor of 5 or 10, resulting in a very substantial loss of head efficiency. The efficiency is defined to be the ratio of the magnetic flux produced by the actual head to the flux produced by an ideal head with no flux leakage.

One significant problem with the use of permalloy in recording heads is its mechanical softness. It can be easily worn away through contact with the recording medium. In recording heads which are designed for use with rigid magnetic discs, this is not so much of a problem because the head rides on a thin (0.2 - 0.4 μm) cushion of air. The head is in contact with the disc when it starts and stops, however, so that some wear is expected. In thin film heads, the core material and windings are usually surrounded by alumina (polycrystalline Al_2O_3). Owing to the hardness of this material, the lifetime of thin film heads can be rather long, in spite of the fact that permalloy is used in the core. A lifetime of at least 10,000 starts and stops is commonplace.

The active part of the head, consisting of the permalloy core, the windings, and the insulation, rests on a block of material known as the slider (see Fig. 4). This object constitutes the bulk of the head, and is responsible for creating the air cushion which separates the head from the disc. In order that a cushion may be established and maintained, the slider must have certain well defined mechanical properties. It must be possible to machine the slider material to very high tolerances in order to give it a contour which will establish the correct air flow. The presence of an excessive amount of roughness on the slider's lower surface could cause turbulence which might destroy the air cushion. It must therefore be possible to give the underside of the slider a very high polish, with a small number of pits and scratches. The slider material must also be hard, so that head abrasion may be minimized. In addition, the slider material must have good thermal stability, low electrical conductivity, and low magnetic activity. These requirements are met by a variety of advanced ceramics. An example of such a material is

a 70% alumina, 30% titanium carbide alloy made by sintering the constituent materials at high temperatures and pressures[24].

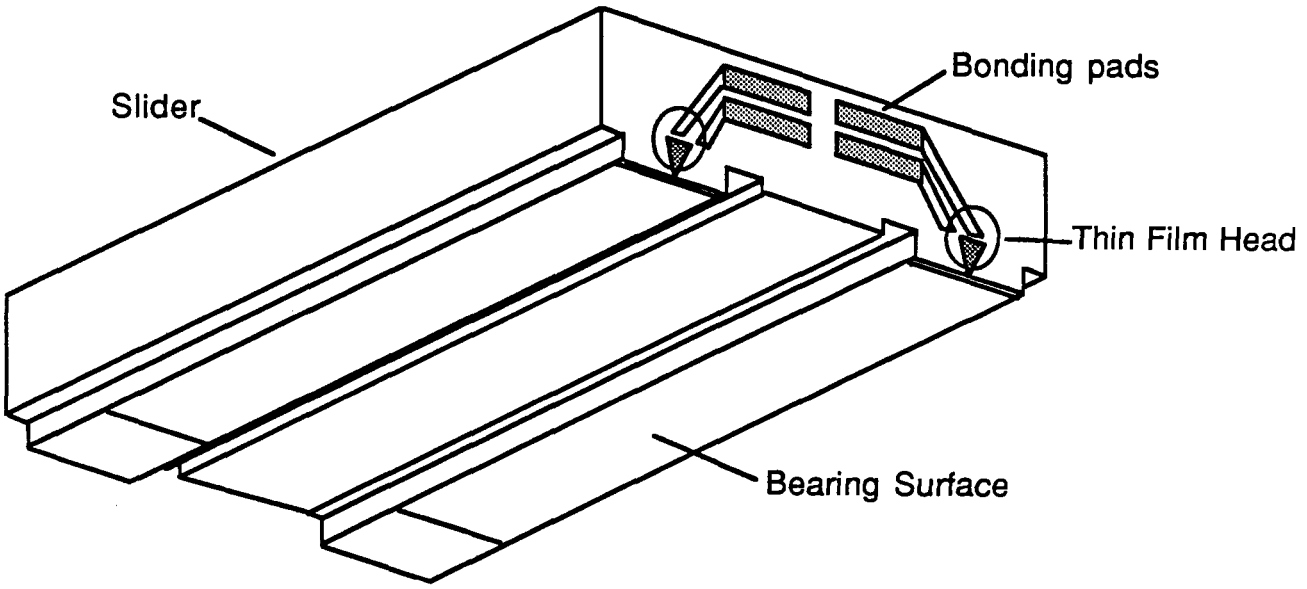

Fig. 4. Thin film head slider

The saturation induction of the permalloy in thin film heads is on the order of 10 kG, but this is almost a factor of ten greater than the maximum fringing field produced near the gap. Hoyt has measured the fringing fields produced by thin film heads using small wire loops[25]. These were fabricated by ion beam milling Au-Ti films which had been evaporated on glass substrates. To make the measurement, a substrate was mounted over an inverted head, which was controlled using an x-y-z translator. By exciting the head windings using a high frequency oscillator and monitoring the voltage induced in the loop using a lock-in amplifier, Hoyt was able to determine the head fields as a function of current. He found that the maximum field which the heads could produce was about 1 kG at a current of about 80 mA. The measurement was made with a head to loop separation of 0.35 μm. Hoyt did not mention which brand of head was being used in the experiments, but it is significant that they were conducted at an IBM research lab. In an earlier paper[26], the same method was used to determine the absolute efficiency of a head as a function of frequency. It was found that the efficiency of the head decreased from a maximum of 76% by no more than about 16% at a frequency of 50 MHz.

The configuration of the domain structures in thin film heads have been studied by several groups using Bitter patterns and Kerr effect imaging[27-30]. These patterns usually take the form shown in Fig. 5. They are essentially variations of the classic Landau domain structure, and are

created by imposing a magnetic field along the indicated axis during deposition. This particular domain arrangement is important to the operation of the head. It insures that the permalloy magnetization process occurs rapidly and smoothly, with no sudden domain movements (Barkhausen jumps). In fact, magnetization of the permalloy involves only the continuous rotation of domains and the displacement of domain walls (see Fig. 6) during which the formation of poles at the domain boundaries does not occur. The fact that the magnetization is due mostly to domain rotation means that it can take place quickly, since domain rotation is an intrinsically fast process compared to domain wall translation.

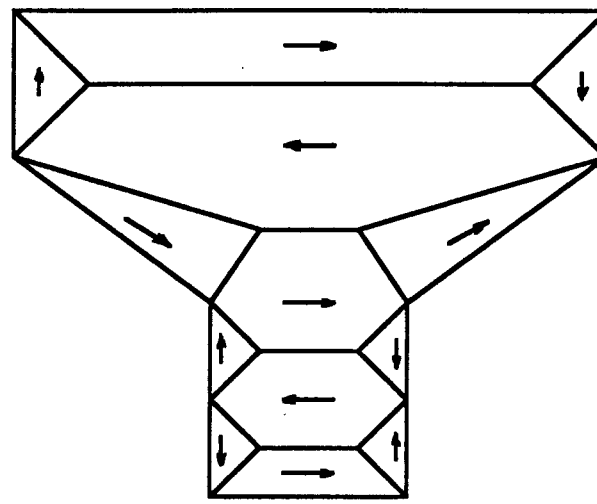

Fig. 5. Domain structure in the core of a thin film head.

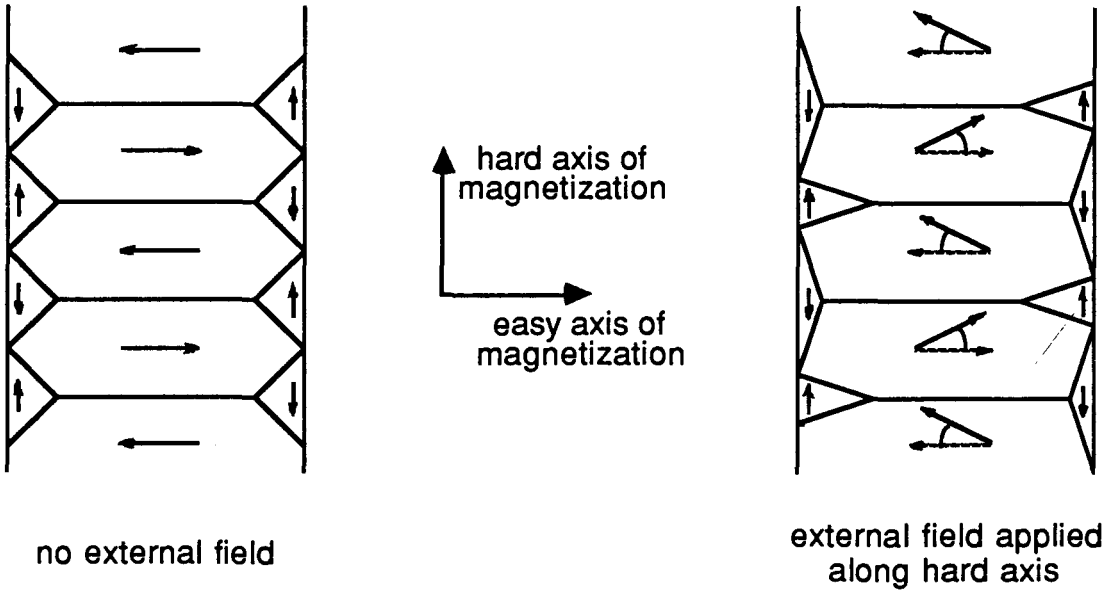

Fig. 6. Magnetization processes in a thin film head.

One important problem concerning the operation of thin film heads involves determining which physical processes limit their frequency response. Several experimental and theoretical studies have been made which imply that it is the translational motion of the edge domain walls in the head, rather than the rotation of main domains, which is the main limitation. Soohoo has done a calculation[31] which suggests that the rotational switching time for the main domains is about 0.5 ns, while the translational switching time for an edge domain wall is on the order of 170 ns. The latter value corresponds to a switching frequency of about 4 MHz. Re and Kryder have experimentally determined, using an IBM 3380 thin film head and Kerr effect apparatus, that the frequency response limits of a head lie between 2 and 12 MHz, and that these limits are set by domain wall motion processes[29]. By the first statement it is meant that the lag in the response of the head domains relative to the phase of the driving field becomes very substantial at these frequencies; reaching 90 degrees at 8.4 MHz. Moreover, they found that the magnetization of the center of the head responds faster to changes in the driving field than magnetization of the edges.

1.3) Using Thin Film Heads in Micromagnetics

Thin film heads are now mass produced for the computer industry, so that they are presently available for a very reasonable price. Their capabilities and low cost became known to my

supervisor (Dr Arrott) sometime in 1984, and it seemed reasonable to suppose that they could be used in the study of magnetic structures. He therefore put Andre van Schyndel, who had recently arrived as a postdoctoral fellow, to work in order to see if this could be done. The basic idea was to take a thin film head and move it rapidly over a magnetic sample in order to produce a voltage in the head windings. This voltage could then be integrated in order to obtain a value for the magnetic field under the head as a function of position.

The first useable apparatus consisted of a pair of opposing loudspeakers, mounted in their original cabinets and bolted to a 3/4" thick plywood board. A stainless steel supporting tube was connected between them, and served to move the head back and forth over the sample. Owing to the inertia of the speaker assembly, it would not have been possible to move the head quickly enough to form an air bearing. A far more viscous fluid than air was needed to provide the lubrication, and oil was chosen for the task. In order to monitor the position of the head, a resistive displacement transducer was constructed. This consisted of a needle which was connected to the support rod at one end, and which dipped into a trough filled with conductive solution (a redox couple[†]) at the other. A voltage could be applied across the trough by way of electrodes at either end, so that the arrangement constituted a potentiometer. Movements of the needle along the trough would result in variations of the voltage between the needle and one of the electrodes. This system had the virtue of being simple, and the disadvantage of measuring only the position of the connecting rod - not the head itself. Since the head was attached to the rod through a flexible cantilevered arm, highly accurate measurements of head position were inhibited by friction between the slider and the surface on which it was resting. The method was satisfactory for the determination of position to an accuracy measured in tens of microns.

The results obtained with this apparatus were rather inconclusive, at least insofar as they contributed to the understanding of micromagnetics in iron whiskers. It was not too difficult to obtain a signal from the head, but interpreting it in terms of domain structure proved to be very difficult. Such things as bumps and non-magnetic inclusions in the whisker all contributed to the output, so that what one often saw was a trace resembling the one displayed in Fig. 7. None of the data obtained appeared to have its origin in micromagnetic structure.

In spite of the difficulties of conducting micromagnetic studies, the head turned out to be very useful in the study of partially saturated iron whiskers. In particular, it made possible the determination of the location of the interface between the saturated region and the unsaturated region in a whisker as a function of the applied field. Using an oscillating thin film head, it was

---

[†] This solution (10^{-6} M tetraethyl ammonium perchlorate or tetrabutyl ammonium perchlorate) was used to avoid the formation of bubbles at the electrodes.

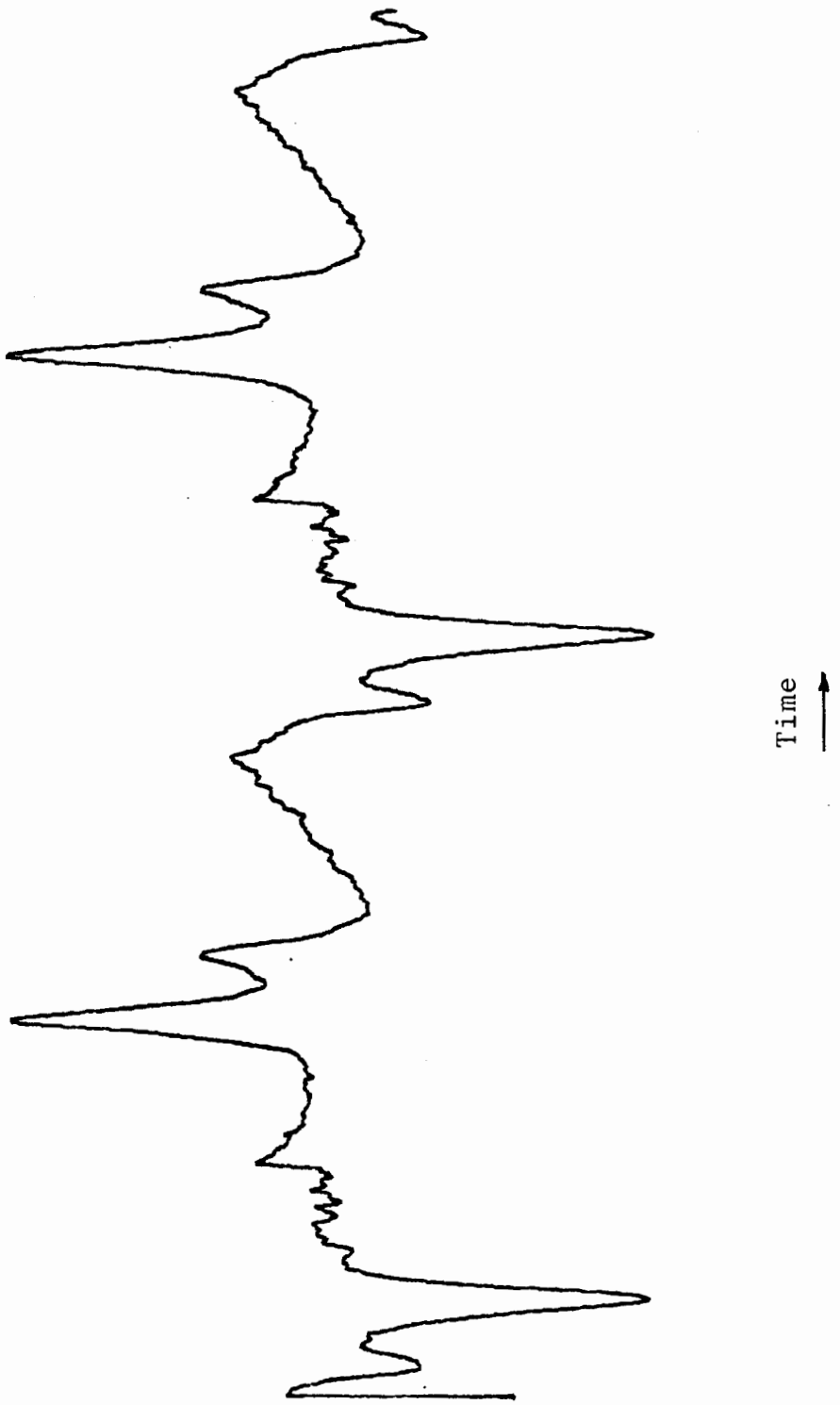

Fig. 7. Signal observed by Andre as a thin film head was moved back and forth over an iron whisker at 54 Hz. The trace represents two cycles of head motion.

possible to confirm an earlier theoretical prediction[32] that the length of the saturated region shows a power law dependence on the difference between the applied axial field, and the applied axial field required to initiate saturation.

A few attempts were made to calibrate the head - to find out how it responded to a known magnetic field produced using an electric current. This was done mainly in order to determine its spatial resolution. The first effort at calibration was made using small (130 μm) wires. The iron whisker was replaced with a pair of these wires in the sample holder. The wires were then supplied with a dc current while the head moved back and forth above them. Unfortunately, while 130 μm wires are small by normal standards, they are not small compared with the characteristic dimensions of the head. The field produced by the wires was long range and uniform on this scale. Consequently, the resolution of the head was observed to be much lower than the thickness of the permalloy pole tips might suggest.

Another attempt was made at calibration by replacing the iron whisker with another head, so that two heads were running face to face. The lower head was supplied with a dc current while the other moved back and forth above it. The results obtained using this arrangement were not very satisfactory. It seemed as if the pole tips were playing no part in coupling flux between the two heads. The resolution was far less than one would expect, knowing the dimensions of the tips.

An interesting effect was observed when the head was positioned over a single 130 μm wire carrying an ac current. The signal produced by the head (see Fig. 8a) appeared to have a discontinuity, as if some kind of Barkhausen jumps were taking place. A digitally smoothed version of the trace (see Fig. 8b) makes the step appear more distinct. The origin of this phenomenon is unknown.

It eventually became clear that current carrying wires and heads were not yielding any useful information on head characteristics, aside from the result mentioned in the previous paragraph. However, it was still desirable to obtain information about the response of the heads to applied fields, in order to find out about their spatial resolution, efficiency, linearity, and frequency response. It was felt that the acquisition of this information was necessary in order to find out how they could most profitably be used in the study of micromagnetics. To this end, I was asked to construct a suitable field source, and use it to determine the needed characteristics.

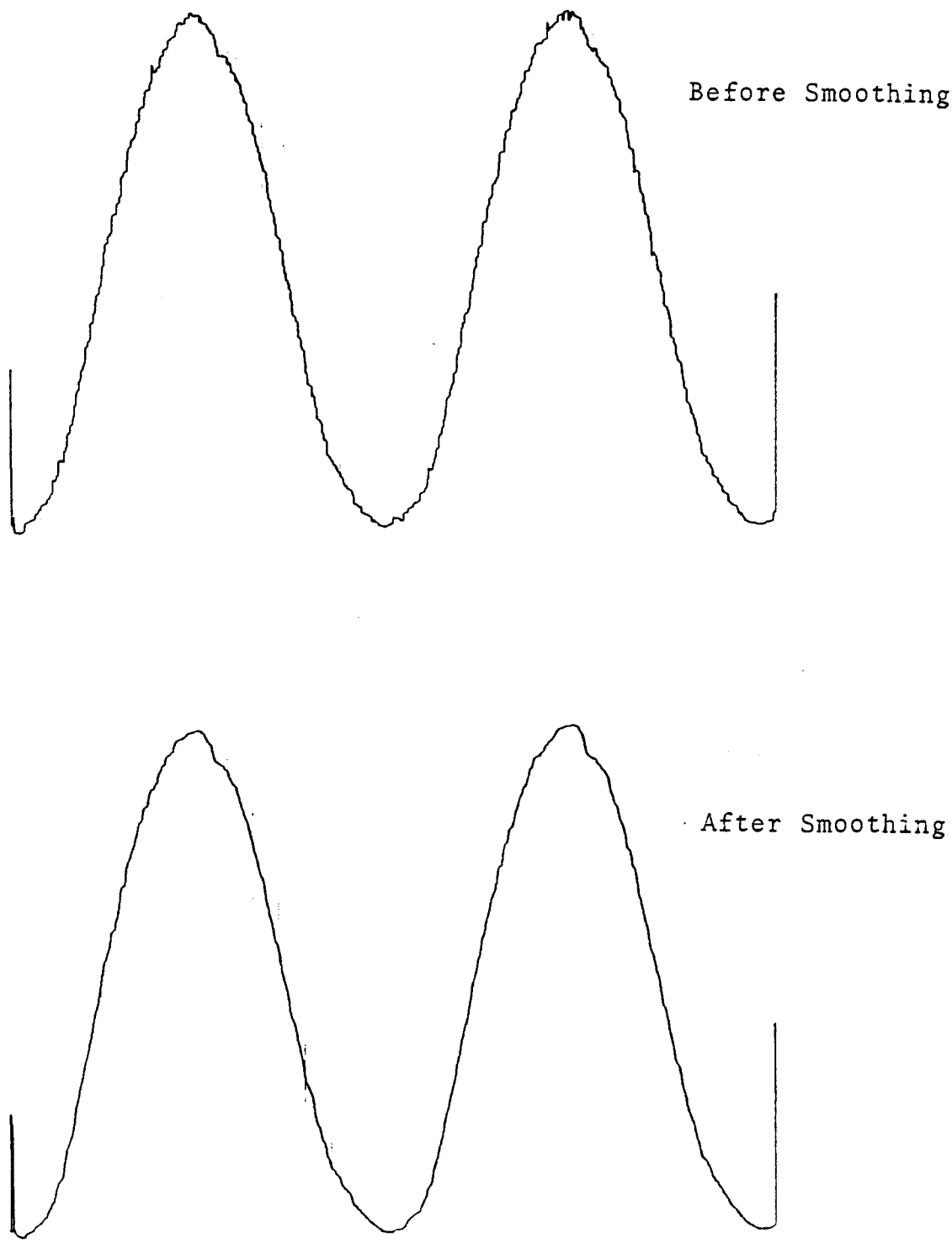

Fig. 8. Signal observed by Andre when a thin film head was used to detect the field produced by a 130 μm diameter ac current carrying wire.

Chapter 2. Apparatus and Experimental Procedure

When one considers what is needed to fabricate magnetic field sources which are capable of resolving the thin film pole tips, it becomes evident that something a little more sophisticated than bulk wire arrays are required. What may be not quite so obvious, however, is that many other things must be dealt with properly if a clean signal representing the spatial resolution of the head is to be obtained. As a consequence, much of this experimental work was devoted to the construction of apparatus which had sufficient stability and precision to permit the acquisition of meaningful data. The following chapter will discuss: 1) The construction and testing of apparatus used to move the head and monitor its position, 2) The preparation of field sources which are capable of resolving the pole tips in the head, and 3) Data acquisition and signal processing.

2.1) The Head Positioning Apparatus

The equipment which had been designed and constructed by Andre Van Schyndel for micromagnetics studies had sufficient spatial resolution to determine the location of domain walls in iron whiskers. For the purpose of resolving the pole tips in a thin film head, however, it was too coarse. The apparatus was therefore redesigned and reconstructed with the objective of positioning the head to submicron resolution. The ultimate configuration took the form shown in Fig. 9. A brief description of this design will now be given, and will be followed by a more elaborate one in successive paragraphs.

Consider the main portion of Fig. 9. Component (1) is one of two loudspeakers which carry out the fine head positioning. These speakers are supported by a cantilevered stainless steel tube (2), and themselves support a much smaller tube (3) which is used to drive the head. The cantilevered tube is attached indirectly to a solenoid (4) and its counterpart, which are used to determine the effects of uniform magnetic fields on head response. The solenoids (which also support the rest of the apparatus) rest on an aluminum plate (5) which is isolated from floor motion by four steel springs (6). A stainless steel plate (7) supports interferometric position monitoring optics, as well as the field source. The plate can be moved in the horizontal plane by means of a motor driven x-y translator (8). This allows the field source to be placed in the desired position with respect to the head. The x-y translator is itself supported by a stainless steel plate (9) which can be moved in the vertical direction with the aid of a micrometer (11). The support plate, its associated guide, and the micrometer are all connected to a stainless steel backplate (12) which is supported by the two solenoids. In order to restrain the lateral movement of the driving tube (3), but still allow axial motion, the tube is connected

Fig. 9. The head positioning apparatus. Component (1) is one of two loudspeakers which carry out the fine head positioning. These speakers are supported by a cantilevered stainless steel tube (2), and themselves support a much smaller tube (3) which is used to drive the head. The cantilevered tube is attached indirectly to a solenoid (4) and its counterpart, which are used to determine the effects of uniform magnetic fields on head response. The solenoids (which also support the rest of the apparatus) rest on an aluminum plate (5) which is isolated from floor motion by four steel springs (6). A stainless steel plate (7) supports interferometric position monitoring optics, as well as the field source. The plate can be moved in the horizontal plane by means of a motor driven x-y translator (8). This allows the field source to be placed in the desired position with respect to the head. The x-y translator is itself supported by a stainless steel plate (9) which can be moved in the vertical direction with the aid of a micrometer (11). The support plate, its associated guide, and the micrometer are all connected to a stainless steel backplate (12) which is supported by the two solenoids. In order to restrain the lateral movement of the driving tube (3), but still allow axial motion, the tube is connected to a pair of pleated brass diaphragms (10 - only one is shown). The two diaphragms are joined by a stainless steel bar and supported by the solenoids. Note that the aluminum plate (5) is 53 cm long.

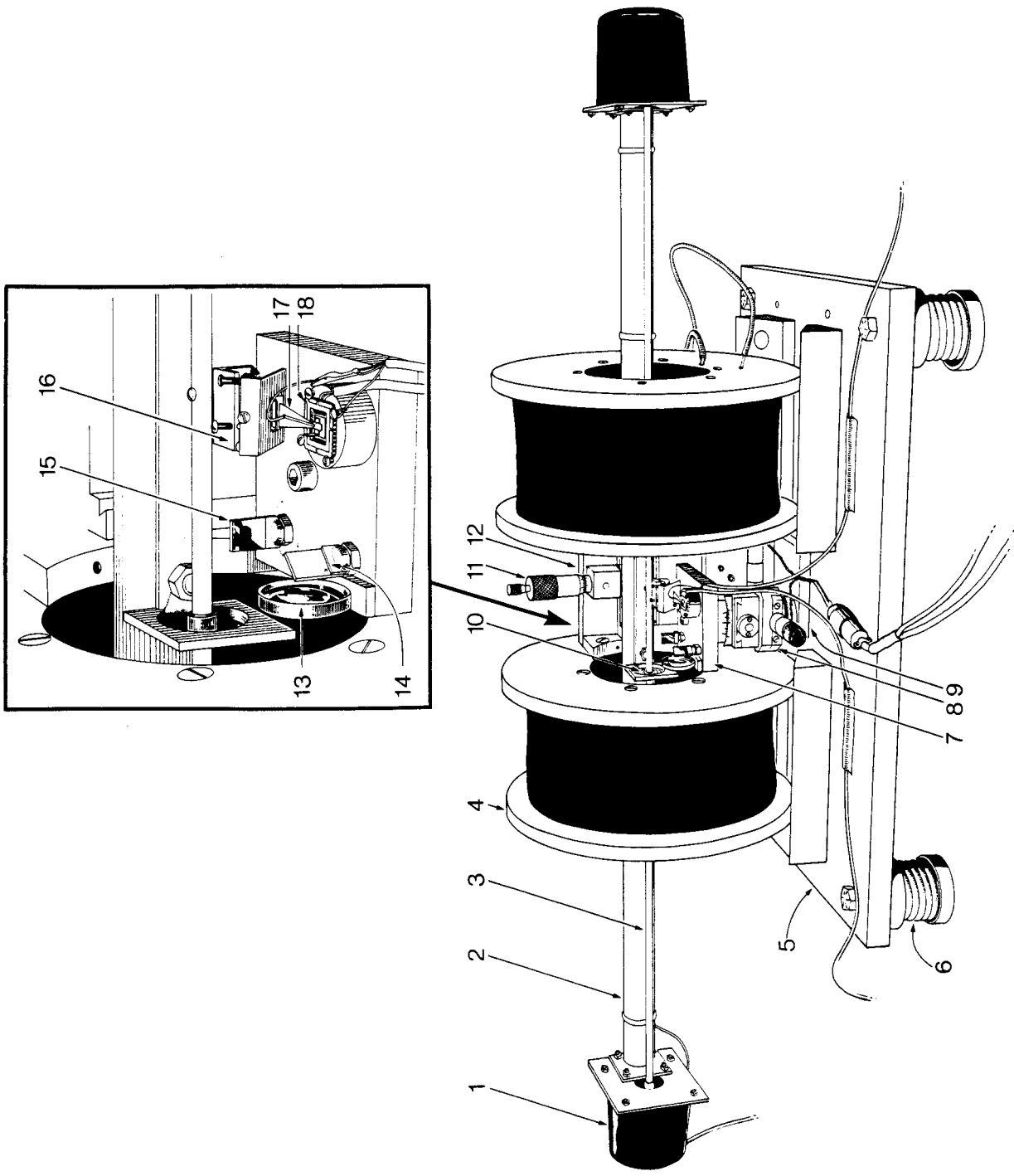
1
2
3
4
5
6
7
8
9
10
11
12
13
14
15
16
17
18

to a pair of pleated brass diaphragms (10 - only one is shown). The two diaphragms are joined by a stainless steel bar and supported by the solenoids.

Now consider the inset of Fig. 9, which is reproduced in enlarged form in Fig. 10. This is a detail of objects on and near component (7). The interferometer consists of a focussing lens (13), beamsplitter (14), reference mirror (15), and a mirror which is fixed to the head (17). The head is connected to the driving rod through an attitude adjustment mechanism (16), which allows the head to be swung about a vertical and a horizontal axis. This device also allows minor adjustments to be made in the position of the head relative to the field source, independent of the micrometer. The field source (mounted in a carrier - 18) is clamped to a brass pedestal using four stainless steel screws. The pedestal is itself attached to the baseplate with a screw.

The loudspeakers which drive the head were chosen because of their small size (7.6 cm diameter), and relatively large power handling ability (30 W when operated at a frequency of 700 Hz to 20 kHz). While they could not accept this power level at very low frequencies, they could accept dc current levels of several hundred mA without damage. They were also provided with a small plastic baffle around one side, which helped to shield them from air currents.

In order to determine whether the speakers were stable enough to drive the head smoothly, small mirrors were fixed to their diaphragms, and they were mounted in one arm of a Michelson interferometer. Visible fringes were formed with this arrangement, but they were observed to shift back and forth randomly over a distance which corresponded to a diaphragm movement of about 1 μm. Air movements across the interferometer arms did not appear to be causing these disturbances, although they did cause some fringe movement. Further investigation revealed that the plastic baffles were hermetically sealed around one side of the speaker diaphragms. Thus, it seemed that barometric pressure fluctuations may have been the cause of these disturbances. Drilling small (1/2 ") holes in the baffles confirmed this hypothesis, as the fringe movement diminished greatly - leaving only small movements due to air motion.

In order to ensure that any changes in the positions of the speakers, relative to the rest of the apparatus and to each other, were as small as possible, it was decided that a cantilevered tube should be used to hold them in place. This also made it possible to carry out very simple calculations about the possible effect of temperature fluctuations and vibrations. The speakers were each bolted to a stainless steel plate with a small hole through which the driving tube could pass. This plate served to protect the diaphragm and shield it from air currents. The plate was connected in turn to a smaller plate which was hard soldered to the cantilevered tube.

Fig. 10. Enlargement of the inset in Fig. 9. This is a detail of objects on and near component (7). The interferometer consists of a focussing lens (13), beamsplitter (14), reference mirror (15), and a mirror which is fixed to the head (17). The head is connected to the driving rod through an attitude adjustment mechanism (16), which allows the head to be swung about a vertical and a horizontal axis. This device also allows minor adjustments to be made in the position of the head relative to the field source, independent of the micrometer. The field source (mounted in a carrier - 18) is clamped to a brass pedestal using four stainless steel screws. The pedestal is itself attached to the baseplate with a screw. Note that the sides of the stainless steel support plate are 7.6 cm long.

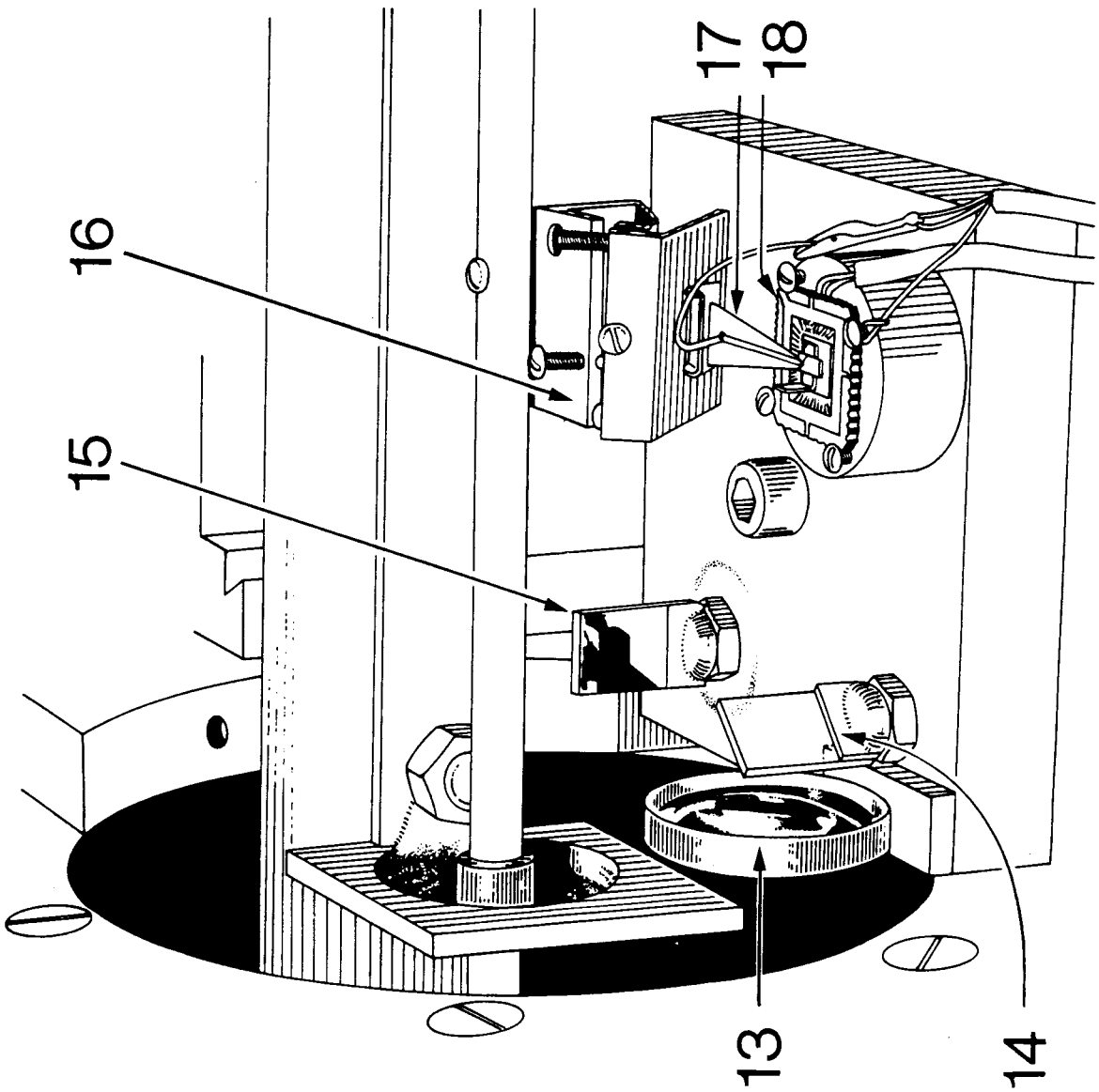
16
15
17
18
13
14

The reason why the speakers are held so far apart is that changes in the magnetic field produced by the solenoids could otherwise cause unacceptable changes in the position of the head, due to interactions between the field and the speaker coils. Experiments were carried out in order to determine what effect the solenoids could have with this configuration. It was found that the position of a freely suspended head changed by about 0.2 μm when the field was swept from 0 to 80 Gauss. This represents an acceptable amount of movement.

The cantilevered tube, the head driving tube, and in fact most parts of the apparatus which in some way determined the position of the head relative to the field source, were made of type 304 stainless steel. This material was chosen because it has a high Young's modulus (2.8×10^7 psi), and a low coefficient of thermal expansion (1.7×10^{-5}/ C) compared to other readily available (and easily machinable) materials. Type 304 stainless steel is also the most nonmagnetic stainless steel commonly produced. This material was often included in the apparatus even when its structural properties were not needed, in order to avoid the kinds of distortion which develop when two materials with different thermal expansion coefficients are held together.

Experiments carried out with partially completed apparatus made it clear that some form of vibration isolation would have to be provided. Such minor disturbances as the vibration set up by a door closing down the hall were enough to significantly disturb the motion of the head. According to one manufacturer of optical tables[†], most floor motion occurs at frequencies between 5 and 30 Hz, with a small amount of motion occurring at frequencies as low as 2 Hz After being provided with four steel springs, the apparatus exhibited a resonance frequency (for linear motion in a vertical direction) of about 2.8 Hz. This turned out to be adequate for the purpose of eliminating the most troublesome vibrations. There were still some problems due to the presence of a machine shop next door, but disturbances from this source were relatively rare, and could be removed by conducting the experiments at night.

In order to move the field source to the desired position with respect to the head, some form of x-y-z translator was required. Movement of the baseplate (7) in the horizontal direction could be accomplished most readily with the aid of a motor driven x-y table. This had previously been used by Andre for micromagnetics experiments, and was suitable for the coarse positioning in this experiment. A control stick, or "joystick" was used to control the speed and direction of the motors while the head and source were observed under a microscope. The x-y table was mounted on an stainless steel L-plate (9), which was moved in

---

[†] Newport Corporation (P.O. Box 8020, 18235 Mt. Baldy Circle, Fountain Valley, Ca., U.S.A. 92728-8020) 1983-84 Catalog, p. 13.

the vertical direction by a micrometer driven dovetail slider. This controlled the z-axis motion of the baseplate.

In order to determine the stability of the driving tube, supporting the head and freely suspended between the two speakers, interferometric tests were carried out. These revealed that if the fringes representing the position of the head were to be observed at all, some method of suppressing lateral motion of the tube would have to be provided. It was decided that this could be most easily achieved by attaching small metal diaphragms to the tube on either side of the head. Ideally, such diaphragms should have concentric circular pleats, in order to permit a reasonable amount of axial motion (at least a few tens of microns).

It turns out that diaphragms of the required form are not easy to obtain, so that it was necessary to make them. In order to do this, male and female stainless steel dies were machined to nearly the correct tolerances on a lathe. They were then pressed together, and lapped to a good fit using various grades of silicon carbide powder (in the form of a slurry). These dies were used to stamp various types of diaphragm material, including beryllium copper, brass, phosphor bronze, and stainless steel. It was found that brass made the best diaphragm, mainly because it could be obtained in 0.002" sheets, whereas the other materials were usually thicker than this. It was usually possible to obtain stainless steel in the required thickness, but it was brittle, and often cracked during the stamping process. The completed brass diaphragms were each attached to a frame. This was done by means of epoxy, since the heat of soldering would have destroyed their elastic properties. They were also provided with collars, so that they could be fixed to the driving tube. interferometric tests were carried out after the installation of the diaphragms, and revealed that the driving tube vibrations which had plagued the apparatus previously had almost completely disappeared.

The interferometric position monitor consists of several parts located in the vicinity of the baseplate (7), as well as a few items which may be a considerable distance away. The latter includes such devices as a low power (1mW) helium neon laser, a phototransistor detector, and an instrument, such as a chart recorder, which can monitor the movement of fringes across the detector. An effort was made to minimize the complexity of the system, in order to reduce the amount of time that would be required to set it up. In particular, most of the components were designed to have as few degrees of freedom as possible.

The beamsplitter (an uncoated glass plate) and the reference mirror (a chromium plated silicon wafer on a brass backing) were to be adjusted once, and left in place thereafter. The focussing lens was mounted on a small brass plate which could be moved freely on the surface of the baseplate. This was a convenient way of allowing the fringe pattern to be accurately positioned on the detector. The orientation of the head could be adjusted to a limited degree,

but once the screws on the attitude adjustment mechanism had been set, they were usually left in place. The head mirror took the form of a small section of a glass coverslide on which a thin layer of aluminum had been evaporated. This was attached to the back of the slider with a small amount of cyanoacrylate adhesive and epoxy. Since the laser light used in the interferometer is highly monochromatic, it was not necessary to include a compensating plate in the apparatus.

A serious problem presented itself when the slider was brought into contact with the field source. The oil lubricating the interface between the slider and the source would creep up onto the head mirror and degrade its optical properties, which resulted in the elimination of the fringe pattern. This behavior can apparently be attributed to the fact that the surface tension of the oil was lower than the surface energy of the aluminum mirror coating. It was found that if the mirror had been used long enough, a contaminating film (probably aluminum oxide) would form on the surface of the coating, and oil creep would no longer occur. In order to avoid having to constantly clean the mirror (or wait until a film had formed), new mirrors were given a thin coating of polytetrafluoroethylene (teflon) by electron beam evaporation. The reason for using teflon is that its surface energy is very low - lower, in fact, than that of any other substance under normal conditions. It was necessary to deposit only a very thin film of the material in order to eliminate oil creep. Typically, a few hundred angstroms were deposited on each mirror[†].

In operation, a beam of laser light is aimed at the beamsplitter from the front of the apparatus. Approximately half the light passes through to the reference mirror, while the other half is reflected to the head mirror. About half of the light from the head mirror and reference mirror respectively pass through and reflect from the beamsplitter to the focussing lens. The light is then directed through a magnet (4), past a loudspeaker (1), and onto the phototransistor

---

[†] It was found that an antiwetting agent (Nyebar - Type CT) developed by the William F. Nye Company (P.O. Box G-927, New Bedford, Mass., U.S.A. 02742) to prevent oil migration was effective at keeping fresh aluminum coatings free of oil contamination. However, there was some concern that this product (consisting of a fluorocarbon polymer dissolved in trichlorotrifluoroethane, which evaporates after application to leave a thin film) might make its way onto the bearing surface of the slider. This could take place while the Nyebar is applied, or while the head is being cleaned. The advantage of vacuum evaporating PTFE is that the evaporant travels in a straight line from the source and stays where it lands. In addition, since it is necessary to bake Nyebar films at 100° C for 15 minutes in order to make them truly effective against diester oils (the type of lubricant used in this experiment), Nyebar is almost as much of a nuisance to apply as vacuum evaporated PTFE.

detector (not shown). A current is produced by the phototransistor which is proportional to the light flux falling on it. This current is converted to a voltage and recorded.

The optics in the interferometer could be used for another purpose besides monitoring the motion of the head, and that is to see whether or not the head slider was resting firmly on the field source. In order to do this, the focussing lens was removed from the baseplate, and the spot produced by light reflecting from the head mirror was observed on a distant screen. A small screw driver was then gently pressed against the top of the slider. If the spot of light subsequently moved in a vertical direction on the screen, it could be inferred that the head was not resting firmly against the source. The optical lever provided by this arrangement gave the method great sensitivity.

When tests were first carried out with the apparatus, fluctuations in the output from the phototransistor were observed even when the head was not being driven. A plexiglass case had been constructed to shield the apparatus from air currents, so fringe movements from this source were not the cause of the variations. In fact, a direct examination of the fringe pattern revealed no movement whatsoever. Changes in the ambient light level were investigated, and discounted, as another possible explanation. If the laser was shone directly into the phototransistor, no variations in the output voltage of the required magnitude could be observed.

Eventually the problem was traced to the fact that the output from the laser was randomly polarized. It seems that the light output from this device always had a preferred direction of polarization, but this could change erratically as a result of small changes in temperature. After reflecting from the surfaces in the interferometer, these changes in polarization manifested themselves as changes in light intensity. The problem was solved by obtaining a laser with an built-in Brewster window. The light produced by this device had a stable angle of polarization, which did not change with temperature. The use of this laser considerably improved the stability of the position sensing apparatus.

In order to determine the linearity and stability of the completed system, a number of experiments were carried out. To begin with, the driving loudspeakers were connected in series in such a way that they moved in phase when a current was passed through them. A current source had been constructed which was capable of passing a current of up to ± 100 mA through the speakers with a linearity and drift of less than 0.1% (see Fig. 11). A potentiometer controlling the output of this source was connected to the shaft of an ac synchronous motor, so that a current ramp could be produced which was related to a fairly accurate time base (the 60 Hz ac mains). The head was suspended freely, so that it was not in physical contact with a field source. A linear current ramp was then produced which started at 0 mA and reached a

Fig. 11. Schematic diagram of the current source. This device was capable of passing a current of up to ± 100 mA through the speakers with a linearity and drift of less than 0.1%. The operational amplifier is a Fairchild mA741C.

-all resistances are in ohms

-all range-set resistors are 1% precision

-all capacitances are in microfarads

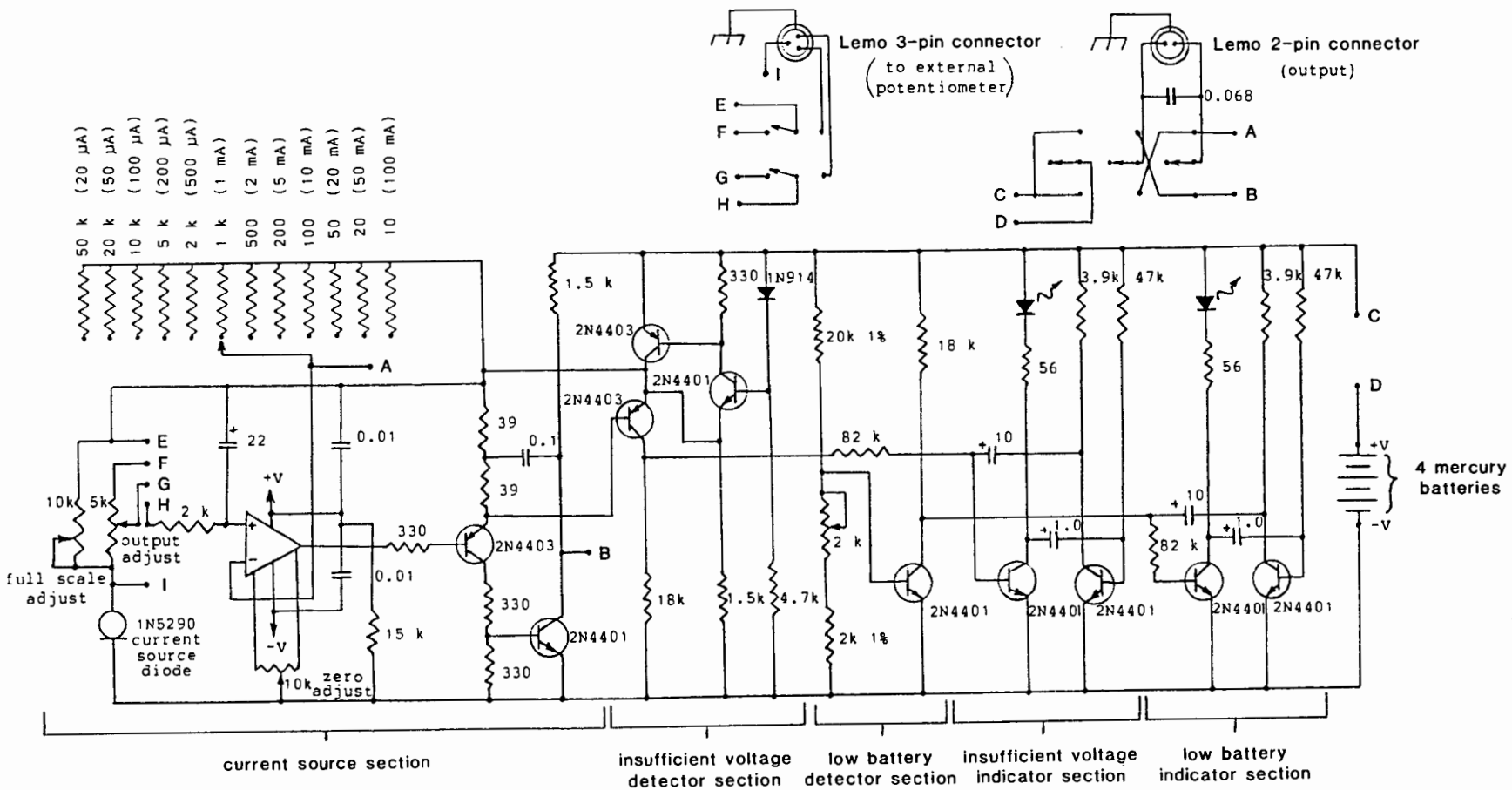

maximum of 100 mA after 100 minutes. The output of the phototransistor, as registered on a chart recorder, is shown in Fig. 12. One oscillation in this plot represents a head displacement of: $\lambda/2 = 0.3164\ \mu m$, where λ is the wavelength of the red helium-neon laser line.

Another experiment was carried out, with no driving current, in order to evaluate the stability of the system against vibrations and thermal drifts. A freely suspended head was left for 150 minutes as the phototransistor output was recorded. The resulting plot, which is reproduced in Fig. 13, shows that the RMS variation in the position of the head over a period of 150 minutes is on the order of $\pm$ 100 Å. For a period of about 15 minutes it can be as small as $\pm$ 30 Å. The rapid oscillations (thick black band) appear to be caused by vibrations of the head slider at the end of its cantilevered leaf spring. These oscillations do not take place if the head is resting on a field source. Both experiments were done with the plexiglass cover in place over the apparatus.

2.2) Construction of the Field Source

For most of the experiments which were carried out to determine the properties of heads, it was not necessary to use an array of fine wires, but merely to use another head of the same kind. Since sliders normally carry two thin film heads, it was always possible to take a slider, invert it, and glue it to a substrate to create a usable field source (see Fig. 14). It was mentioned in the last chapter that Andre had already explored the possibility of doing this, but a reexamination of his apparatus revealed that the lower slider had been mounted in such a way that the upper surface (including the pole tips) was covered by a layer of potting epoxy. Consequently, it appears that the sliders were never close enough together to ensure that most of the flux passing between the heads was going through the pole tips. The spatial resolution of the heads always appeared to be very low, as if flux was being coupled directly between the coils. Therefore, it seemed worth repeating Andre's experiment with a more carefully mounted lower head.

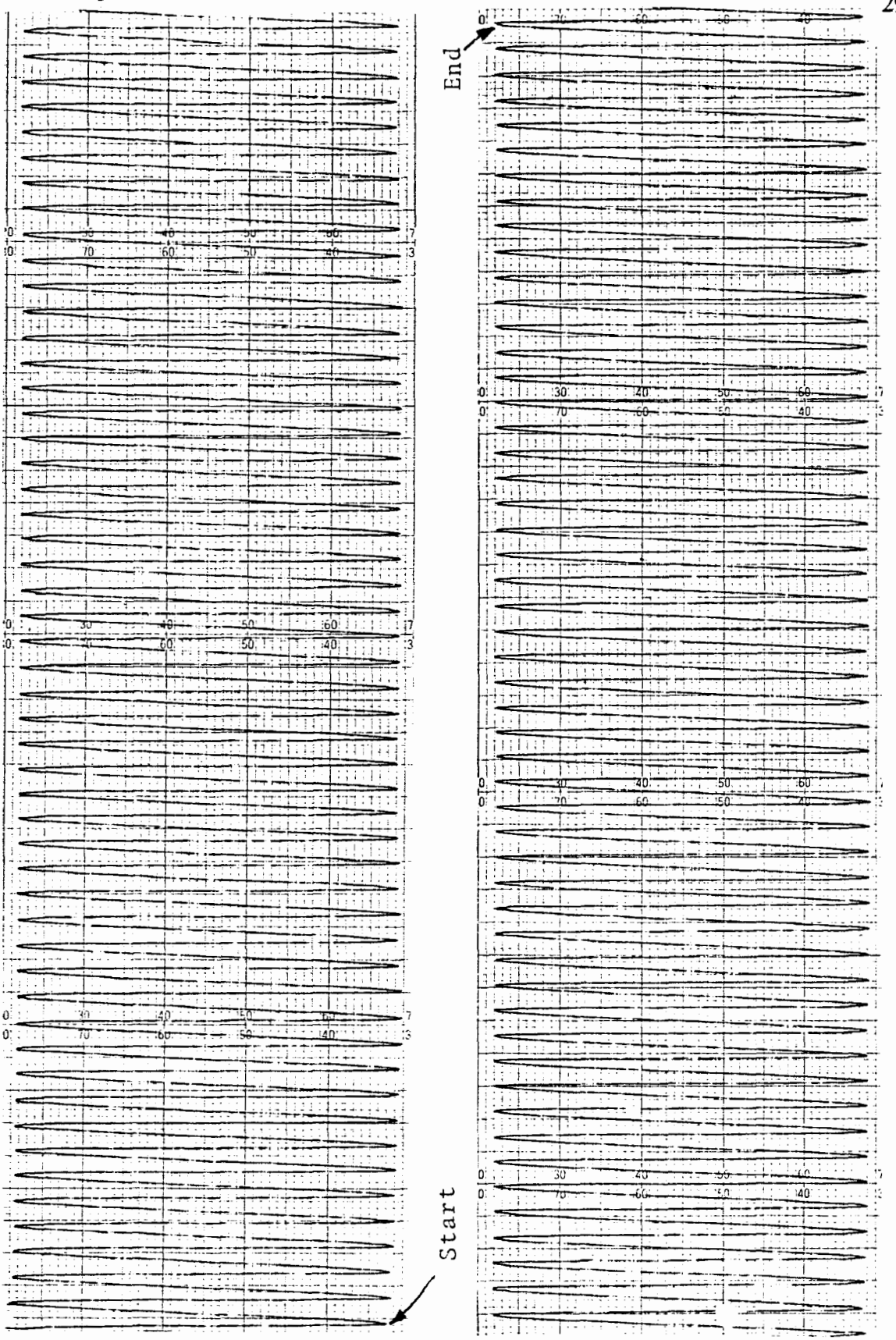

Fig. 12. Interferometer output representing the movement of a freely suspended head during the application of a current ramp to the loudspeakers. The current starts at a level of 0 mA and reaches 100 mA after 100 minutes.

Fig. 13. Interferometer output representing the movement of a freely suspended head in the absence of loudspeaker current. The bar indicates the difference between the maximum and minimum light levels. The plot shows that the RMS variation in the position of the head is on the order of ± 100 Å for a period of 150 minutes, and can be as small as ± 30 Å for a period of 15 minutes. The rapid oscillations (thick black band) appear to be caused by vibrations of the head slider at the end of its cantilevered leaf spring.

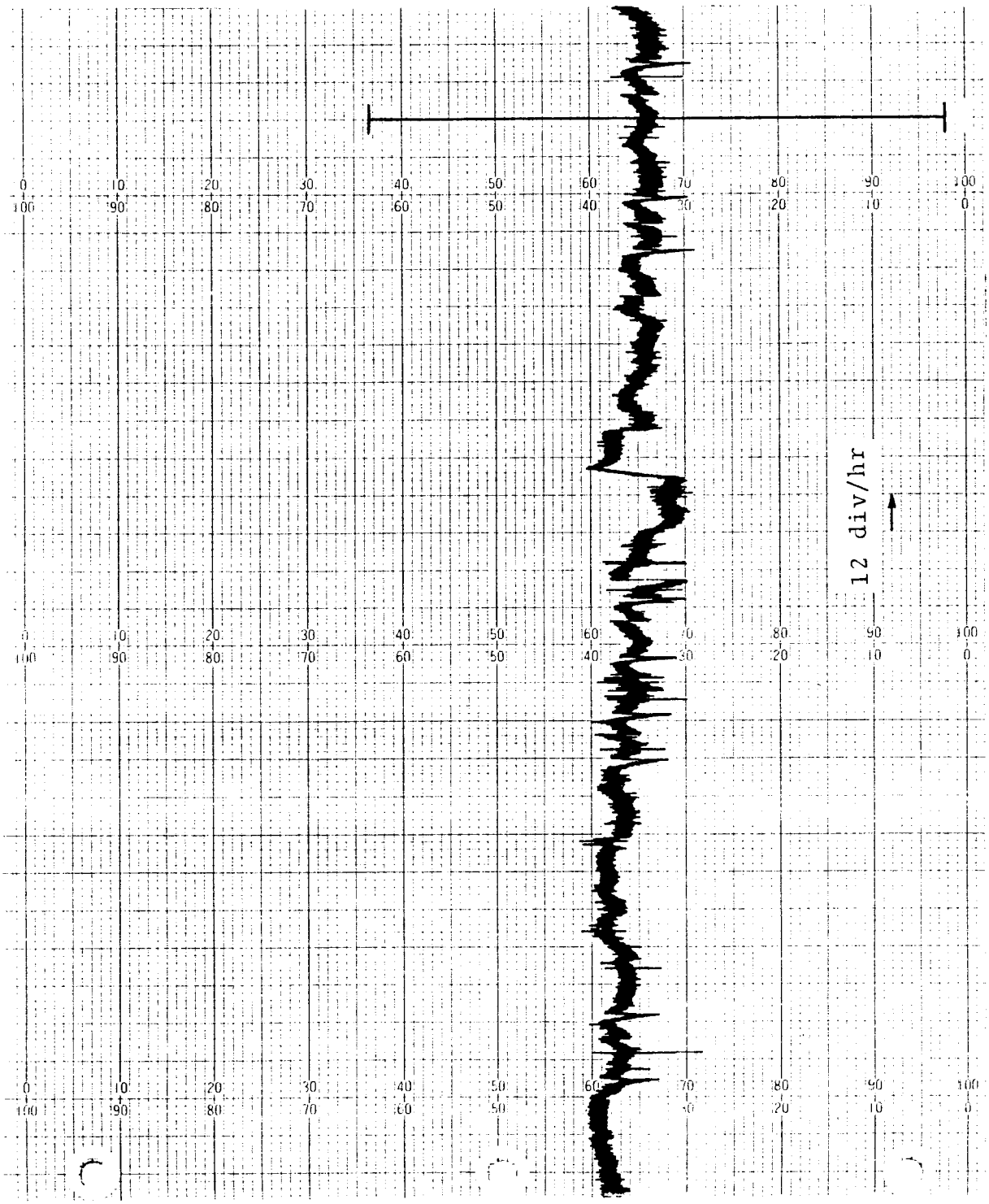
12 div/hr

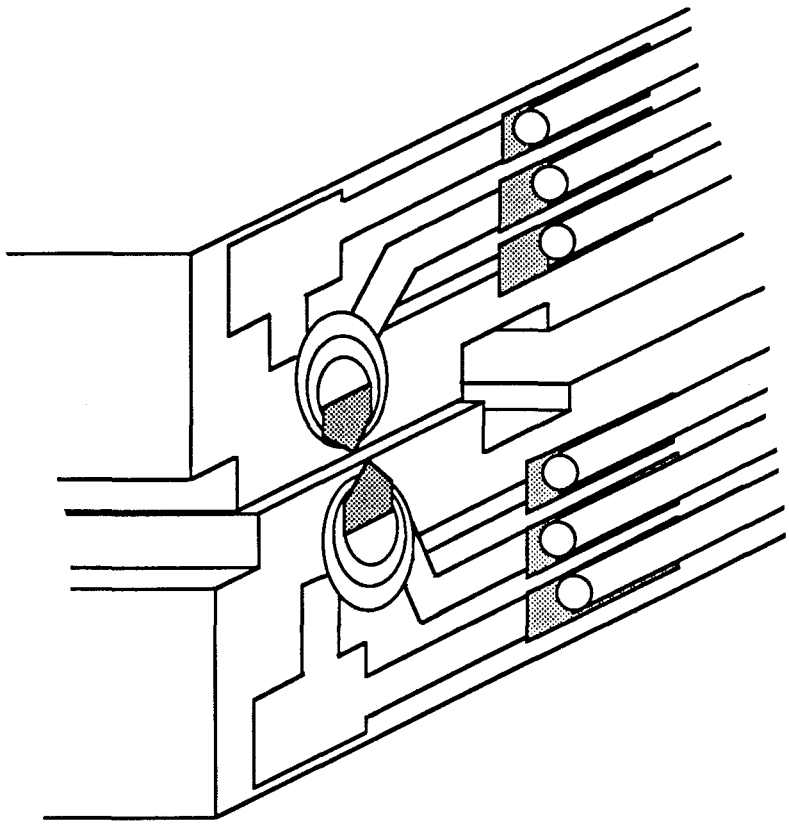

Fig. 14. Using an inverted slider as a field source.

It was found that a head would work quite satisfactorily as a field source, as long as the upper surface was kept free from contamination. In the case of the Cybernex heads, mirror image versions were available which made it possible to match up two heads in the manner shown in Fig. 14. In the case of the IBM heads, the sliders were wired in only one way. Consequently, when they were to be tested it was necessary to rewire one of the sliders so that it would have the correct sense. This involved removing the old lead wires from the slider and attaching new ones to the correct bonding pads by means of ultrasonic welding (a process which will be described later in the chapter).

In order to conduct experiments which required a magnetic field with known (calculable) properties, it was necessary to construct a field source with fine conducting wires. Fabricating this field source turned out to be the most time consuming part of the project. This was partly due to the fact that the devices had to be made using photolithography, and because this had to be done outside the university. It also became necessary to try several different approaches in order to produce exactly what was needed. The nature of these approaches depended to a large degree on what facilities were available to carry out the fabrication. As a result, a very large

amount of interaction with agencies outside the university was required. A few paragraphs in this section of the chapter will be devoted to a discussion of the unsuccessful approaches, in order to show how the successful one was finally chosen. The remainder of the section will discuss how the ultimate design was implemented, and how it was incorporated into the rest of the apparatus.

It became apparent that field sources constructed using conventional materials (bulk wire stored in the form of a reel) are unsuited to the investigation of thin film heads. Clearly, the most appropriate method of constructing the needed devices is to make use of the same techniques which are used to fabricate the heads themselves. With this in mind, a thin film field source was fabricated using techniques which have been developed by the electronics industry for the manufacture of integrated circuits.

A diagram of this device can be seen in Fig. 15. Current enters the source through the boxes at the bottom of the diagram, which represent bonding pads onto which gold wires are connected. Current travels from these pads through 20 μm wide conductors to a region near the top of the diagram, where the wires narrow to about 4 μm, and the right hand wire climbs atop the left hand one. The wires retain this configuration over a distance of 200 μm, until they connect through the small box (a "via") located at the top of the diagram. This 200 μm long pair of wires is the field source over which the pole tips pass. The crosses located at the left and right of the pattern near the middle of the diagram are alignment marks. They are needed because the source is constructed using three thin film layers, which must be placed on top of each other with the correct orientation. Each layer had its own mark, and together these marks allow the layers to be aligned by visual inspection.

The first layer in the source is the left hand wire, which consists of 0.6 μm thick evaporated aluminum. The second layer, which provides the insulation between the two wires, is a form of polyamide with a thickness of about 0.5 μm. The third layer is the right hand wire, which is also made from aluminum and has about the same thickness as the left wire. The substrate which supports the wires and their insulation is silicon coated with silicon nitride. The silicon nitride serves to insulate the first layer from the silicon substrate, which is a semiconductor, and which would otherwise produce a short circuit.

Field sources of the kind just described were used in thin film head investigations, but it became clear after a while that they were not going to do what was required of them. It was possible to explore the nonlinearities and frequency response of the head, but not its spatial resolution. The width of the response function of the head was far larger than one would

Fig. 15. The first field source. The lead wires are 20 μm wide and are separated horizontally by 10 μm. The source wires are 4 μm wide, and are separated vertically by 1 μm.

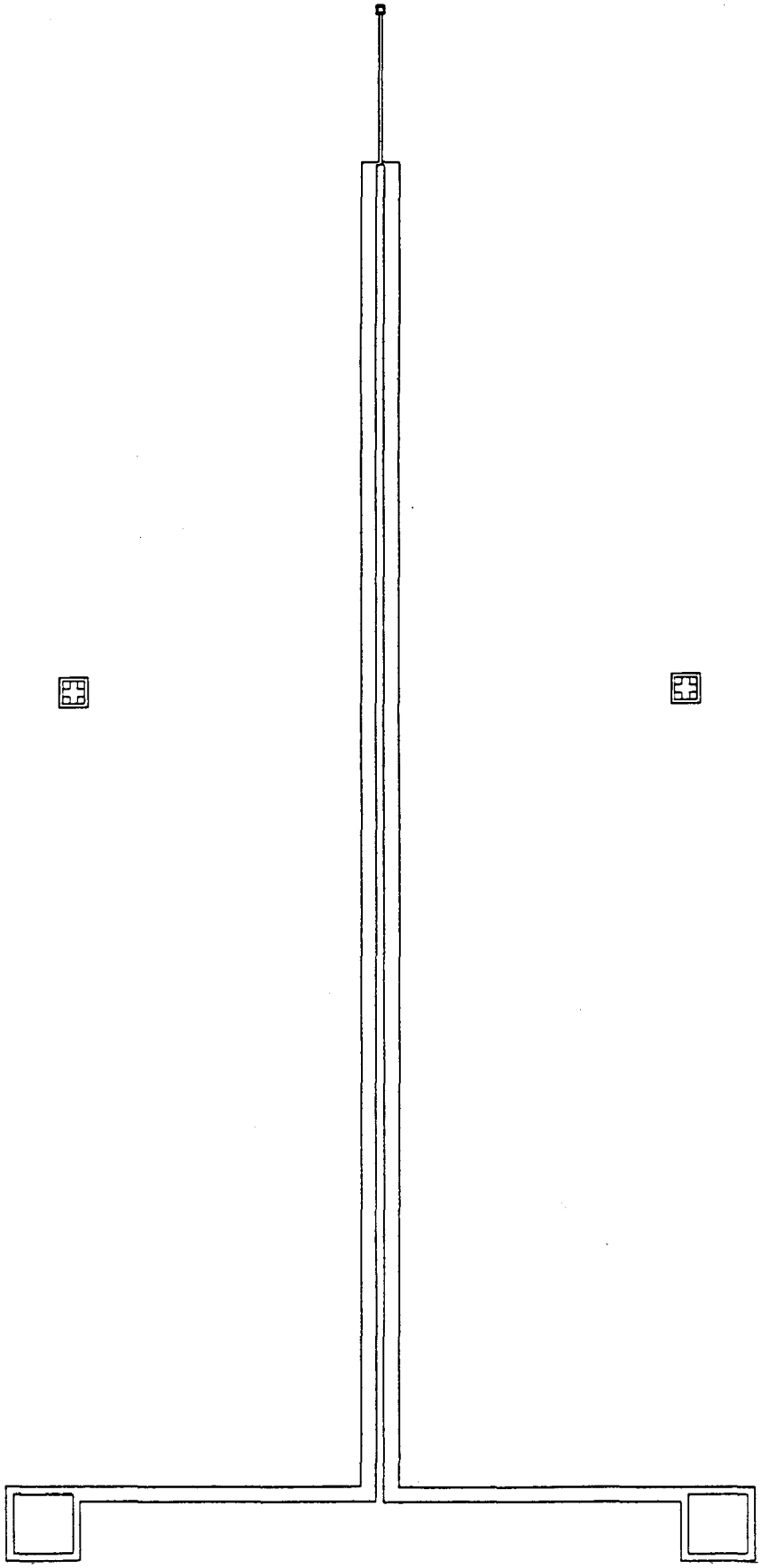

expect after considering the width of the wires in the field source and the thickness of the pole tips (see Fig. 16).

There appears to be a reasonable explanation for this. It could be that the design of the source made it impossible to get the slider close enough to the wires to resolve the pole tips. There was no method, using this design, by which one could determine the distance between the head and the wires. One could only assume that the pole tips were in contact with the wires. This actually may have been part of the problem. It could be that the head, in moving back and forth across the source, peeled some of the aluminum up, so that the pole tips were prevented from coming close to the wires. A layer of oil was applied to the source to provide it with lubrication, but this may not have been enough to protect it against abrasion. It is significant that reproducibility from one measurement to the next was often difficult to achieve.

It is also significant that the same kind of resolution function was observed when the pole tips were not running over the source wires. The same lineshape and the same signal strengths were observed when the pole tips passed below the via connecting the two wires. This indicates that parts of the head other than the pole tips had been responsible for detecting most of the signal. Further evidence came when the pole tips were located near, but not over, the 20 μm wires leading up to the source. Despite the fact that the pole tips were not passing over these wires, the response function began to take on the shape that one would expect to see if they were. These kinds of phenomena are similar to the ones which Andre observed, and their origin is probably similar. It seems likely that in both cases it was not possible to produce a large magnetic field gradient close to the pole tips. In the case of Andre's experiment, the wires were too big to produce such a gradient. In the case of this experiment, it seems that the wires were small enough to produce the gradient, but the poletips could not be moved near enough to them.

In order to find out why the source illustrated in Fig. 15 was producing such unexpected results, calculations of the field produced by the source were carried out. The details of this analysis are given in the next chapter. Stated briefly, the calculations support the notion that the source was never close enough to the head to produce a response in the pole tips, and that the rest of the head (the permalloy core and the coil) was capturing most of the flux.

Another analysis was carried out in order to find out the character of the field near a magnetic disc, in order to find out what magnetic heads encounter when they are reading information stored on a disc. It turns out that if one assumes that adjacent domains in a magnetic disc are oriented in opposite directions (i.e the surface of the disc looks like a 2-D antiferromagnet), the fields will decay exponentially in a direction perpendicular to the surface of the disc. In fact the functional form is actually more complicated than this, but it is

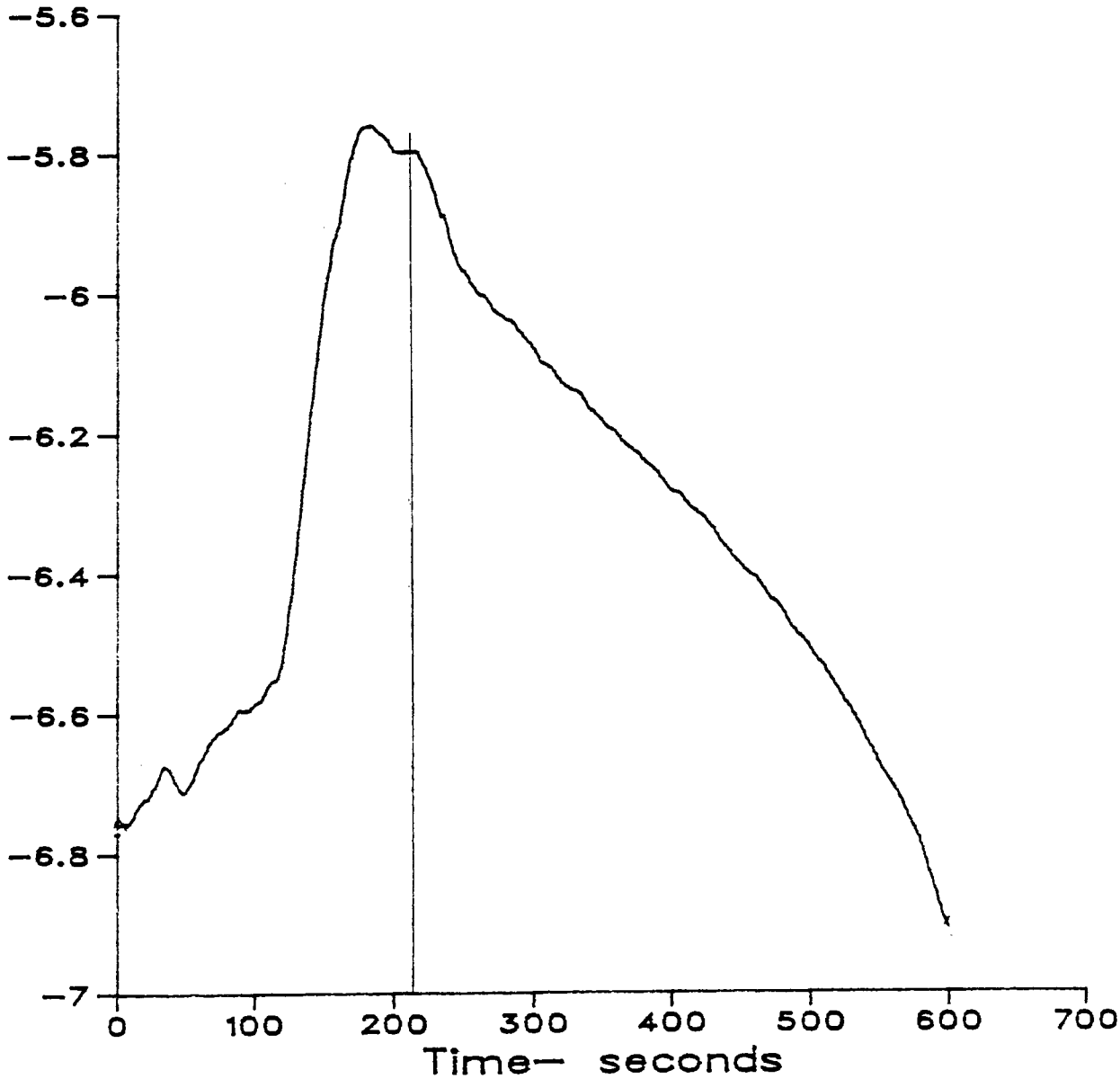

Fig. 16. Signal detected as a Cybernex head was moved over a copy of the first field source which was carrying a current of 138 mA at a frequency of 2.7 kHz. A period of 100 s represents a travel distance of 233 mm.The vertical line in the middle of the plot indicates the position of the source wires. The width of the line indicates the approximate width of the source wires on this scale. Each division in the vertical scale represents 10 nV.

essentially exponential. The characteristic length in this decay is set by the periodicity of the domains.

This result suggests the following arrangement. What is needed is a field source which will only produce a response in the pole tips, if there is to be any response at all. Such a source can be constructed by fabricating an array of parallel wires, in which adjacent wires carry current in opposite directions. The analysis shows that the fields from this source will decay exponentially in a direction perpendicular to the plane of the wires. As a result, any detected signal will have to be caused by fields acting at the pole tips. Of course, since any real wire array must be finite, the form of the field decay will not be a true exponential. If it is large compared with the dimensions of the permalloy core and coils in the head, however, the difference should not be of practical significance.

A diagram of a source which was designed to have these characteristics can be seen in Fig. 17. Each of the lines represents a wire which is 2 μm wide, 998 μm long, and which is separated from its neighbors by 2 μm. There are a total of 256 wires in the array. Unlike the previous source, this one consists only of conductors on a single level. As with the idealized magnetic disc, the field from this source will decay exponentially - in some region which is fairly close to the plane of the wires, but not too close to the boundaries. As with the disk, the characteristic decay length is set by the periodicity of the array. Detailed calculations of these fields are presented in the next chapter. In order to minimize stray fields from large area loops, the thin film lead wires are extended for about 2 mm before connecting to bonding pads.

The construction of the source began by entering its design into a computer using a computer aided drafting system at TRIUMF. This information was subsequently stored on magnetic tape, and sent to a commercial facility for mask fabrication[†]. In this facility, another computer used the information to drive a device which uses a laser to expose selected areas of a photographic plate. This plate, which contains an image of the source pattern, was mounted in a machine which made many copies of the pattern on another plate. The machine simultaneously reduced the size of the image by a factor of ten, so that 20 μm wide lines became 2 μm ones. The new plate, called the "master", was used to produce images of the source on yet another plate, which was to become the actual photomask. This plate did not contain a photographic emulsion, but consisted of layers of gold and chromium (several hundred Å thick) deposited on glass, which were selectively removed (using a process similar to one described later) to form images of the source pattern. The chromium is deposited first, to provide abrasion resistance. The gold is then deposited to reduce backreflections of

---

[†] Precision Photomask (4950 Fisher St., St. Laurent, Que., H4T 1O6).

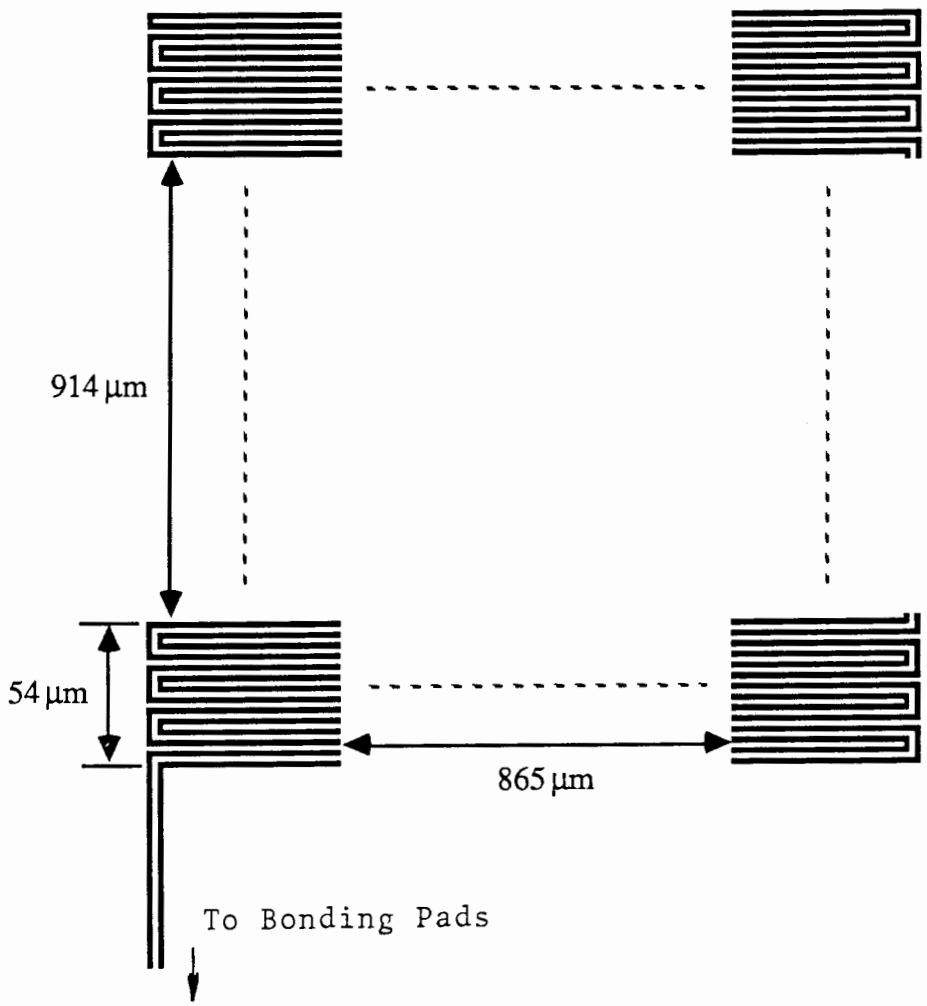

Fig. 17. The second field source. The wires (black lines) are 2 µm wide and are separated by 2 µm.

ultraviolet light, which is used in the photolithography.

In order to produce a source, a 0.4 mm thick silicon wafer must first be given some form of dielectric coating. Previously, silicon nitride had been used. For this source, however, it was decided that thermally grown SiO_2 should be used, because of its outstanding resistance to abrasion and the formation of pinholes. The oxide is created by exposing the wafers to oxygen at a temperature of 850 C for about 2 days. This results in a 5000 Å thick layer.

The next step in the process was the deposition of a suitable metal, which was to form the source wires. Aluminum is a satisfactory material for this purpose, since it is a good electrical conductor. Its chief disadvantage is its lack of abrasion resistance. It will be shown later, however, that this need not be a liability. A good method of depositing almost any substance is rf planar magnetron sputtering, since it is capable of producing a very good bond between the material and its substrate[33]. Consequently, this form of sputtering was used to deposit the wire metal. The thickness of the layer was chosen to be about 5000 Å, since it does not take too long to create a layer of this thickness, and because calculations indicated that the resistivity of the resulting source wires would not be too high (about 8 kΩ for aluminum). It is also true that 5000 Å is comparable to the thickness of the film in magnetic disks.

A pattern must be created in the conducting film, and this is accomplished by means of a photolithographic process. A 1.5 μm layer of a light sensitive chemical called photoresist is applied to the wafer by a process known as spinning. This consists of applying the photoresist, in liquid form, to the wafer, which is then spun at a speed of about 4500 RPM. Excess photoresist is thrown off the wafer by its rotational motion, and the material which remains is smoothed to form a uniform film. The wafer is subsequently baked in an oven in order to dry the photoresist. To create the pattern, the wafer is placed in a device called a mask aligner, along with the mask. The mask is pressed into direct contact with the substrate, so that the gold-chromium patterns come into contact with the photoresist. A beam of ultraviolet light is then shone through the mask onto the wafer. The areas of the photoresist which are not protected by the mask are rendered susceptible to chemical removal by the light. The wafer is baked once again in order to prepare it for the development step. It is then placed in a developing solution, which removes the photoresist which had not been protected. What remains afterwards are patterns of photoresist which sit atop the conductive film.

In order to remove unwanted conductive material and form the wires, the wafers must at this point be placed in some kind of reactive environment. The easiest way to produce such an environment is to place the wafer in an aqueous etching bath. In the case of aluminum, this is usually hydrochloric acid or sodium hydroxide in water. Wet chemical etching was used to process some wafers, but the resulting patterns were of very poor quality. The lines were

often uneven, and there were usually many bridges or breaks in the wires. In fact, no acceptable devices were produced using this method.

The alternative to wet chemical etching is dry etching, or plasma etching (there is actually another method, called reactive ion etching, which will not be discussed here). In plasma etching, the material to be etched is placed in a vacuum chamber, from which most of the air is removed. An suitable etching gas is then admitted to the chamber at low pressure, and a high frequency electrical discharge is initiated. Although the etching gas by itself may not be reactive, the act of passing a current through it creates species which may be highly reactive. These species combine with the material to be etched and form volatile residues, which can then be pumped away. This process is continuous, of course, so that new gas is constantly replacing gas which has been removed. The chief virtue of plasma etching is the complete absence of such factors as surface tension, viscosity, and bubble formation, which make it difficult for wet etching to produce fine features. For this reason, a decision was made to use plasma etching to create the source wires.

The problem with plasma etching is that it is a process which involves hazardous gases, and complicated equipment to handle them. Plasma etching the refractory metals molybdenum, titanium, and tungsten can be done with carbon tetrafluoride (Freon 14), and a fabrication facility was found which could deposit these metals and etch them using this gas[†]. This facility was used to fabricate source wires containing a tungsten-titanium alloy. Such sources were used in an attempt to conduct thin film head investigations.

Unfortunately, the resistances of these devices turned out to be extremely high (about 500 kΩ). This caused a number of problems. For example, in order to pass a reasonable amount of current (at least 10 μA) through the wires, it was necessary to apply a large potential difference between them. As a result, very high voltage gradients (about 50 kV/cm) were produced. These gradients often caused electrolysis to take place, which resulted in the destruction of the wire material (see Fig. 18). It was also impossible to attach lead wires to bonding pads made out of this alloy using the standard methods. Instead of creating a metallurgical bond between the lead wires and the bonding pads, the wires were attached to the pads using silver epoxy. This turned out to be an uncertain process, and very often an electrical connection could not be established.

It is possible to etch aluminum using a carbon tetrachloride or boron trichloride plasma. A commercial microelectronics facility (Microtel Pacific Research) had acquired the ability to plasma etch aluminum, as well as carrying out some of the other steps needed to fabricate the

---

[†] The Department of Electrical Engineering at the University of British Columbia.

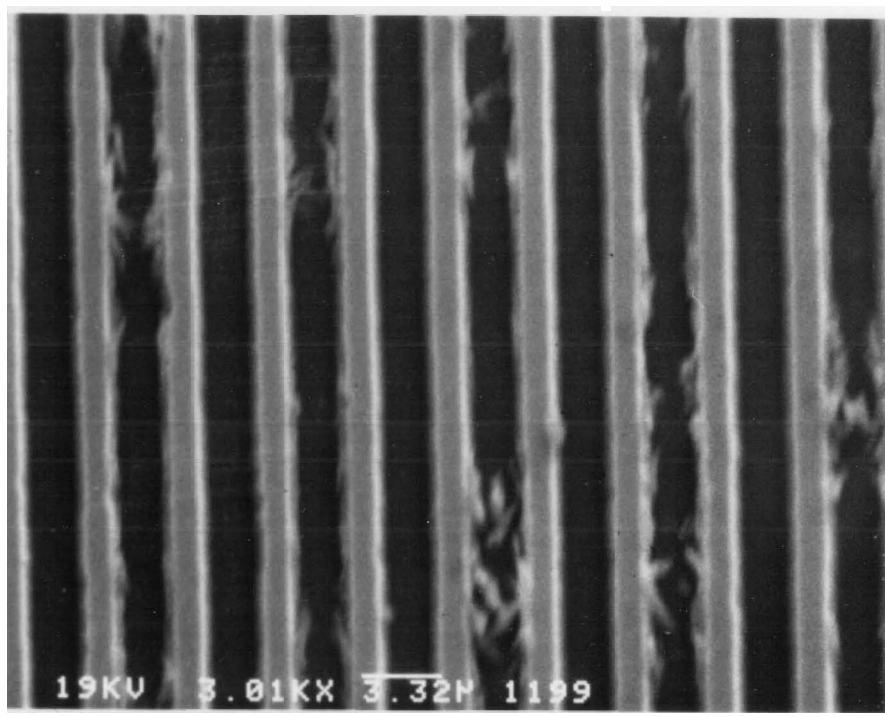

Fig. 18. Electron micrograph of W-Ti field source wires which have been subjected to a voltage gradient of about 50 kVRMS/cm for several hours.

source. They had also installed a good contamination free enclosure (a "clean room"), which meant that the presence of a large number of dust particles during photolithography would be unlikely. Microtel was approached about the possibility of using their facilities to make some sources. They agreed, and the fabrication was carried out.

The substrates for the sources were standard 4" silicon wafers. This particular material was chosen because it could be handled by the machinery at Microtel. The first step in the fabrication involved growing an insulating layer of SiO_2 on the wafers by thermally assisted oxidation. To do this, the wafers were placed in a tube furnace at a temperature of 850 C. Then, 99.999% pure oxygen was passed over them at a rate of 5 l/min for a period of two days.

In order to desposit the aluminum, the wafers were loaded into a MRC 902A sputtering machine. sputtering took place at a pressure of 15 mTorr and a power level of 5.5 kW dc. The wafers were passed under the target at a speed of 13.4 cm/min (corresponding to a deposition rate of 0.46 μm/min) for 1.1 min.

After depositing the photoresist and carrying out the photolithography, the wafers were placed in a Perkin Elmer Omnietch plasma etching machine. The unwanted aluminum was removed using a mixture of BCl_3 (flowing at a rate of 15 scc/min), CH_3Cl (at 52 scc/min) and Cl_2 (at 25 scc/min). The pressure inside the reaction vessel was 2.5 Torr, and the plasma power level was 250 W. The endpoint of the etching process was determined spectroscopically. Radiation from the plasma was analyzed in order to detect a characteristic emission line of aluminum. When this line dissappeared (an event which took place about 120 s after the start of etching), the machine was left to run for 20 s before being shut off.

After the wires were formed on the silicon substrates, it was necessary for these substrates to be divided into sections containing the individual sources. In some cases this was done using an scribing machine, which uses a diamond stylus to create scratches on the wafer at precisely determined intervals and in the correct directions. The correct directions are determined by the crystalline axes of the silicon, which the manufacturer indicates by creating a flat on one side of the (otherwise circular) wafer. In order to create smooth separations, the wafers must be scribed in directions parallel and perpendicular to this flat. The wafers were aligned during photolithography so the circuits could have the desired orientation after scribing. After the scratches were made, it was necessary to exert only a small amount of pressure in the appropriate places to break the wafer up.

The wafers were usually divided using a diamond saw. This is a specialized machine which is used by the semiconductor industry for the production of integrated circuits. The advantage of sawing wafers is that the resulting cuts are relatively straight and clean compared

with the ones produced by scribing and breaking. The main disadvantage of this method is that it creates a large amount of silicon dust. This dust often found its way into the crevices between the wires, and often scratched through the aluminum wires during subsequent cleaning operations. Because of this hazard, scribing and breaking is (in this application) the preferred method of dividing wafers.

Before the sources were subjected to any further processing, they were examined in various ways for signs of damage. The first step in this process consisted of a cursory visual inspection under an optical microscope. Following this, the resistivities of the sources were measured in order to find out if they contained any shorts or open circuits. These measurements were conducted under a microscope, and made use of small wire probes which could be moved about with micromanipulators. Many defective devices could be easily found and discarded at this point before more time consuming tests were done. The last step in screening the sources consisted of examining them under a scanning electron microscope. Using this device, openings in the wires could be found, and lumps of material which might produce shorts could be detected. A subsequent analysis using x-ray photoelectron spectroscopy usually revealed whether these lumps of material were pieces of photoresist, dust or metallic shorts. Electron microscope images of a functional source can be seen in Fig. 19.

In order to insure that the pole tips, as they travelled across the field source, remained at a constant distance from the wires, a structure had to be created which would support the slider. It was clear that the surface of such a structure would have to be parallel to the surface of the wafer holding the field source, and it would have to be very smooth. The best way of achieving this seemed to be to deposit a layer of material around the source in such a way that the head could be supported everywhere except in a small region surrounding the pole tips. This idea is illustrated in Fig 20. In order to reduce abrasion of the source, it was desirable to leave a small gap between the head and the source wires. This could be accomplished by making the support layer slightly thicker than the source, which is fairly easy to do using thin film deposition methods.

The easiest way of depositing a film with the required properties is to use vacuum evaporation through a mask. A mask was therefore constructed out of tantalum with a hole having the required shape. Since it would be necessary for the support layer to resist abrasion and the embedding of foreign particles, it seemed reasonable to try evaporating hard refractory materials such as molybdenum. This necessitated the use of an electron beam evaporator containing an electron gun and a water cooled copper crucible. A vacuum system containing these elements was located, and a variety of hard materials with high melting points were evaporated on suitable substrates. The evaporated layers were first inspected visually for

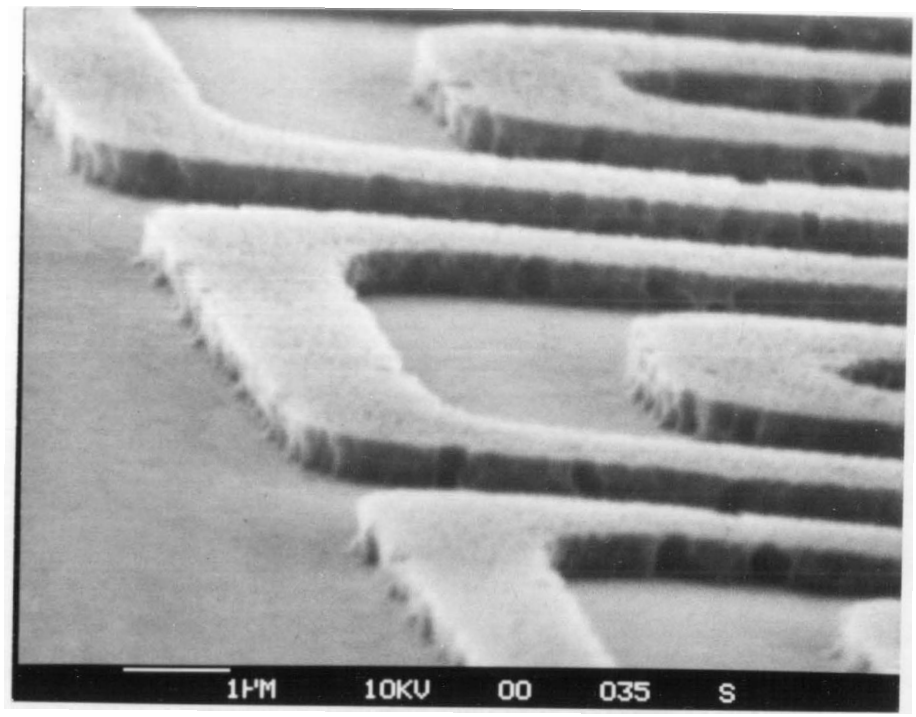

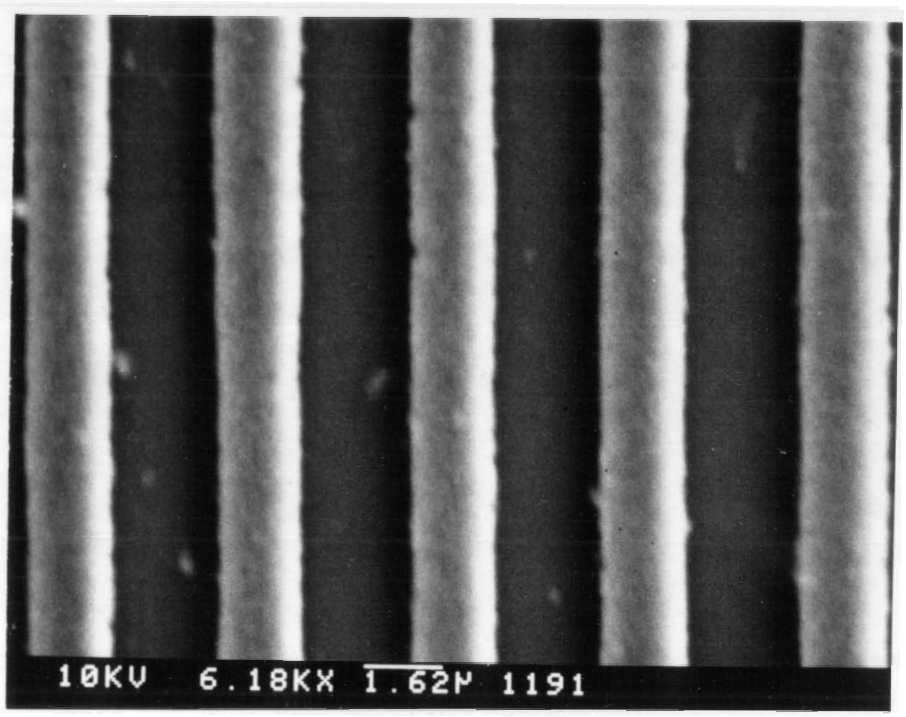

Fig. 19. Electron micrographs of a functional field source which uses aluminum wires.

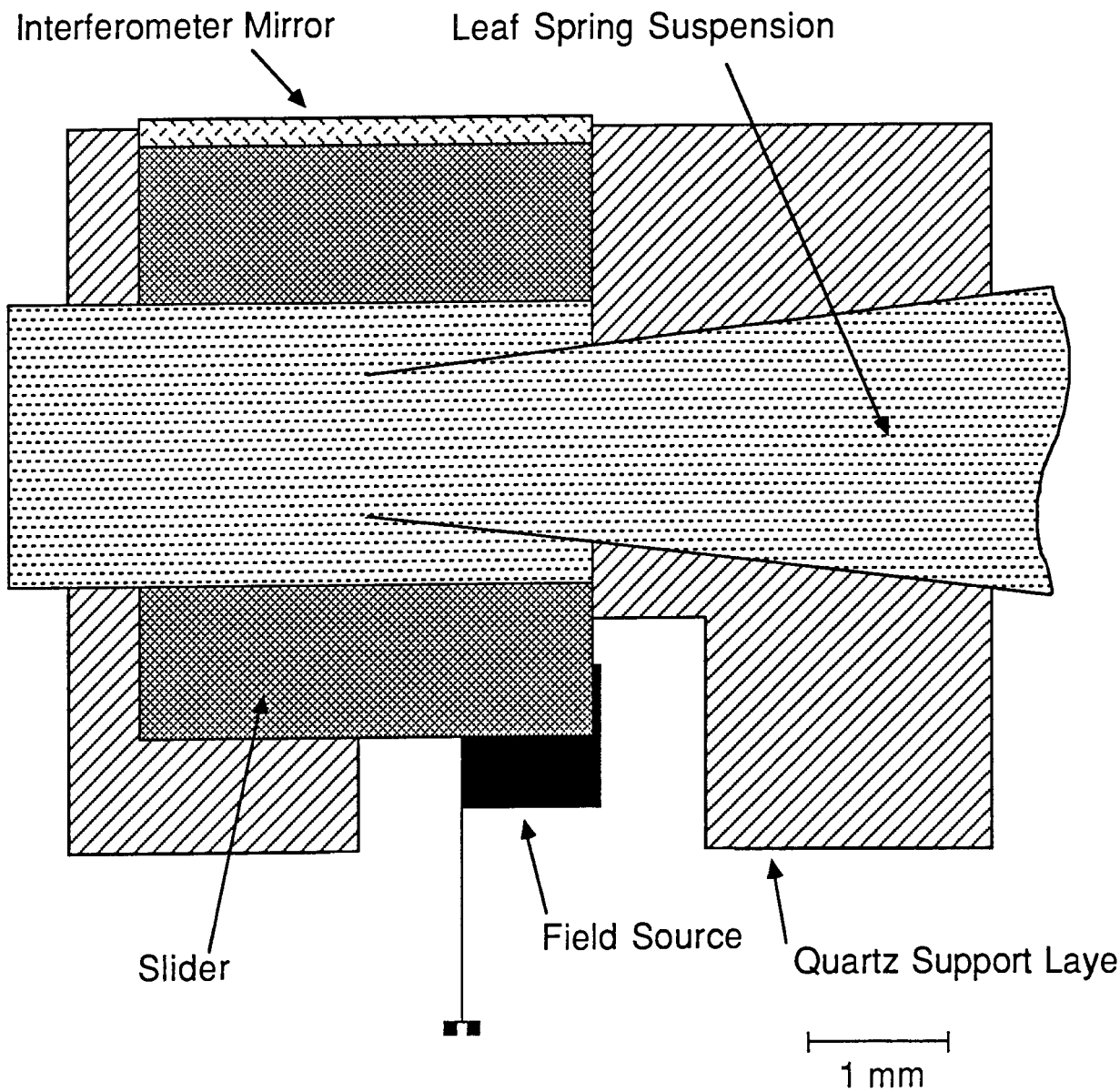

Fig. 20. Diagram showing the relative positions of the thin film head, the quartz support, and the field source.

cracks and bumps. A head slider was then rubbed on them (with and without lubrication) in order to determine their ability to withstand abrasion. Materials which were tried and rejected include molybdenum, chromium, nickel, and alumina. quartz was the only material which could be used to form a film with the desired properties. This could partly be due to the fact that the substrate itself was thermally grown quartz. One expects that a given material will adhere very well to an identical substrate.

Questions pertaining to the uniformity of thin films can be answered using a variety of optical and mechanical methods. The silicon wafers which come from the factory are already polished to optical standards of flatness. If the evaporated films are some transparent dielectric, such as alumina or silica, nonuniformities can be detected by noting the interference pattern formed between the film and its substrate. In most of the quartz films, a uniform color was normally observed over virtually the entire area, except in regions near the boundaries. This means that deviations in the thickness of the film could be no more than about 0.1 μm from an average value of about 0.6 μm. A variety of mechanical surface profilers are available to measure the topography of thin films. Measurements made by one such instrument (a Tencor surface profiler) confirmed the optical results.

A very important consideration, from the point of view of conducting experiments on heads, is whether the slider can be placed in close proximity to the SiO_2 supporting film. It is possible that dust particles or surface protrusions are present which might prevent the head from coming into uniform contact with the quartz. To test this, a 0.5 μm layer of quartz was evaporated through the tantalum mask onto a glass plate. The quartz deposit was lubricated with a very fine oil (more about this later), and a clean head was brought into contact with it. The interface between the head and the quartz layer was viewed in white light and light from a mercury lamp in order to observe interference fringes. In order to bring the head against the quartz, one edge of the slider was brought down first, and then rotated so as to bring the other edge down. interference bands could be seen only as the oil was squeezed out of the interface, or if the head was moved off the end of the quartz deposit (so that a wedge could be formed). Otherwise, no variations in light intensity could be observed. This result indicates that any gap between the head and the quartz was no more than about 1000 Å.

This experiment does not indicate that a larger gap will not be present if an experiment is performed with a real source. It does indicate, however, that the creation of a narrow and reproducible gap between the head and the pole tips should always be possible to achieve. There was never any difficulty, as long as the slider and quartz were clean, in bringing them into intimate contact. The only completely reliable method for making sure that the gap is small during an actual experiment is to look for reproducibility.

Another consideration which arose during the course of this work is that of how to best lubricate the interface between the slider and the quartz. Experiments were carried out in which the head was moved across the source in the positioning apparatus while interferometric measurements were made. Various lubricants were placed in the interface, and the fringe patterns were observed for evidence of non-uniform head motion. Materials which were tested include vacuum pump oil, watch oil, oleic acid, silicone oil, teflon (evaporated on the quartz), electric shaver lubricant, slidewire lubricant, and various light synthetic oils. The electric shaver lubricant (an old product provided by the Remington company) and the slidewire lubricant worked quite well. In general it was found that low viscosity fluids were better lubricants than the higher viscosity ones.

It was eventually realized, however, that since quartz is a polar structure, a lubricant composed of molecules with dipole moments might be the best substance to use. This is because such a lubricant would be expected to adhere very well to the surface of quartz, even in the form of a very thin film. A sample of a low viscosity diester oil was provided by the William F. Nye company (Nye Synthetic Oil 223), and subsequent tests confirmed this hypothesis. An interferogram taken during a run with this oil can be seen in Fig. 21. It is shown above an earlier interferogram taken with a much poorer lubricant (Silicone oil), to illustrate the importance of using the correct lubricant. In order to reduce the possibility that particles in the oil could prevent good head-source contact, a precleaned batch of the 223 oil was purchased. It had been passed through a 0.45 μm filter before leaving the factory, which removed most of the particles and slightly reduced the viscosity. The kinematic viscosity of the filtered oil at 40 C was measured at the factory, and found to be 5.22 centistokes.

Since it was essential that the head and source be very clean before they were brought together, a cleaning procedure was developed which could accomplish this without disruption of the experimental work. The best cleaning fluid for the removal of dust and oil was found to be trichlorotrifluoroethane (Freon 113). This liquid can be readily obtained in a form which is pure enough that it will not leave a residue, and it evaporates very quickly. It was usually sprayed onto the surface of the head and source to remove contamination which had accumulated since the previous run. In order to allow residual moisture and dust to be removed from the head and source, a dry nitrogen line was installed next to the apparatus. This took the form of a flexible hose with a nozzle, which allowed last minute cleaning to be done before the lubricant was applied and the source raised to the head. A 0.6 μm filter was installed in the line in order to remove particles (such as dust and pipe scale) which could otherwise contaminate the apparatus.

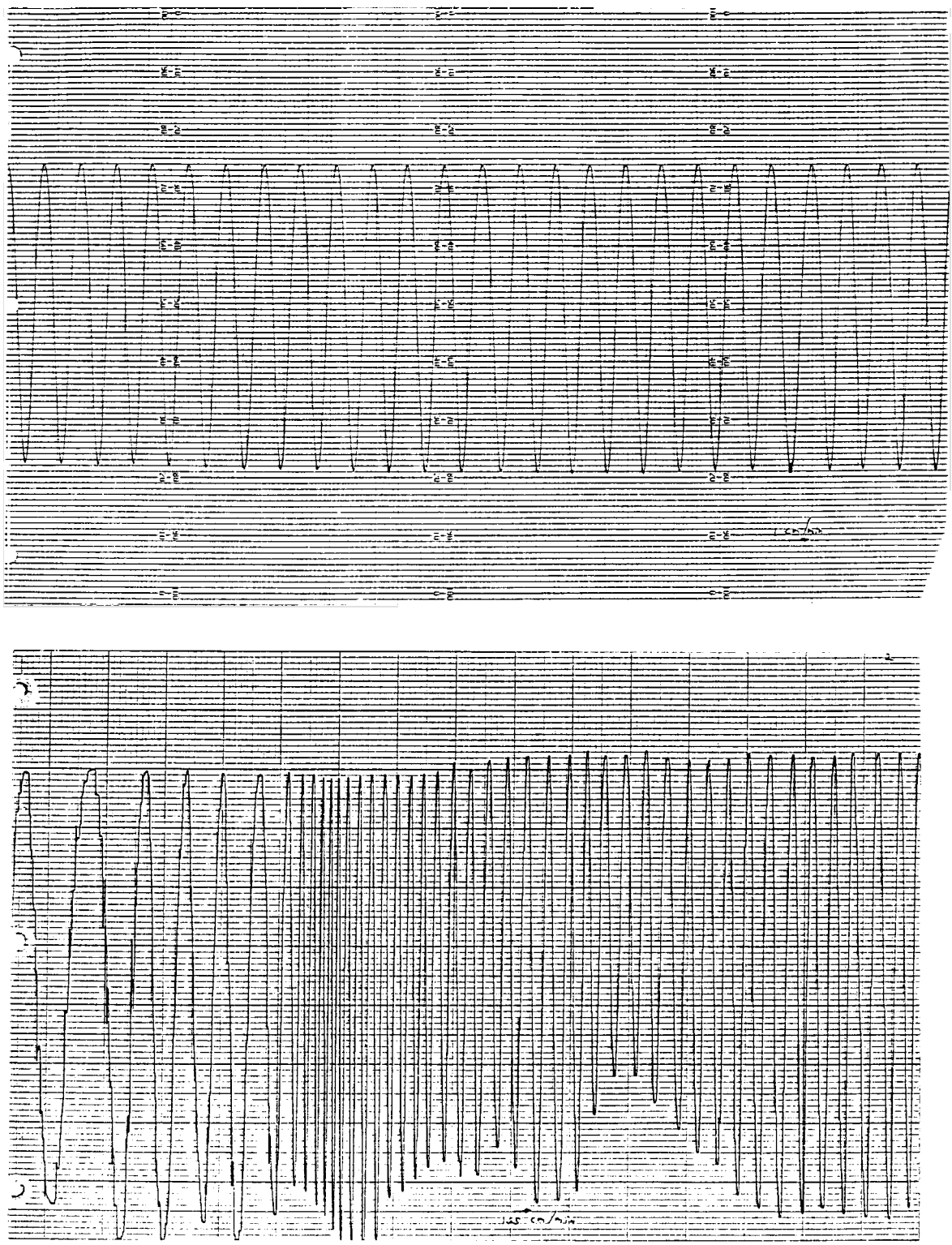

Fig. 21. Interferograms produced by a slider running on a field source lubricated by Nye Synthetic Oil 223 (top) and silicone oil (bottom). The variations in the amplitude of the lower plot are a result of polarization angle instabilities in the laser which was used when the measurement was made.

In order to connect the source wires up to an external supply of current, some means must be found to attach macroscopic wires to the bonding pads. In the microelectronics industry, connections between bonding pads and bulk wires are normally made by ultrasonic welding methods. This involves taking a small (25 μm) gold wire and pressing it against a pad with a ceramic holder. A burst of ultrasound is created on the arm attached to the holder, which vibrates the wire against the pad. This heats up the interface, breaks up oxides and surface contamination on the pad, and permits a metallic bond to form. The other end of the gold wire is then attached to a gold plated copper lead on a chip carrier. The latter is a small package which holds the silicon and provides electrical connections between the circuit and external wires.

2.3) Data Acquisition and Signal Processing

One of the purposes of this work was to explore the linearity of the head response over a wide dynamic range. To this end, it was decided that phase sensitive detection would be the best way of measuring signals from the head, especially at amplitude levels where Johnson noise starts to become important. A block diagram of the experimental setup for measurements involving spatial resolution, linearity, and frequency response is shown in Fig. 22.

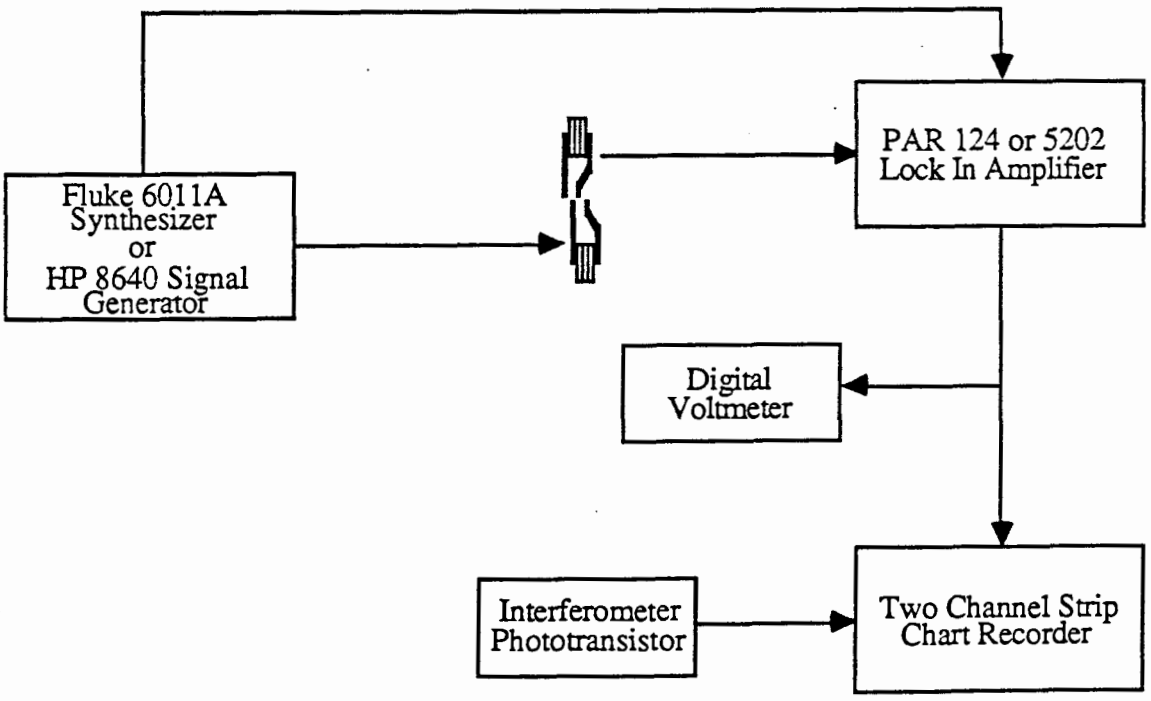

Fig. 22. The standard experimental arrangement.

The oscillator which was used to drive the field source in most experiments was a Fluke 6011A Synthesized Signal Generator. This could produce sinusoidal signals in the frequency range from 10 Hz to 11 MHz at amplitudes ranging from 0.8 mV rms to 10 V rms into an open circuit (>50 kΩ). The accuracy with which frequencies could be specified depended on the frequency. In the range from 10 Hz to 110 kHz, the resolution was 0.1 Hz, while from 110 kHz to 11 MHz, it was 10 Hz. The amplitude could be specified to 4 decimal places. A square wave signal could be obtained from this instrument which had the same frequency as the sinusoidal output, but with a constant amplitude of about 2 V. This was used as the reference signal for phase sensitive detection.

For experiments which were to be carried out at a high frequency (up to 50 MHz), a Hewlett-Packard 8640A Signal Generator was used as the signal source. Although this instrument was not provided with an accurate (digital) frequency display, it was stable (10 ppm/10 min), and the frequency could be read directly by an external counter. Similarly, although the amplitude of the signal was indicated by a comparatively crude analog display, it was stable and measurable using external instruments (such as an oscilloscope).

The choice of lock-in amplifier depended on the frequency range which was to be explored. For the range 2 Hz to 210 kHz, the PAR Model 124 was very useful. It had the capability to detect signals with amplitudes ranging from 1 nanovolt to 500 millivolts. The machine can be used with two different plug-in preamplifiers. The PAR Model 116 could be used in the frequency range 1.5 Hz to 10 kHz, if it was being operated with a built-in transformer. The transformer was necessary to provide a good impedance match between the head coils (18 ohms) and the input of the preamplifier (> 4 kilohms). The PAR Model 119 could be used in the frequency range 1 kHz to 210 kHz, under the same conditions. Both preamplifiers could accept differential inputs. This turned out to be a very useful feature, since a large common mode signal was usually present which was sometimes larger than the signal of interest. Consequently, this kind of input was used for most of the experiments. The Model 124 could also pass the signal through a bandpass filter which had an adjustable frequency and Q. This was normally used to limit noise signals which might otherwise overload the amplifiers.

For high frequency work, a PAR Model 5202 lock-In amplifier was used to detect and amplify signals from the head. It had the ability to operate in the frequency range from 100 kHz to 50 MHz at amplitude levels ranging from 100 μV to 250 mV. This machine had two disadvantages compared with the Model 124 amplifer, which made it cumbersome to use for some experiments. There was no bandpass filter with an adjustable frequency and Q, and there was no provision for the use of differential input.

If the permalloy in the head has some form of nonlinear threshold response at low amplitudes, then such a response could show up as a third harmonic of the signal applied to the field source. An arrangement for detecting these third harmonics is shown in Fig. 23. The square wave output from the frequency synthesizer was passed through the filter section of a PAR Model 124 amplifier in order to remove all components of the square wave but its third harmonic. The resulting signal was retrieved from the amplifier before passing through the phase sensitive detector, and sent to the reference input of another Model 124. The output signal from the head was sent to the input channel of the same amplifier, and signal detection proceeded in the usual way. A frequency counter (Model 1615, made by the Eldorado Electrodata Corp.) was used to ensure that the frequency of the reference signal was really the third harmonic of the fundamental.

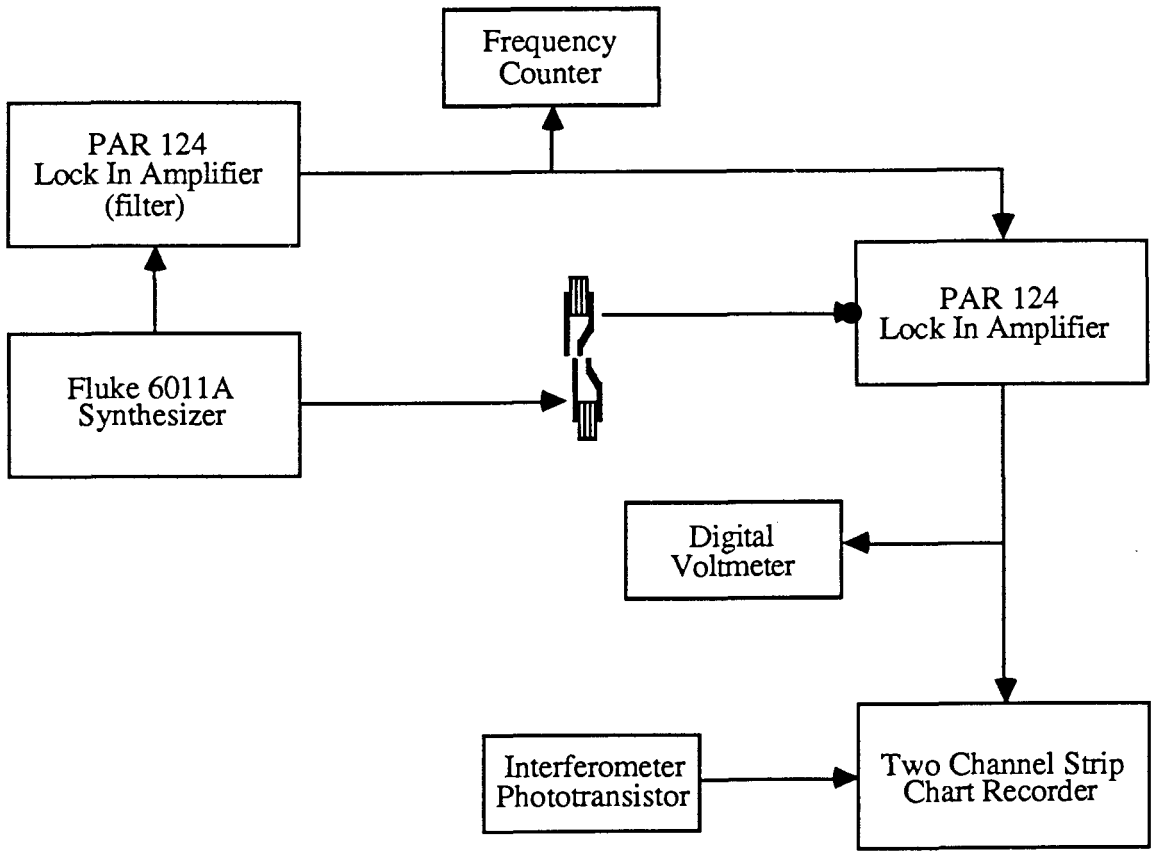

Fig. 23. The experimental arrangement used to investigate nonlinear head response.

One of the experiments consisted of monitoring the signal from the head during the application of a slowly varying magnetic field. In many cases it was necessary to carry out signal averaging while this was done. For this purpose, the arrangement shown in Fig. 24

was employed. Timing for the field sweep was provided by a Krohn-Hite 5100 function generator. This produced a triangular ramp which controlled the magnet power supply (a Kepco bipolar operational amplifier/power supply), and provided trigger signals for the signal averager. A Nicolet 1072 instrument computer accepted head signals from the lock-in amplifier and started a new averaging cycle whenever it recieved a trigger signal from the function generator. Data recorded by the signal averager could be plotted out on an x-y plotter.

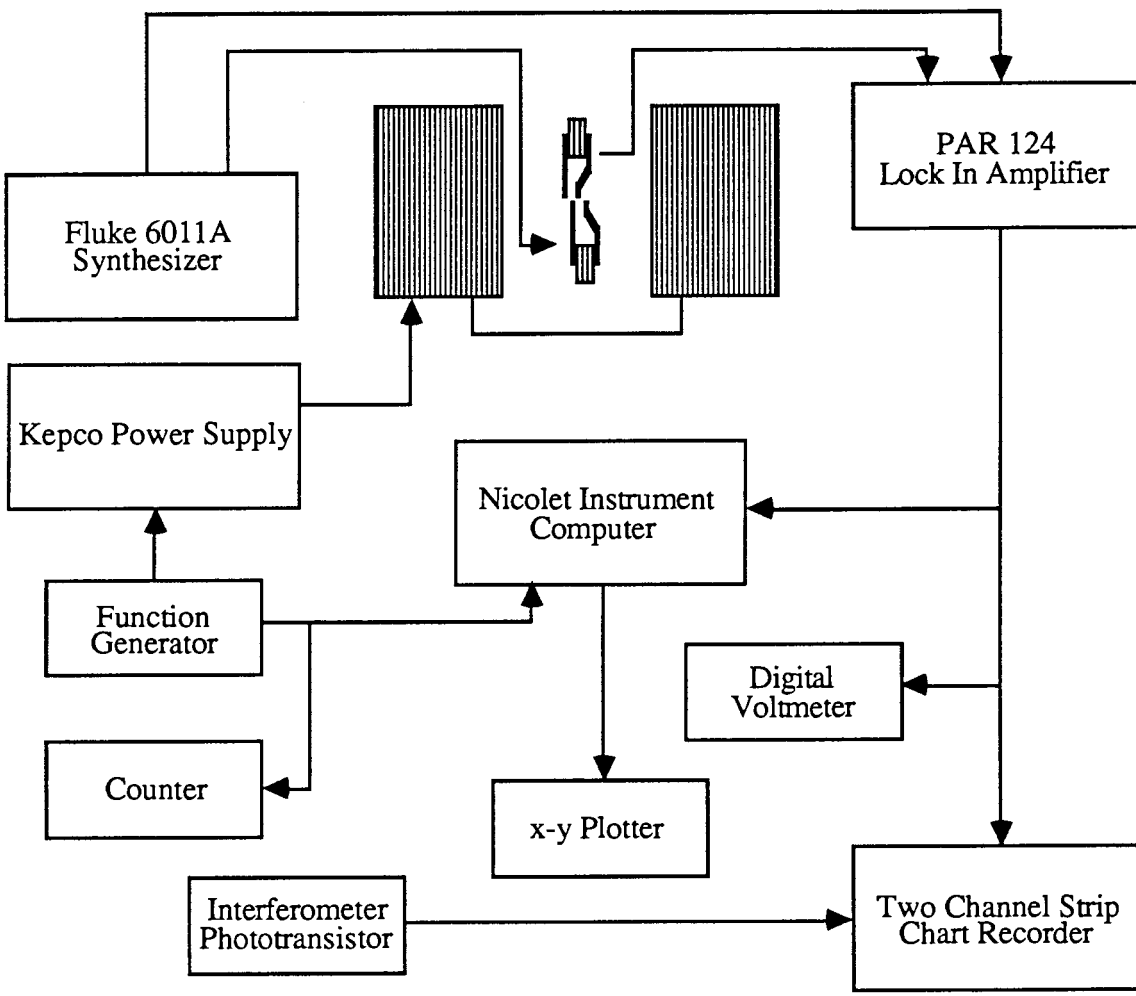

Fig. 24. The experimental arrangment used to investigate head response in the presence of uniform external magnetic fields.

The Nicolet had no system of indicating how many averaging sweeps it had done, although it could be programmed to stop after a specified number. Since it was often necessary to terminate the runs prematurely, the aforementioned frequency counter was connected to the

trigger output of the function generator and used as a pulse counter. This made it possible to find out how many sweeps had been carried out at any given time.

Chapter 3. Models and Calculations

In order to calculate the fields produced by the heads and the fine wire arrays, it was necessary to create mathematical models of these systems. It is the purpose of this chapter to show how these models were created. The results of some calculations which were carried out using the models will also be presented.

3.1) Fields from Rectangular Wires

Before proceeding with the algebra, let us state our assumptions and specify our coordinate systems. Assume that we are dealing with straight rectangular wires which have faces oriented parallel to the x-y, x-z, or y-z planes. In addition, suppose that the wires themselves are oriented parallel to either the x or the y axes. This means that current will be allowed to travel only in directions parallel to these axes. The current density will be uniform everywhere inside the wires, even at those places where the current must turn corners. There are two reasons for making the last assumption. Firstly, the total area of the regions in which the current turns corners is small compared with the total area of the other regions, so that their contribution to the total field (at positions which are far away from these corners) will be small. Secondly, determining the actual current density in the corner regions and incorporating it into the field calculations would be a difficult task.

We will make use of two sets of coordinates during the calculations. Unprimed coordinates will refer to positions in space where currents exist, while primed coordinates will refer to the positions for which fields are being calculated. It is convenient to define two angles, θ and ϕ, which allow us to relate these two positions. These angles are shown in relation to the coordinate systems in Fig. 25.

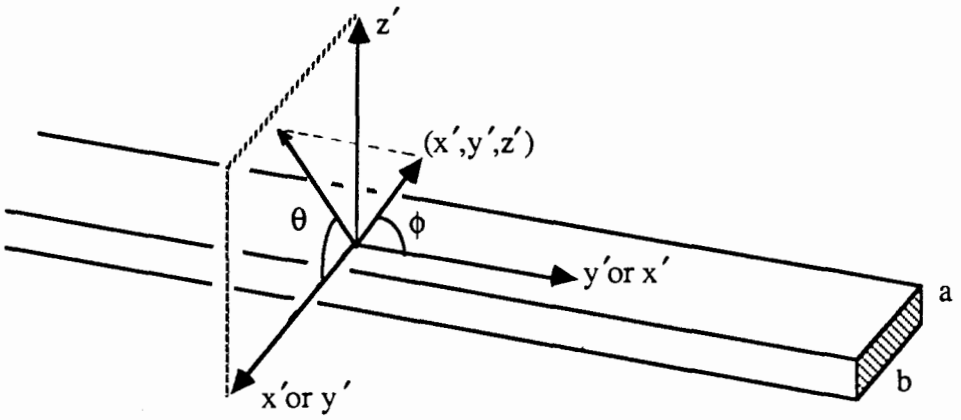

Fig. 25. Coordinate system used in the field calculations. The origin of the system is at (x,y,z).

The correct expression for calculating fields arising from currents is the Biot -Savart law. In our case, this can be expressed simply as:

$$dB = \frac{\mu_0 I \sin(\phi)\, dl\, \hat{\theta}}{4\pi r^2}$$

where dl is an element of length, and r is the distance from the source point to the field point - i.e. $r = |\mathbf{r} - \mathbf{r}'|$. Since we are really dealing with a current distributed over a conductor of finite dimensions, a more appropriate relationship is:

$$dB = \frac{\mu_0 J \sin(\phi)\, dA\, dl\, \hat{\theta}}{4\pi r^2}$$

where dA is an element of conductor cross sectional area, and J is the current density. Now consider the particular case involving the calculation of the field component oriented in the x direction.Then:

$$dB_x = \frac{\mu_0 J_y \sin(\theta)\sin(\phi)\, dA\, dl}{4\pi r^2}$$

$$= \frac{\mu_0 J_y \left[\dfrac{(z-z')}{\sqrt{(x-x')^2+(z-z')^2}}\right]\left[\dfrac{\sqrt{(x-x')^2+(z-z')^2}}{|r-r'|}\right] dx\, dy\, dz}{4\pi\,|r-r'|^2}$$

$$= \frac{\mu_0 J_y\,(z-z')\, dx\, dy\, dz}{4\pi\,|r-r'|^3}$$

Similarly, for dB_y and dB_z we will have:

$$dB_y = \frac{\mu_0 J_x\,(z-z')\, dx\, dy\, dz}{4\pi\,|r-r'|^3}$$

and:

$$dB_z = \frac{\mu_0 J_x\,(y-y')\, dx\, dy\, dz}{4\pi\,|r-r'|^3}$$

Hence, the fields at any point (x',y',z') in space are given by the following:

$$B_x\,(x',y',z') = \left(\frac{\mu_0 I_y}{4\pi ab}\right)\iiint\left\{\frac{(z-z')}{\left[(x-x')^2+(y-y')^2+(z-z')^2\right]^{3/2}}\right\} dx\, dy\, dz$$

$$B_y\,(x',y',z') = \left(\frac{\mu_0 I_x}{4\pi ab}\right)\iiint\left\{\frac{(z-z')}{\left[(x-x')^2+(y-y')^2+(z-z')^2\right]^{3/2}}\right\} dx\, dy\, dz$$

$$B_z\,(x',y',z') = \left(\frac{\mu_0 I_\zeta}{4\pi ab}\right)\iiint\left\{\frac{(\eta-\eta')}{\left[(x-x')^2+(y-y')^2+(z-z')^2\right]^{3/2}}\right\} dx\, dy\, dz$$

where (ζ,η) corresponds to (x,y) or (y,x) depending on whether the wire is oriented in the x or y direction, respectively.

While it is possible to carry out the integrals over x, y, and z numerically, the savings in computer time can be very large if at least one, or preferably two of the integrals are done in closed form. The first integral is fairly simple. If for B_z we evaluate:

$$\int \left(\frac{(x-x')}{\left((x-x')^2+(y-y')^2+(z-z')^2 \right)^{3/2}} \right) dy$$

we find:

$$\frac{(x-x')\,(y-y')}{\left((x-x')^2+(z-z')^2 \right) \sqrt{(x-x')^2+(y-y')^2+(z-z')^2}}$$

The next integral is more complicated. If the above expression is integrated with respect to z, one finds (after a little algebra):

$$\frac{i}{2} \ln \left\{ \frac{\left[(y-y')+i(z-z')\right]\sqrt{(x-x')^2+(y-y')^2+(z-z')^2}+(x-x')\left[(y-y')+i(z-z')\right]+i\left(\frac{z-z'}{x-x'}\right)\left[(y-y')^2+(z-z')^2\right]}{\left[(y-y')-i(z-z')\right]\sqrt{(x-x')^2+(y-y')^2+(z-z')^2}+(x-x')\left[(y-y')-i(z-z')\right]-i\left(\frac{z-z'}{x-x'}\right)\left[(y-y')^2+(z-z')^2\right]} \right\}$$

In the case of B_x or B_y, the result is:

$$\frac{i}{2} \ln \left\{ \frac{\left[(x-x')+i(y-y')\right]\sqrt{(x-x')^2+(y-y')^2+(z-z')^2}+(z-z')\left[(x-x')+i(y-y')\right]+i\left(\frac{y-y'}{z-z'}\right)\left[(x-x')^2+(y-y')^2\right]}{\left[(x-x')-i(y-y')\right]\sqrt{(x-x')^2+(y-y')^2+(z-z')^2}+(z-z')\left[(x-x')-i(y-y')\right]-i\left(\frac{y-y'}{z-z'}\right)\left[(x-x')^2+(y-y')^2\right]} \right\}$$

This result is the correct one for the case in which the current is flowing in the x direction. If the current is flowing in the y direction, the substitution: $(x-x') \Leftrightarrow (y-y')$ must be made. It can be demonstrated that the above expressions produce real numbers (as they must do), even though they contain imaginary parts.

It was found that the most convenient way of carrying out the last steps in the integration is to use a numerical procedure. A computer program was written which could evaluate the integrals, and sum the contributions from the various source wires for all three components of the field. This program is listed in the appendix.

Calculations were carried out to determine the fields produced by the first field source. The coordinate system which was used in these calculations is shown in Fig. 26. In addition to the assumptions stated earlier, it was assumed in this case that contributions to the total field near the thin film source wires from the bulk lead wires would be small. Hence, the calculations took into account only the fields produced by the thin film wires. The results are shown in Figs. 27-30.

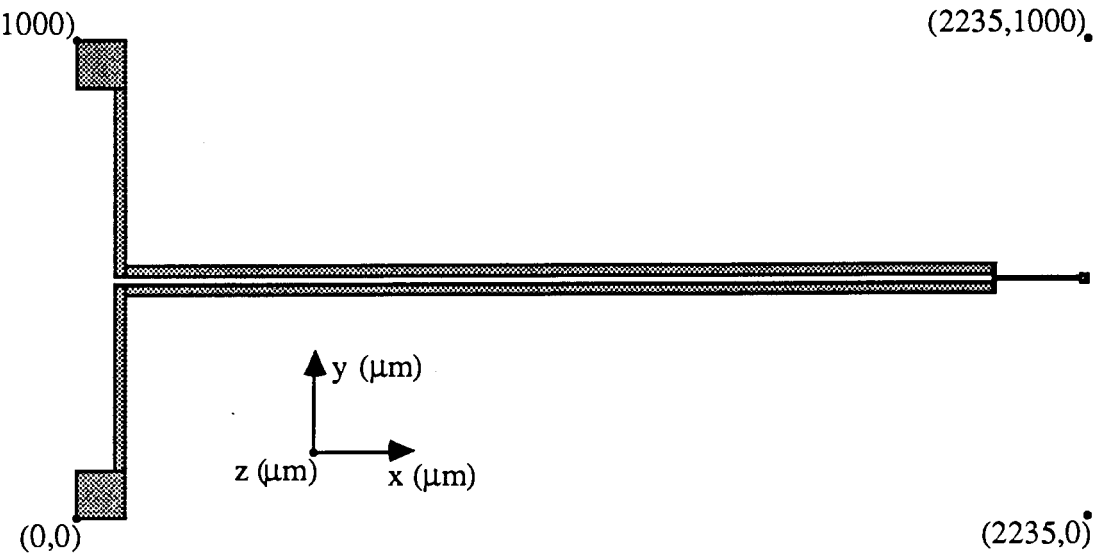

Fig. 26. Coordinate system used for calculations involving the first field source.

Since the fields appear to decay very rapidly in the neighborhood of the source wires, one would expect that if the pole tips of a thin film head were moved close enough to them, a very narrow response function would be observed. The narrowness of the calculated field functions (close to the source wires), in comparison with that of the experimentally determined response function shown in the last chapter (Fig. 16), indicates that there must have been something seriously wrong with the experimental arrangement. In particular, the result seems to show that the pole tips were nowhere near the source wires.

3.2 Fields Produced by Magnetic Discs and the Second Field Source

After calculations were carried out to determine the fields produced by the first field source, other calculations were performed in order to determine the fields produced by magnetic discs,

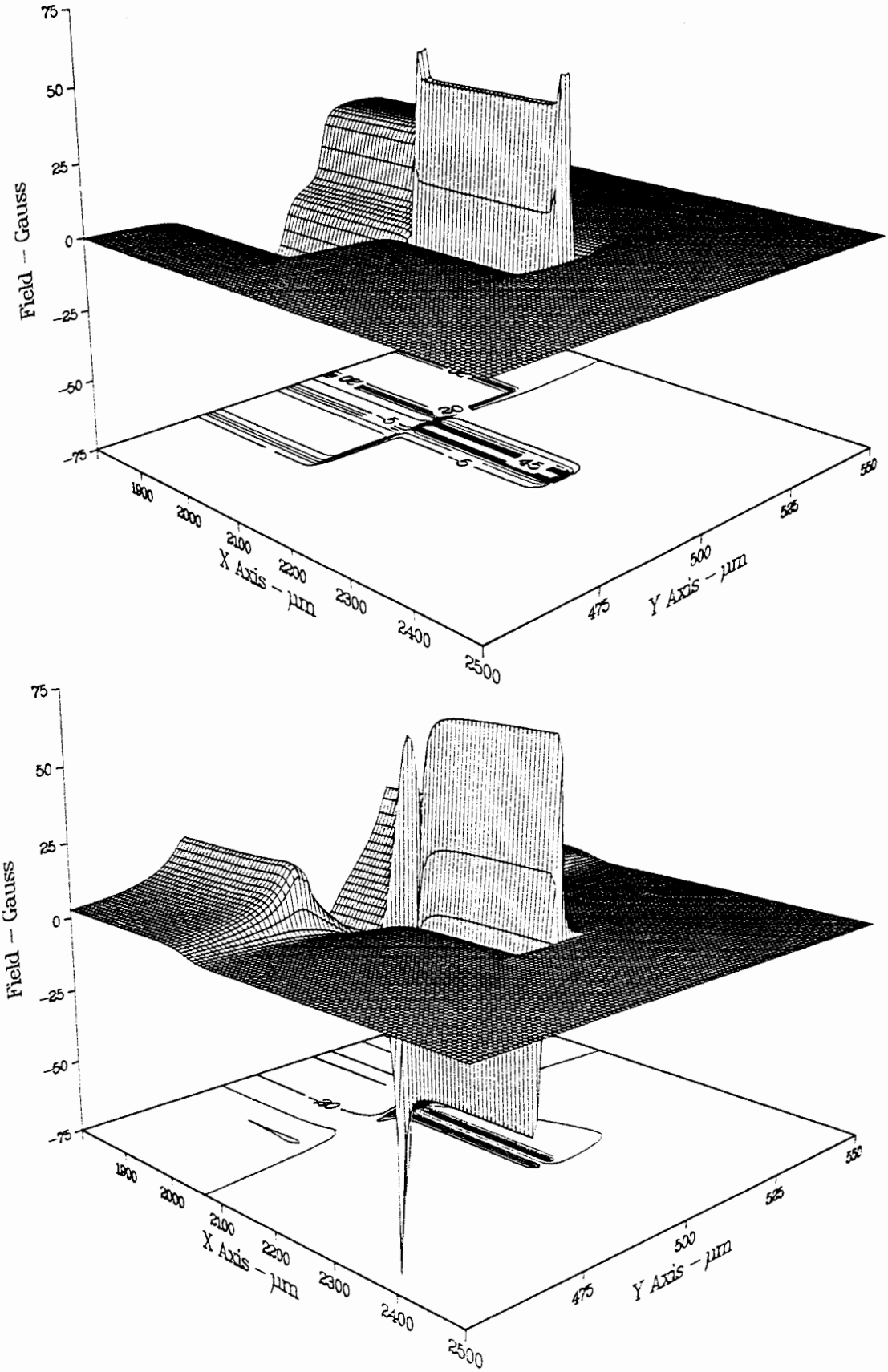

Fig. 27. Calculated values of the y field (top) and z field (bottom) 2 μm above the first field source for a 100 mA source current. The thicknesses of the upper and lower wires are assumed to be 0.64 μm and 0.68 μm respectively.

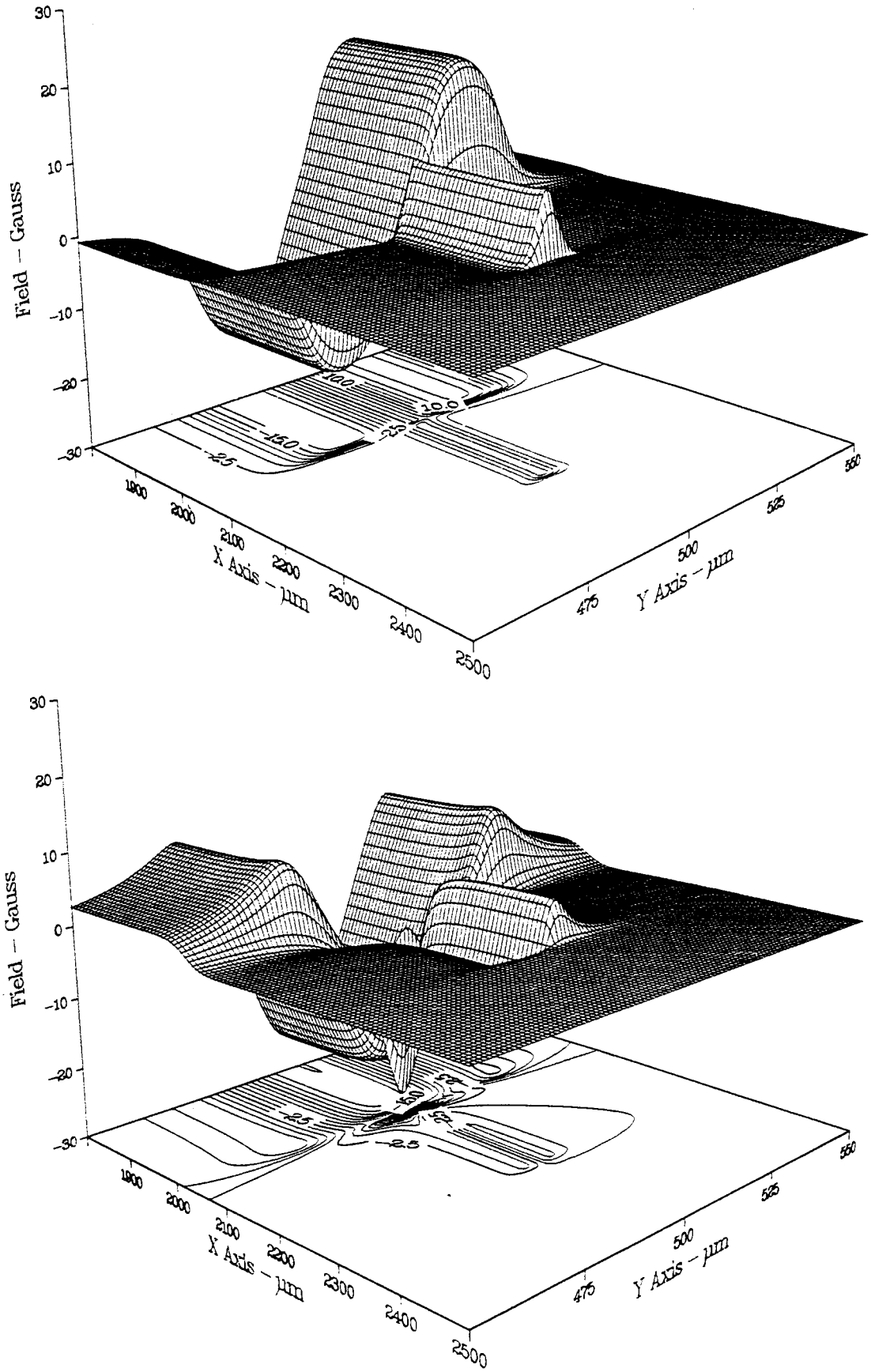

Fig. 28. Calculated values of the y field (top) and z field (bottom) 6 μm above the first field source for a 100 mA source current. The thicknesses of the upper and lower wires are assumed to be 0.64 μm and 0.68 μm respectively.

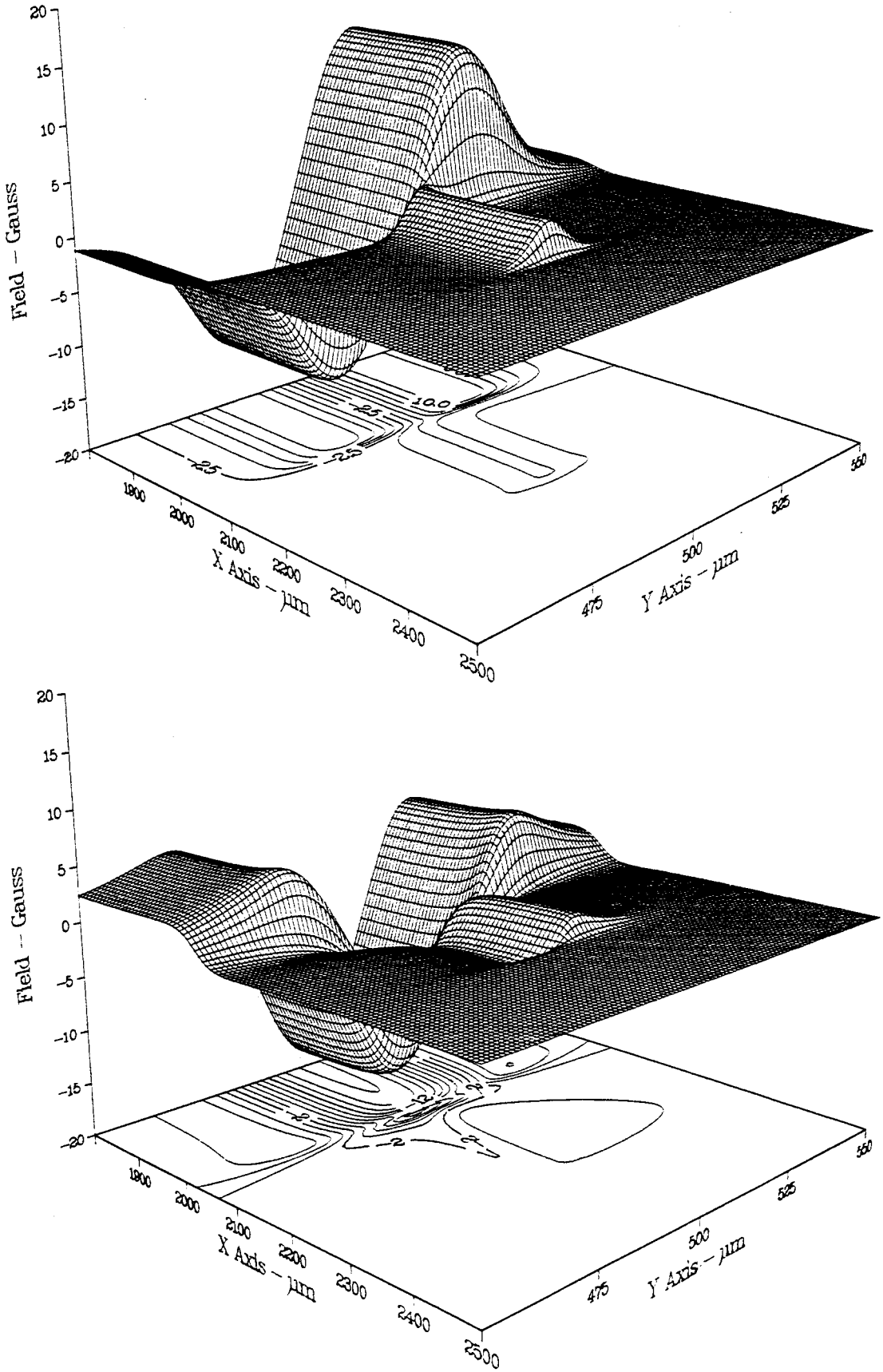

Fig. 29. Calculated values of the y field (top) and z field (bottom) 10 μm above the first field source for a 100 mA source current. The thicknesses of the upper and lower wires are assumed to be 0.64 μm and 0.68 μm respectively.

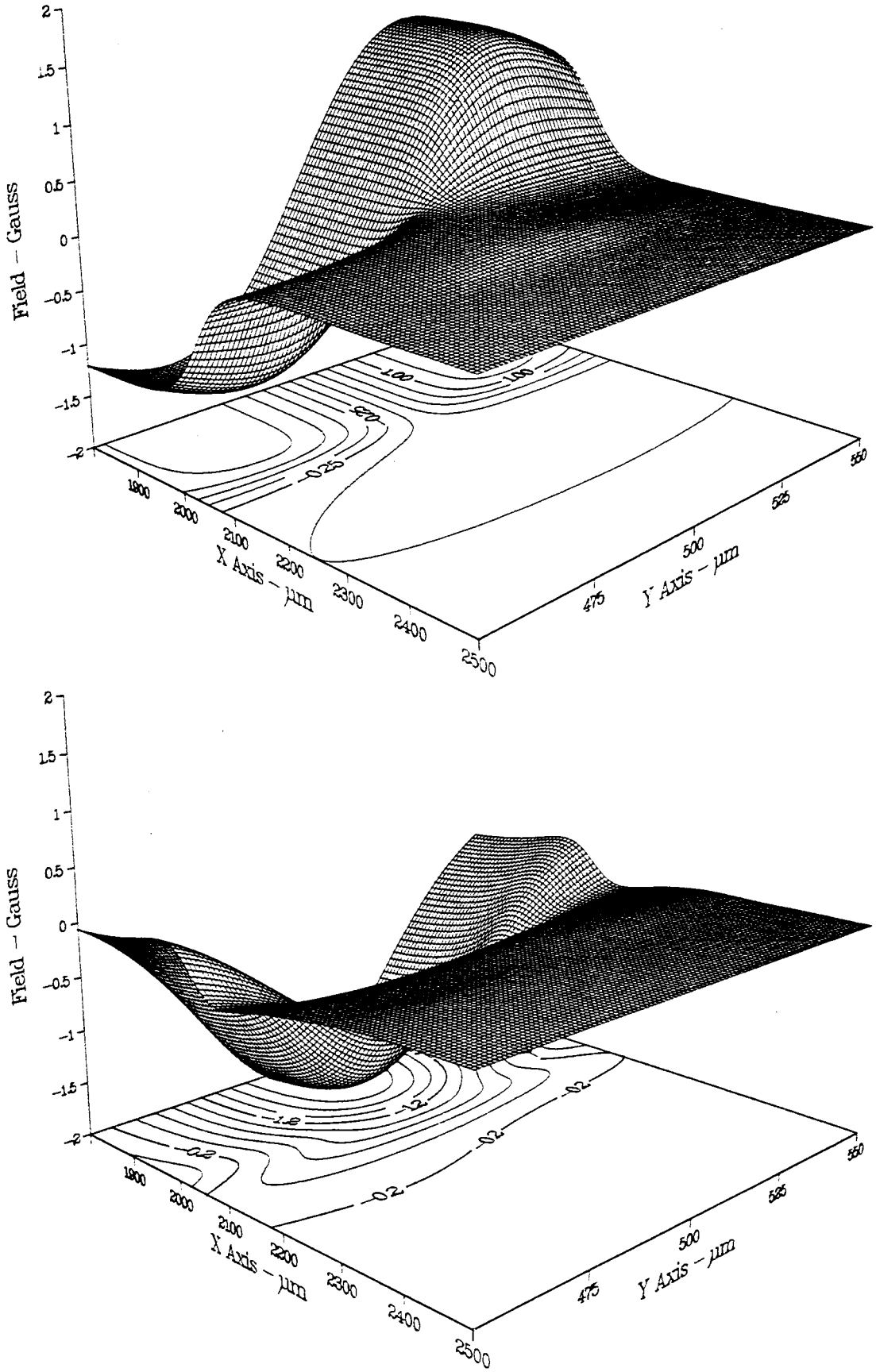

Fig. 30. Calculated values of the y field (top) and z field (bottom) 50 μm above the first field source for a 100 mA source current. The thicknesses of the upper and lower wires are assumed to be 0.64 μm and 0.68 μm respectively.

using certain simplifying assumptions about the distribution of magnetization. These calculations indicated that the fields decay very rapidly as one moves away from the surface of a disc. As a result, it was expected that only the pole tips of a head will collect flux from the magnetic structures on a disc, since the slowly varying long range fields will be too small to have any effect on other parts of the head. Consequently, there was some concern about the possibility that thin film heads could not be used to detect isolated magnetic structures. Later experimental results negated these fears; it appears that short range fields are not responsible for the ability of thin film heads to detect small structures on magnetic discs.

In order to calculate the disc fields, it is desirable to have a model disc which is simple enough to permit us to carry out closed form calculations. Hence, let us consider the surface of an infinitely large disc, which has been divided up into tracks. Assume that we are interested in a region of the disc which is so far away from the center that the domains point only along directions parallel to a given axis (the x axis). For the purpose of simplicity, we will make the assumption that successive bits which have been recorded on a given track will alternate in sense. We will further suppose that adjacent tracks will alternate, so that bits which are side by side on two different tracks will have opposite senses. The model disc has the magnetic appearance of a two dimensional antiferromagnet:

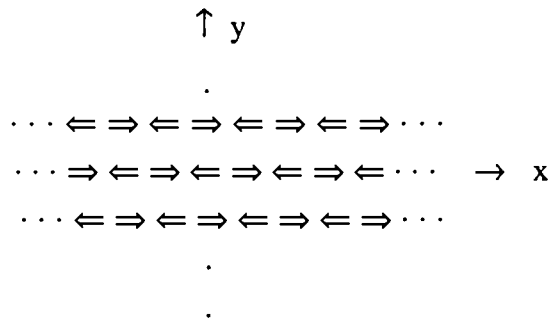

In reality, of course, the patterns recorded on magnetic discs do not have this appearance. However, this should be a good approximation for small regions of an actual disc.

Now suppose that there exists above the surface of the disc a magnetic scalar potential $\phi(x,y,z)$ which results from the charges produced by these magnetization patterns. Assume that this potential has a form which looks something like: $\phi(x,y,z) = \phi_0 \sin(ax) \sin(by) f(z)$. This potential must satisfy Poisson's equation, so:

$$\phi_{xx}+\phi_{yy}+\phi_{zz} = -\phi_0 \left[a^2 \sin(ax) \sin(by) f(z) + b^2 \sin(ax) \sin(by) f(z) + \sin(ax) \sin(by) f''(z)\right] = 0$$

Hence:

$$0 = -\phi_0 \sin(ax) \sin(by) [(a^2 + b^2) f(z) - f''(z)]$$

$$\Rightarrow \quad f''(z) - (a^2 + b^2) f(z) = 0$$

$$\Rightarrow \quad f(z) = \exp(-\sqrt{a^2+b^2}\, z)$$

$$\therefore \quad \phi(x,y,z) = \phi_0 \sin(ax) \sin(by) \exp(-\sqrt{a^2+b^2}\, z)$$

(The other solution, involving a positive exponent, is physically unrealistic.)

If a different form of $\phi(x,y)$ were needed to match the potential in the plane of the disc, a suitable solution could be constructed using a Fourier series. Regardless of its final form, $\phi(x,y,z)$ must have some kind of exponential z dependence.

Given this result for the scalar potential, the magnetic field must have the form:

$$\begin{aligned} \mathbf{B}(x,y,z) &= -\nabla\phi \\ &= -\phi_0 \exp(-\sqrt{a^2+b^2}\, z) [a\, \phi_0 \cos(ax) \sin(by)\ \hat{x} \\ &\qquad + b\, \phi_0 \sin(ax) \cos(by)\ \hat{y} \\ &\qquad - \sqrt{a^2+b^2}\, \phi_0 \sin(ax) \sin(by)\ \hat{z}] \end{aligned}$$

The fields produced by the model magnetic disc are apparently of short range, with a decay length equal to the diagonal distance between adjacent domains. In a real magnetic disc, only small collections of recorded bits will have the necessary antiferromagnetic character required to produce this behaviour. Consequently, it is to be expected that stray fields from the domains will fall off rapidly (according to an exponential law) near the surface of the disc, and more slowly (according to some power law) at larger distances. This conclusion is not a good one from the point of view of applying thin film heads to the study of micomagnetics, since it seems to indicate that heads may not necessarily have to resolve isolated magnetic structures in order to retrieve recorded information. Fortunately, experimental results later showed that heads are able to resolve isolated structures, so short range fields are not necessary for their operation.

The results of the magnetic disc calculations suggested a field source structure which appeared to be well suited to the investigation of head efficiency. This would consist of a grating of fine wires, in which adjacent wires carry currents in opposite directions. The fields thus produced could be expected to decay exponentially in a direction perpendicular to the plane containing the wires, with a characteristic decay length set by the periodicity of the array. Such a field source would have two advantages over the simpler ones which had been used previously. Firstly, no signal can be detected by the head unless it is within a few characteristic lengths of the wires. Consequently, the existence of a signal by itself indicates whether the head is resting properly against the field source. Secondly, since the far fields of the source have a negligible

strength, magnetic flux which has not been intercepted by the pole tips will not contribute to the total signal detected by the head. This makes it somewhat easier to make comparisons between experimentally determined efficiencies and theoretically determined ones.

In order to determine the fields which would be produced by this source (which is described in detail in the last chapter), use was made of the same computer program which had been developed for the earlier one. A few modifications were made to the program to take advantage of the periodicity of the wires in the new source. In addition, stray fields produced by wires near the bonding pads have been ignored. The coordinate system used in the calculations is shown in Fig. 31. The program itself is listed in the appendix.

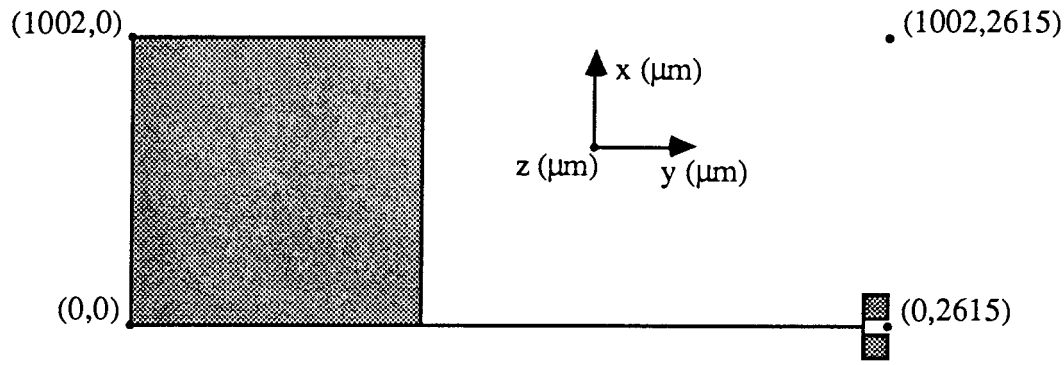

Fig. 31. Coordinate system used for calculations involving the second field source.

The results of field calculations for this source are shown in Figs. 32,33.

In order to determine the efficiency of a head, it was necessary to calculate how much flux an ideal head could be expected to pick up as it passed over the field source. In the calculation it was assumed that only the part of the source field which was intercepted by the bottom of the pole tips would contribute to the total flux.The following expression was used:

$$\Phi_{total} = \frac{1}{2}\left(\int_{pole\ 1} B_z \cdot dS - \int_{pole\ 2} B_z \cdot dS \right)$$

What this means is that only the difference in the flux entering the two pole tips contributes to the total flux passing through the detection coils. Clearly, if equal amounts of flux enter each pole tip in the same direction, the total flux passing through the permalloy circuit will be zero. The factor of 1/2 ensures that the same flux is not counted twice. The calculations were done on a computer using a program which is listed in the appendix. The results are shown in Fig. 34.

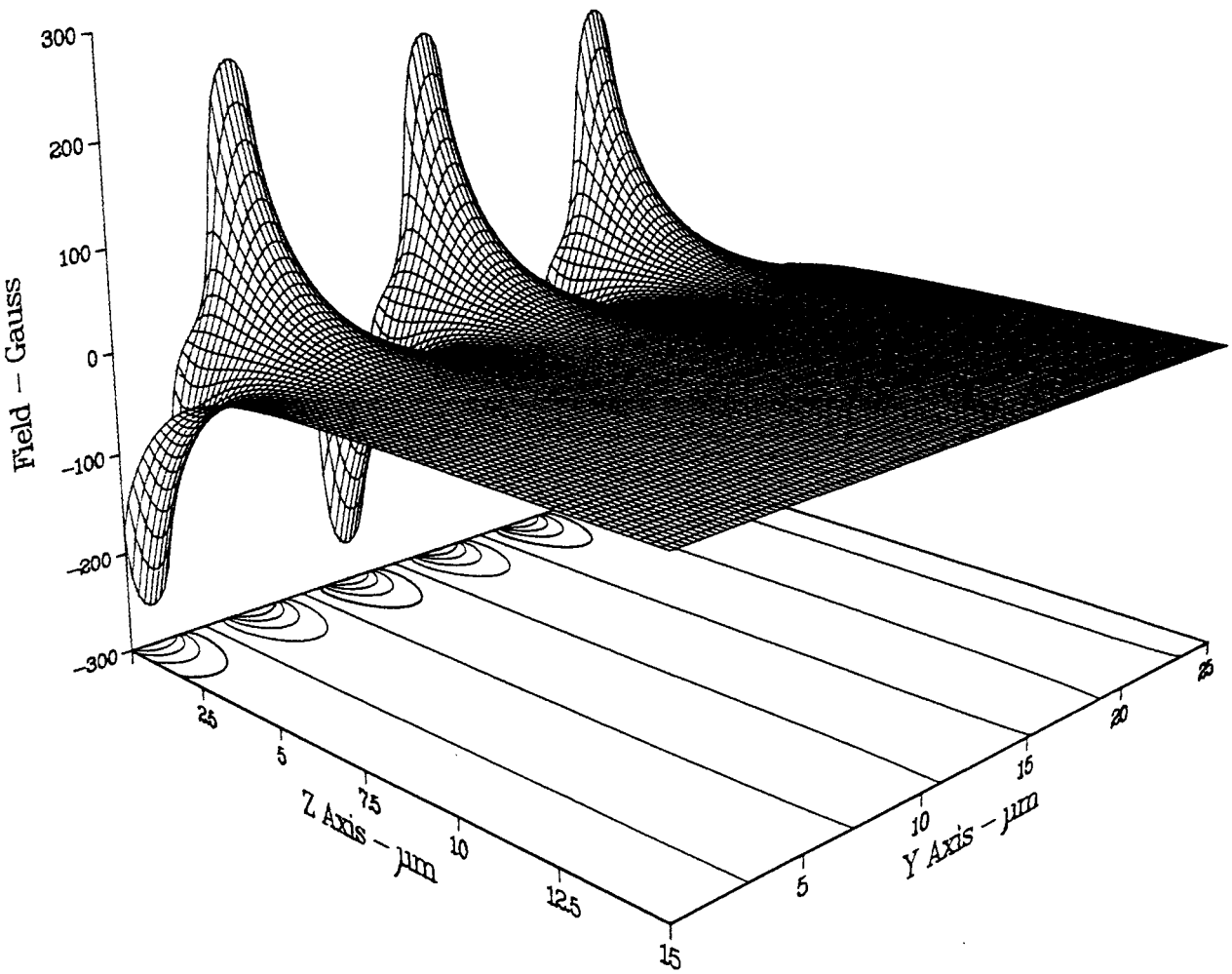

g. 32. Calculated values of the y field above the second field source for a 100 mA source current. The ckness of the wires is assumed to be 0.3 μm. One must add 760.3 μm to the y axis values in order to obtain e correct y coordinates (with respect to the coordinate system shown in Fig. 31). The z axis begins at a sition 0.1 μm above the source wires.

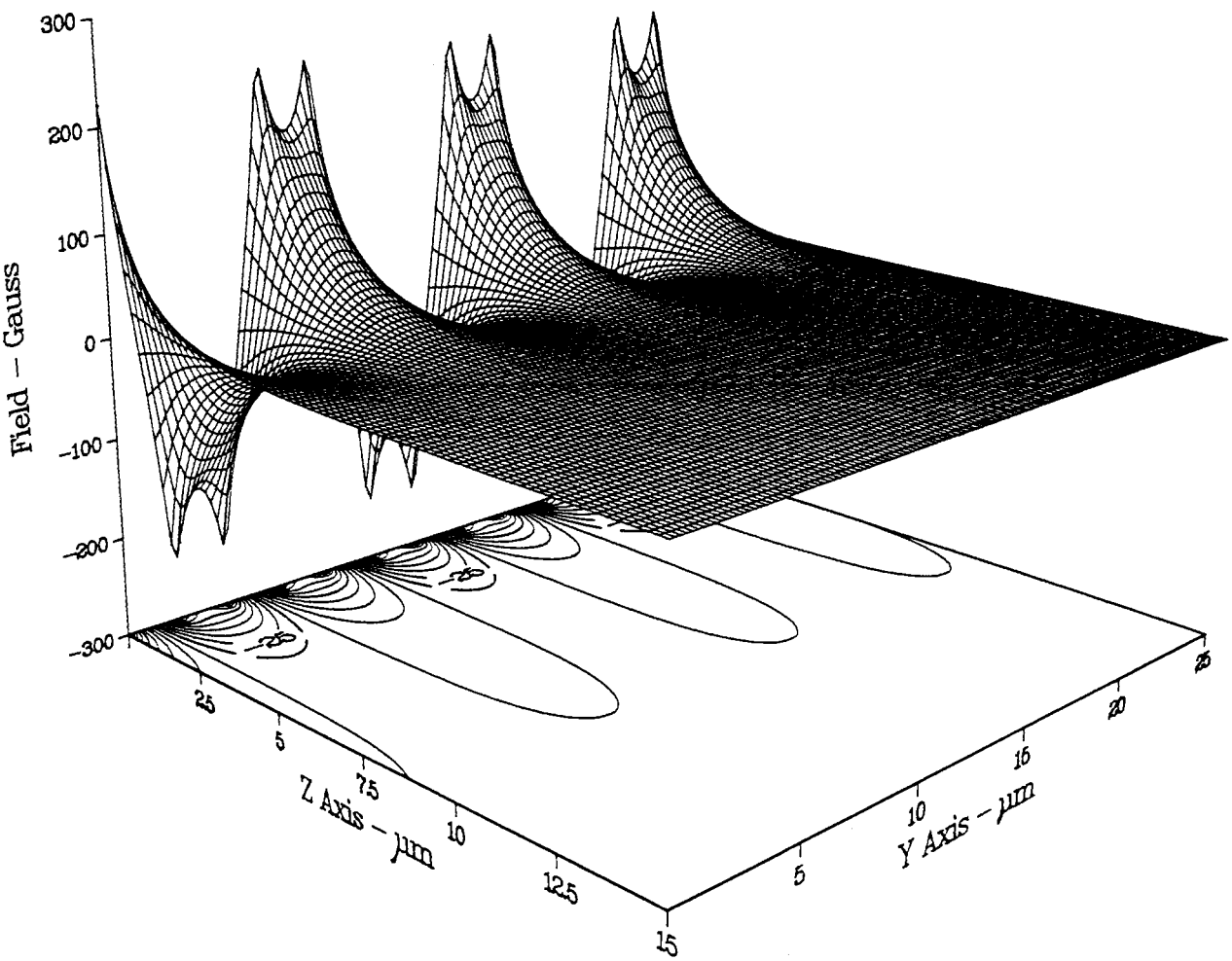

Fig. 33. Calculated values of the z field above the second field source for a 100 mA source current. The thickness of the wires is assumed to be 0.3 μm. One must add 760.3 μm to the y axis values in order to obtain the correct y coordinates (with respect to the coordinate system shown in Fig. 31). The z axis begins at a position 0.1 μm above the source wires.

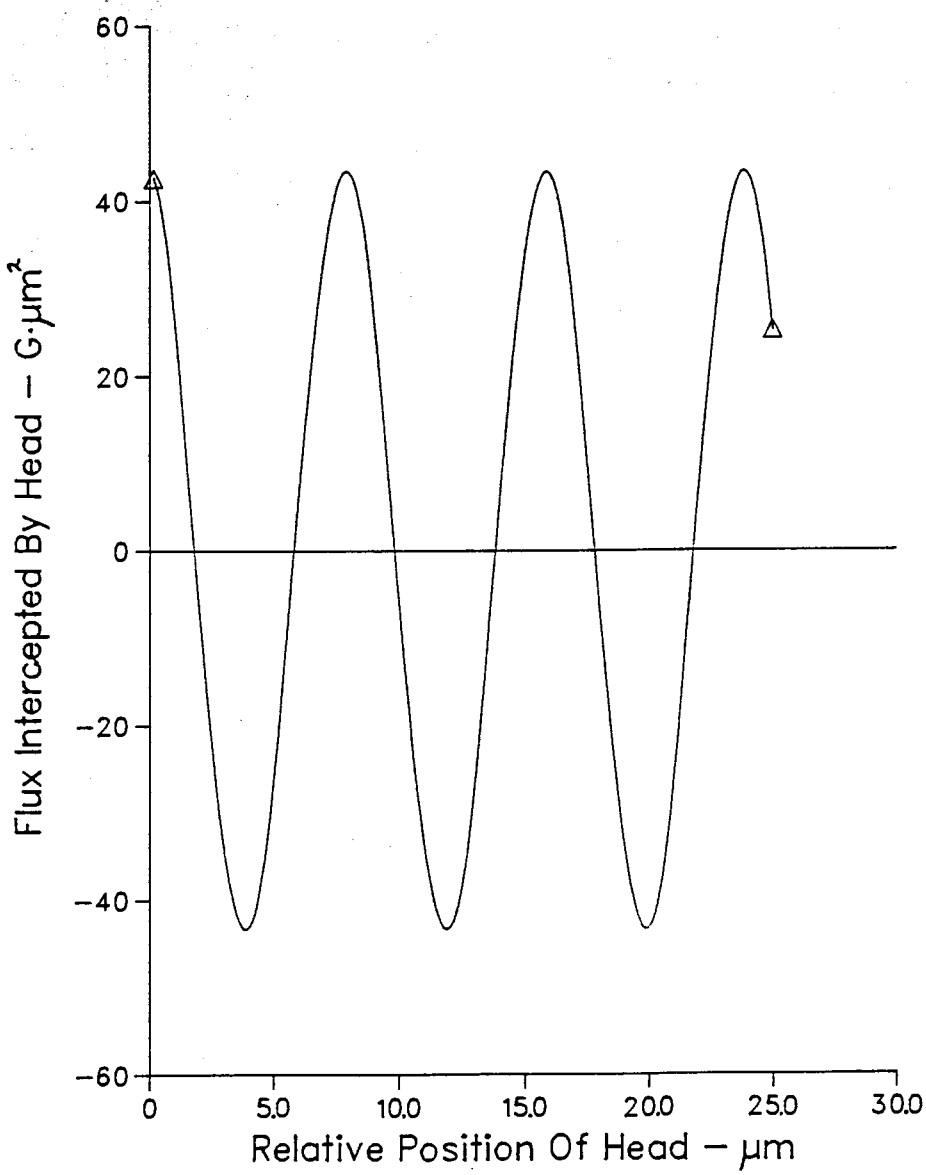

Fig. 34. Calculated values of the flux intercepted by a head for a 1.06 mm head to source distance and a 1.63 mA source current. It is assumed that the head and source dimensions have the values listed in the table in chapter 4, section 4.5.

3.3) Fields from Thin Film Heads

An approximate two dimensional model for the fringe field of a head with pole tips of equal and finite width has been developed by Potter[34]. He postulated a scalar potential in the plane of the pole tips based on some conformal mapping calculations, and used this potential to determine the field in a direction parallel to this plane - the direction of motion of the head. The field component perpendicular to the plane of the pole tips was not calculated. However, a model of this component was needed in the present work to determine the amount of flux which would be intercepted by one head as it passed over another. Also, the pole tips in both the IBM and the Cybernex heads are of unequal thickness. Consequently, in order to make use of Potter's analytic result, it was necessary to generalize the potential to include cases where the pole tips are of unequal thickness. This potential was then used to calculate the field components.

We will make use of the following coordinate system:

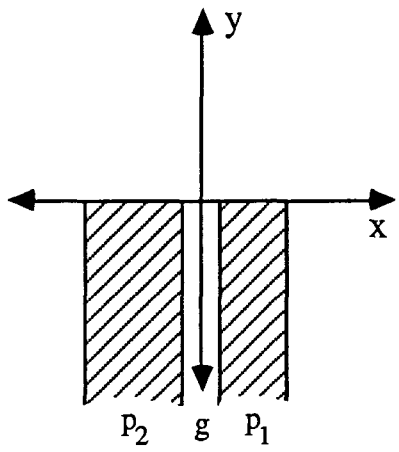

Fig. 35. Coordinate system used for the calculation of fields produced by thin film heads.

Assume that the potential has the following form along the line y = 0:

$$\phi(x,0) = \frac{I}{4}\left(1-\frac{g+2p_2}{2x}\right) \quad \text{for } x \le -\left(\frac{g}{2}+p_2\right)$$

$$= \frac{I}{2} \quad \text{for } -\left(\frac{g}{2}+p_2\right) \le x \le -\frac{g}{2}$$

$$= \frac{-Ix}{g} \quad \text{for } \frac{-g}{2} \le x \le \frac{g}{2}$$

$$= \frac{-I}{2} \quad \text{for } \frac{g}{2} \le x \le \frac{g}{2}+p_1$$

$$= \frac{-I}{4}\left(1+\frac{g+2p_1}{2x}\right) \quad \text{for } x \ge \frac{g}{2}+p_1$$

Now, using the Green's function:

$$G(x,y,x',y') = \ln\left(\frac{(x-x')^2+(y-y')^2}{(x-x')^2+(y-y')^2}\right)$$

we can obtain an expression for the potential everywhere in the x-y plane[35]:

$$\phi(x,y) = \frac{-1}{4\pi}\int_{-\infty}^{\infty}\phi(x,0)\frac{\partial G(x,y,x',0)}{\partial y'}dx'$$

But:

$$\frac{\partial G}{\partial y'} = \frac{-4y}{(x-x')^2+(y-y')^2}$$

For $y' = 0$ this becomes:

$$\frac{\partial G}{\partial y'} = \frac{-4y}{y^2+(x-x')^2}$$

So, upon integrating:

$$\phi = \frac{I}{16\pi g\,(x^2+y^2)}\left\{ gy\,(2p_1+g)\,\ln\left[\frac{(2p_1+g)^2}{4\left(x-p_1-\frac{g}{2}\right)^2+4y^2}\right]\right.$$

$$+\,gy\,(2p_2+g)\,\ln\left[\frac{(2p_2+g)^2}{4\left(x+p_2+\frac{g}{2}\right)^2+4y^2}\right]+8y\,(x^2+y^2)\,\ln\left[\frac{\left(x+\frac{g}{2}\right)^2+y^2}{\left(x-\frac{g}{2}\right)^2+y^2}\right]$$

$$+2g\left[x\,(2x-2p_1-g)+2y^2\right]\operatorname{atan}\left(\frac{2x-2p_1-g}{2y}\right)+2g\left[x\,(2x+2p_2+g)+2y^2\right]\operatorname{atan}\left(\frac{2x+2p_2+g}{2y}\right)$$

$$+\,8\left[x\,(2x^2-gx+2y^2)-gy^2\right]\operatorname{atan}\left(\frac{2x-g}{2y}\right)-8\left[x\,(2x^2+gx+2y^2)+gy^2\right]\operatorname{atan}\left(\frac{2x+g}{2y}\right)$$

$$\left.-2\pi gx\,(p_1+p_2+g)\right\}$$

Now, since $H_x(x,y) = \frac{-\partial\phi}{\partial x}$, we find:

$$H_x = \frac{-I}{8\pi g\left(x^2+y^2\right)^2}\left\{ gxy\,(2p_2+g)\,\ln\left[\frac{(2p_2+g)^2}{4\left(x+p_2+\frac{g}{2}\right)^2+4y^2}\right]\right.$$

$$\left.-gxy\,(2p_1+g)\,\ln\left[\frac{(2p_1+g)^2}{4\left(x-p_1-\frac{g}{2}\right)^2+4y^2}\right]+8\left(x^2+y^2\right)^2\left[\operatorname{atan}\left(\frac{2x-g}{2y}\right)-\operatorname{atan}\left(\frac{2x+g}{2y}\right)\right]\right.$$

$$+ g\,(x^2-y^2)\left[(2p_1+g)\,\mathrm{atan}\left(\frac{2x-2p_1-g}{2y}\right) - (2p_2+g)\,\mathrm{atan}\left(\frac{2x+2p_2+g}{2y}\right)\right]$$

$$+gx^2\left[4y + \pi\,(p_1+p_2+g)\right] + gy^2\left[4y - \pi(p_1+p_2+g)\right]\Bigg\}$$

And, since $H_y(x,y) = \frac{-\partial\phi}{\partial y}$:

$$H_y = \frac{-I}{16\pi g\left(x^2+y^2\right)^2}\Bigg\{ g\,(2p_2+g)\,(x^2-y^2)\ln\left[\frac{4\left(x+p_2+\frac{g}{2}\right)^2 + 4y^2}{(2p_2+g)^2}\right]$$

$$+ g\,(2p_1+g)\,(y^2-x^2)\ln\left[\frac{4\left(x-p_1-\frac{g}{2}\right)^2 + 4y^2}{(2p_1+g)^2}\right] + 8\left(x^2+y^2\right)^2\ln\left[\frac{\left(x+\frac{g}{2}\right)^2 + y^2}{\left(x-\frac{g}{2}\right)^2 + y^2}\right]$$

$$+ 4xyg\left[(2p_1+g)\,\mathrm{atan}\left(\frac{x-p_1-\frac{g}{2}}{y}\right) - (2p_2+g)\,\mathrm{atan}\left(\frac{x+p_2+\frac{g}{2}}{y}\right)\right] - 4xg\left[2(x^2+y^2) - \pi y(p_1+p_2+g)\right]\Bigg\}$$

Plots of H_x and H_y calculated using these expressions are shown in Figs. 36 and 37.

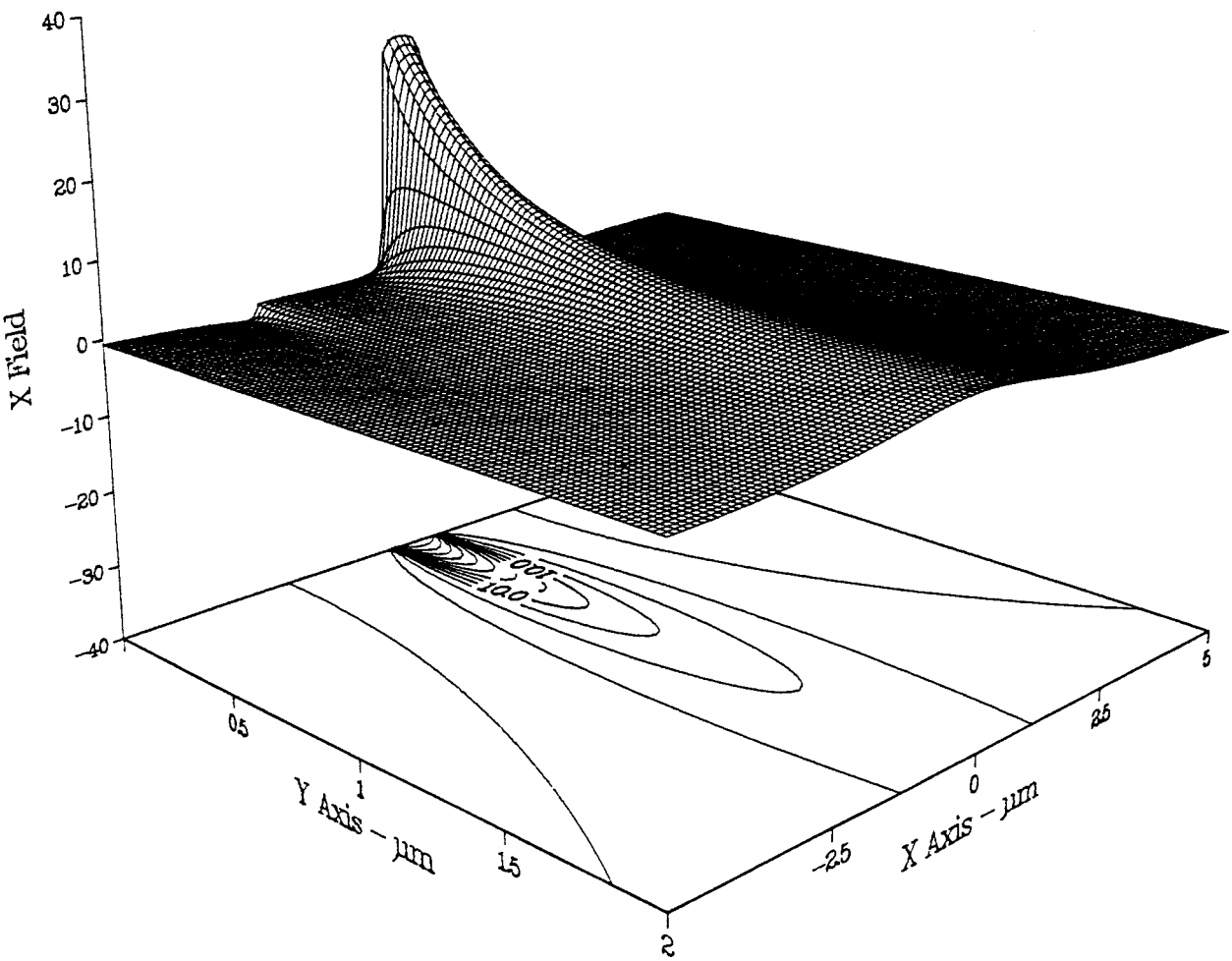

Fig. 36. Calculated values of the x field produced by a thin film head. Multiplying these values by (500·NI) = 12 gives the correct field (in Gauss) for a Cybernex head with a 1 mA excitation current. It is assumed that p_1 = 1.75 µm, p_2 = 2.2 µm and g = 0.75 µm in this calculation.

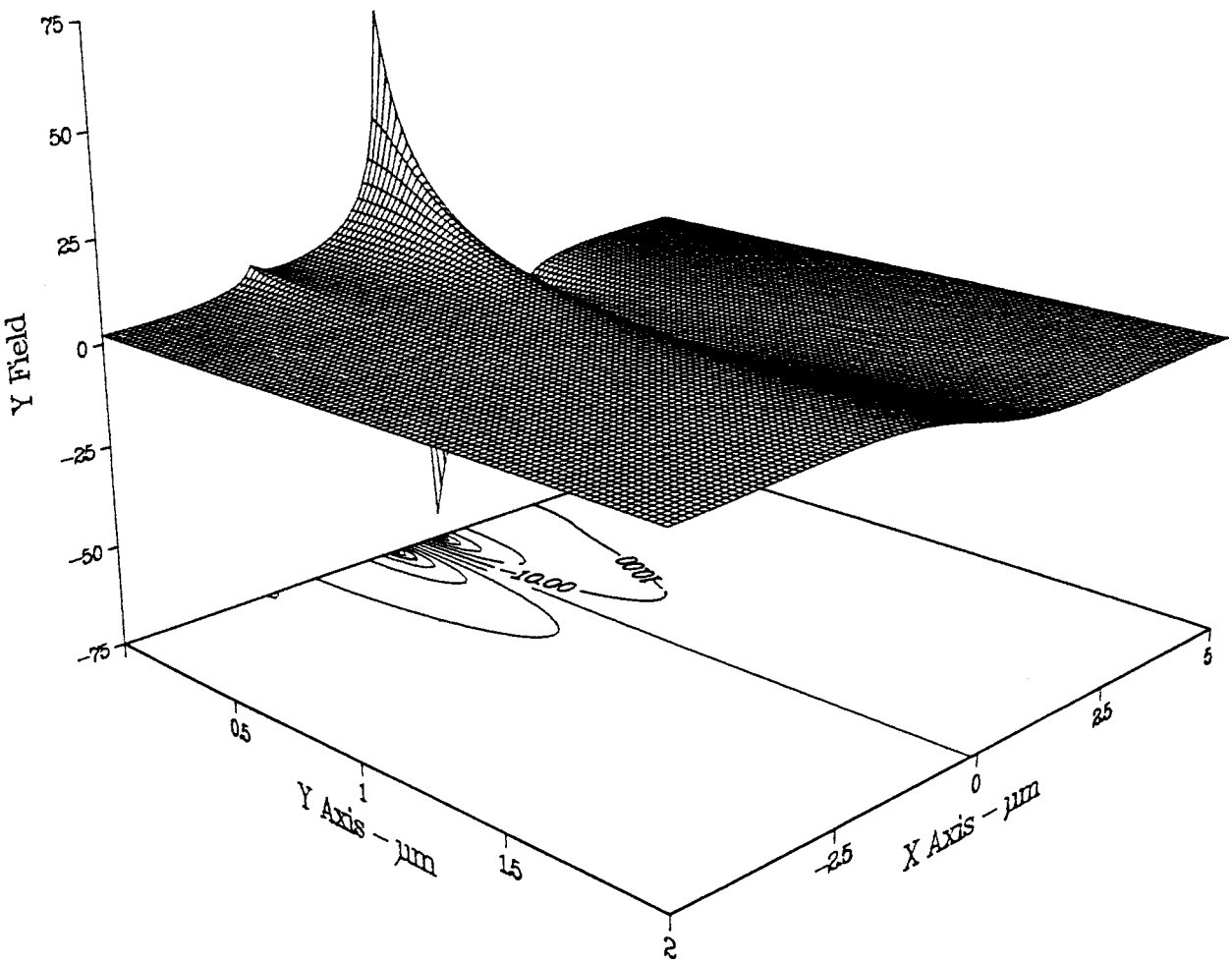

Fig. 37. Calculated values of the y field produced by a thin film head. Multiplying these values by (250·NI) = 6 gives the correct field (in Gauss) for a Cybernex head with a 1 mA excitation current. It is assumed that p_1 = 1.75 µm, p_2 = 2.2 µm and g = 0.75 µm in this calculation.

Chapter 4. Results and Discussion

The following chapter is divided into several sections, each of which will discuss (and attempt to answer) a question which arose during the course of the research. They are: 1) The spatial resolution of the head, 2) Nonlinearities of the head response at zero applied field, 3) Frequency dependence of the amplitude and phase response, 4) Effects caused by external applied fields, 5) The efficiency of the head, 6) Using the head as a probe of other systems.

4.1) Spatial Resolution of the Head

The first question which presented itself was that of whether or not the head could do what we expected it to do. In other words, we have a magnetic sensing device which has characteristic dimensions measured in microns. Can this device be made to detect magnetic field variations which have a similar scale? Common sense tells us that it should be possible, since the heads are designed with this purpose in mind. On the other hand, previous investigations have not produced measurements with spatial resolutions of the expected order. Is this due to imperfections in the apparatus, the experimental procedure, the head, or all three?

Experiments were performed in which heads (made by IBM and Cybernex) were inverted and supplied with an ac signal, while other heads of the same variety were moved overtop. Before carrying out a measurement, the head sliders were aligned under an optical microscope. Further alignment was then accomplished by optimizing the signals produced by the lock-in amplifier. Examples of signals produced by these runs, with their accompanying interferograms, are shown in Fig. 38. Note that the head travel distance represented by the peak to peak spacing in the interferograms is 0.3164 μm.

The fact that the features in the data, especially in the case of the IBM heads, are not symmetrical (as one might expect them to be) requires a word of explanation. It was never possible to align the sliders so that they were running perfectly parallel to one another. As a result, the amount of flux coupled between the two pole tips during the first drop in the signal level and the second will not necessarily be the same.

In order to determine whether the data which was recorded is really the data one expects to see (on the basis of simple notions about the characteristics of heads), a few calculations were carried out. These calculations were based on the analytic model of thin film head fields developed in the last chapter, and the reciprocity theorem[36]. According to the reciprocity theorem, the flux induced in a head is the convolution of the normalized field function of that

Fig. 38. Signals produced as two heads (one generating a field which the other detects) pass across each other. The upper and lower plots respectively represent the signals produced by IBM 3380E heads and Cybernex ones. In the case of the IBM heads, an EMF of 300 mVRMS at a frequency of 50 kHz was applied to the lower head. In the case of the Cybernex heads, an EMF of 50 mVRMS at a frequency of 10 KHz was applied to the lower head.

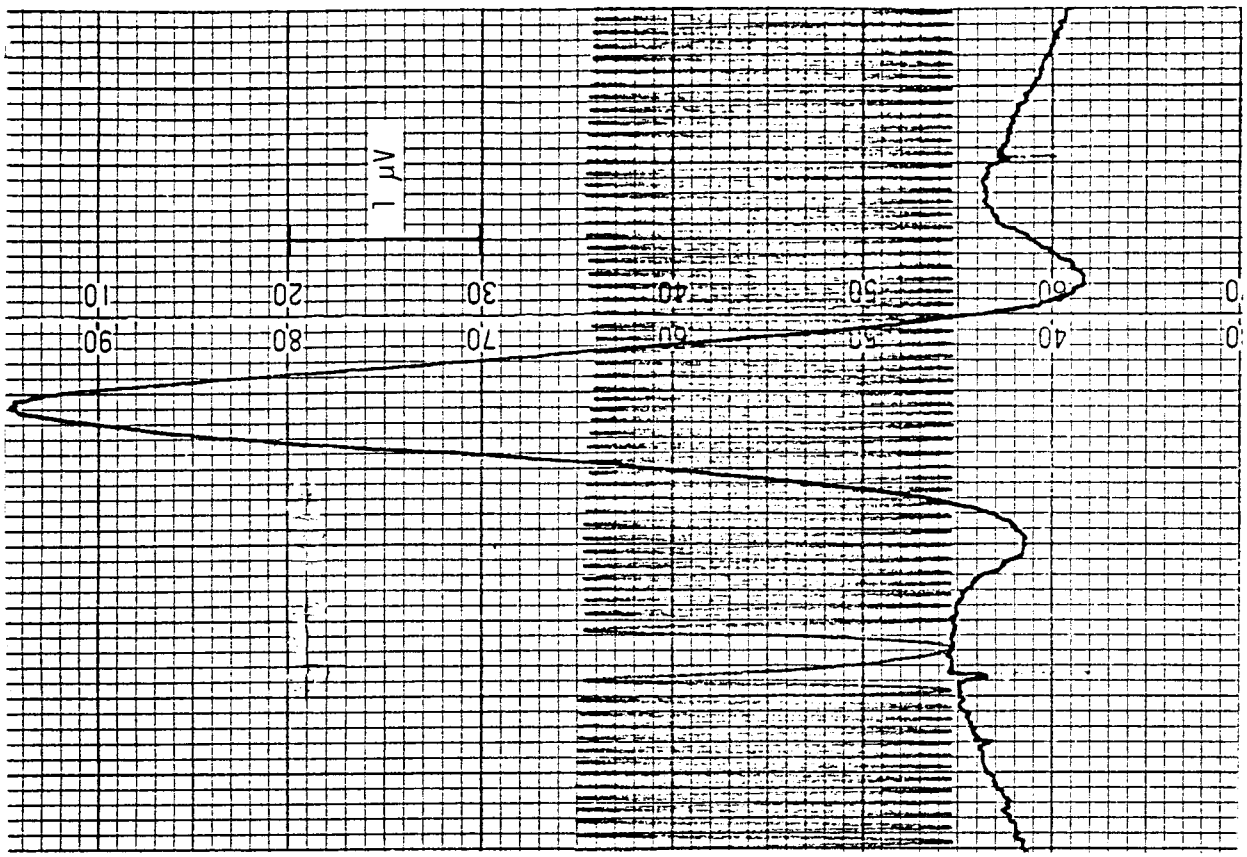
1 μV

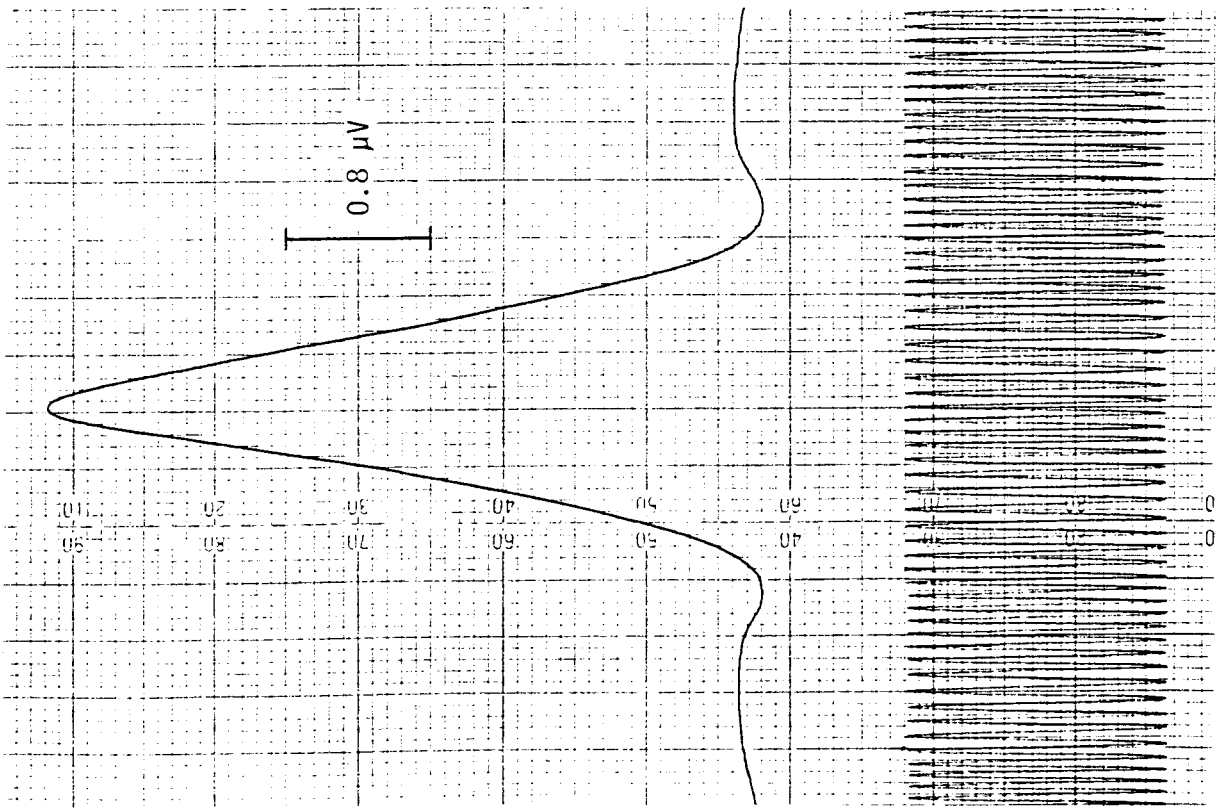
0.8 μV

head with the magnetization of the medium which is producing the flux (which, in this case is just another head):

$$\Phi(\mathbf{r}) = \frac{-4\pi}{gH_g} \int_V \mathbf{H}_1(\mathbf{r}) \cdot \mathbf{M}(\mathbf{r}-\mathbf{r}') \, d^3\mathbf{r}'$$

In this case the region of integration is just the space external to the head receiving the flux. To carry out the calculation, we make the assumption that the magnetization in the pole tips of the head producing the flux is constant and oriented in the same direction as the pole tips. We also assume that the magnetization is normalized in such a way that flux is conserved. In other words, the magnetization in one of the pole tips is adjusted so that it produces just as much flux as the other tip, regardless of the relative size of the other tip. It should be remarked that these assumptions do not make full use of the power of the reciprocity theorem, since we could have postulated more complicated (and realistic) forms for the magnetization. Incorporating such elaborations into the analysis will be left to future investigation.

In order to compare a calculation such as this with an experimental result, it was necessary to add a background flux to the field produced by the pole tips. This took into account the fact that other parts of the heads exchanged some small and slowly varying flux. A detailed model of these sources would have been complicated, and not very illuminating. Consequently, the background flux was represented by a simple peaked function: a quadratic. The asymmetry appearing in the data in Fig. 38 was not included in the model.

The comparison between model and data took the form of a least squares curve fit. This made it possible to extract such information as the distance between the heads and the magnetization of the permalloy in the pole tips from the data. To perform the least squares minimization, the program MINUIT was employed. The subroutine used to generate χ^2 for MINUIT is listed in the appendix.

The data which was fitted is the same data presented in Fig. 38 for the Cybernex head. The data is displayed again with the fitted curve in Fig. 39, along with the parameters resulting from the least squares minimization. Notice in particular the value of B, the thickness of the gap separating the two heads. It appears to agree fairly closely with the interference measurements of head to substrate spacing. In both cases, the value of B was on the order of 1000 Å. Notice also that the value of the upper limit of integration T has not been allowed to vary in the minimization (see the appendix, section 6.5). This is because the value of T used in the minimization is, roughly, the position at which the actual thin film head starts to look substantially different from the model head. In addition, it turns out that χ^2 is very insensitive to variations of T about this value.

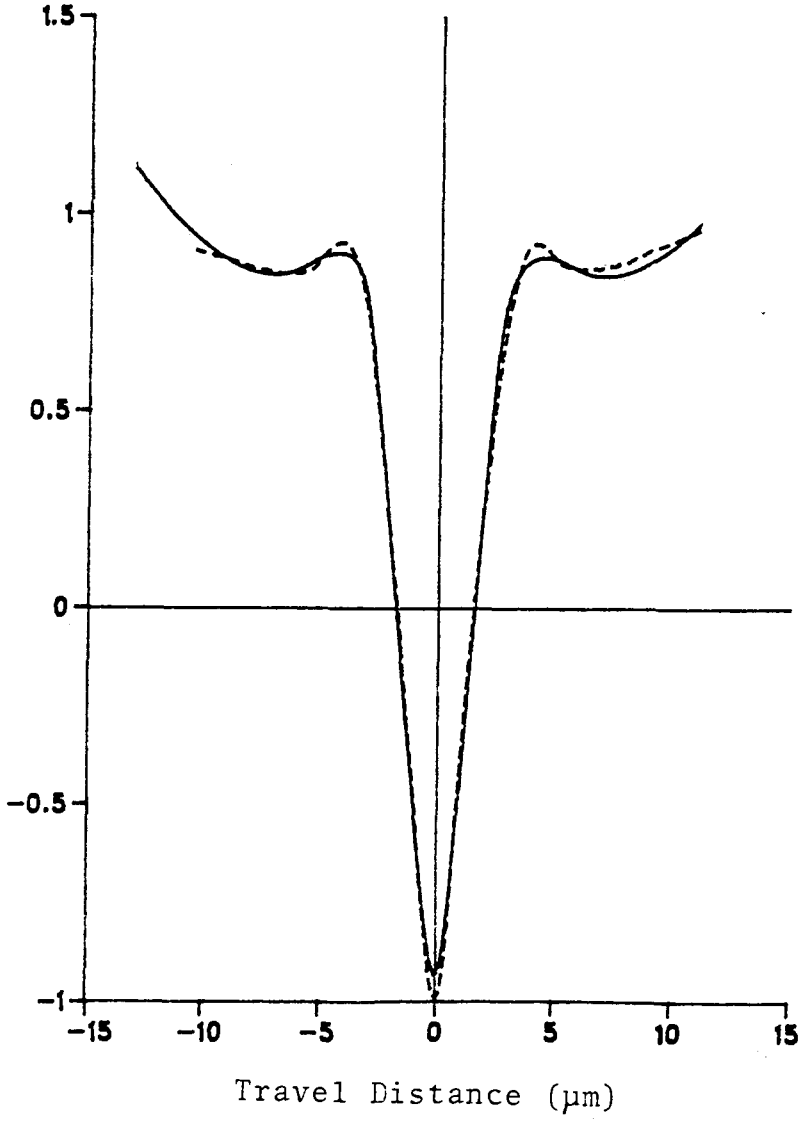

Fig. 39. A digitized version of the Cybernex head data shown in plot (a) of Fig. 38. (dashed line) plotted with the fitted curve (solid line). Some of the parameters produced by the least squares minimization are as follows: head-to head spacing = 0.29 mm (the actual value was probably somewhat less than this, about 0.1 mm), p_1 = 3.0 mm (actual value: 1.7 mm), p_2 = 2.6 mm (actual value: 2.8 mm), g = 0.15 mm (actual value: 0.7 mm). For the sake of simplicity, the parameters used for the lower and upper heads were the same. It was thought that this would be a reasonable simplification since, in reality, the dimensions of the two heads were approximately equal.

The model of the head magnetization used in these calculations is fairly crude, of course, so that one should be somewhat suspicious of the numerical values which emerge from it. Nevertheless, the fact that the fit is as good as it is indicates that the basic notions which have been incorporated into the model are probably sound. For example, recall that the pole tip field model is a two dimensional one, so we are making the implicit assumption that the width of the pole tips is much larger than their thickness (i.e. $w >> p_1+p_2+g$). Now if this assumption is acceptable for Cybernex heads, then it is certainly acceptable for the IBM ones, since $w/(p_1+p_2+g) = 3.2$ for Cybernex, whereas $w/(p_1+p_2+g) = 6.4$ for IBM.

The important question which these results have answered is that of whether the heads are capable of resolving isolated magnetic structures having dimensions on the order of a few microns. An important distinction should be made at this point between isolated magnetic structures, and structures which form one part of a periodic (or nearly periodic) group. In the former case we can include such things as the magnetic anomaly which surrounds a defect in an otherwise perfect crystal, a domain wall, a crosstie, etc. In the latter case we can include information stored as patterns on a magnetic recording disc. The reason for making this distinction is that the magnetic structures which are part of a periodic group do not (as we have seen in chapter 3) produce a large long range field. The field falls off very quickly as one moves away from the structure. Hence, it is conceivable that a magnetic recording head might work very well in resolving magnetic transitions which are part of a collection of similar transitions, because the long range fields are small, but very poorly in resolving isolated transitions. If this were the case, then isolated transitions might manifest themselves as the kind of very broad response functions seen by Andre, and not the very narrow ones which can be observed with clean sliders.

4.2) Nonlinearities of the Head Response in the Absence of a Uniform External Field

It was mentioned in the first chapter that some of the features which Andre observed in the large wire measurements were reminiscent of Barkhausen noise. This brings up the question of whether the head is a linear device. It is to be expected that the head will saturate, and hence become nonlinear, if it is driven at a high current, or if some external magnetic structure drives enough flux through its poletips. However, it is possible that some rapid reorganization of the domain structure will take place at lower fields, producing the kinds of discontinuous changes in magnetic susceptibility that result in Barkhausen noise.

A good method of testing this possibility is to look for harmonics emerging from a two head arrangement which is being driven by some pure sinusoidal signal. Such an experiment was carried out, using the apparatus described in the second chapter and a pair of Cybernex heads. It was found that if any harmonics were being generated by the heads, they must have been at least about 50 dB smaller than the main signal. Measurements were made of both the second and third harmonics, and no signal could be detected in either case. Care was taken to ensure that the heads were being driven at a current level which would not saturate the pole tips. The current used was about 2 mA (peak) at a frequency of 10 kHz. Second and third harmonic data are plotted with the fundamental in Figs. 40 and 41.

4.3) Frequency Dependence of the Amplitude and Phase Response

Results have appeared in several publications which concern the changes which occur in the amplitude and phase response of thin film heads at high frequencies. For example, it was mentioned in the first chapter that Re and Kryder have measured very large phase shifts in IBM heads at frequencies of several MHz.[29] Brief mention has also been made of the fact that Hoyt detected a gradual decrease in the response of (unspecified) thin film heads at frequencies of up to 50 MHz.[26] It seemed desirable to investigate these claims, since they have a bearing on eddy current and domain wall behavior. Consequently, pairs of IBM heads were aligned and energized with high frequency signals in order to investigate their amplitude and phase response.

When we discuss phase behavior, we mean the variation in the phase of magnetization of some part of a head versus the phase of its driving current. At the frequencies where phase response appears to become important (according to Re and Kryder), one has to be very careful about the effects of stray capacitances. The first experiments which were conducted to determine phase response yielded some interesting effects, including large phase shifts and even resonances under certain conditions. However, some investigation revealed that the effects were due entirely to the capacitance of the lead wires. The results were very tempting, because the frequencies at which large phase shifts occurred corresponded, approximately, to the frequencies at which Re and Kryder observed large shifts. A plot of this data can be seen in Fig. 42.

It was the resonances, during which the lock-in amplifier ceased to function properly, which indicated that something was seriously wrong with the experimental setup. A major effort was consequently undertaken to rid the apparatus of stray capacitances. All excess wiring was eliminated, to the point of disconnecting any apparatus which was not immediately needed for the experiment . Included among the cables was a low noise twisted wire variety which had a high

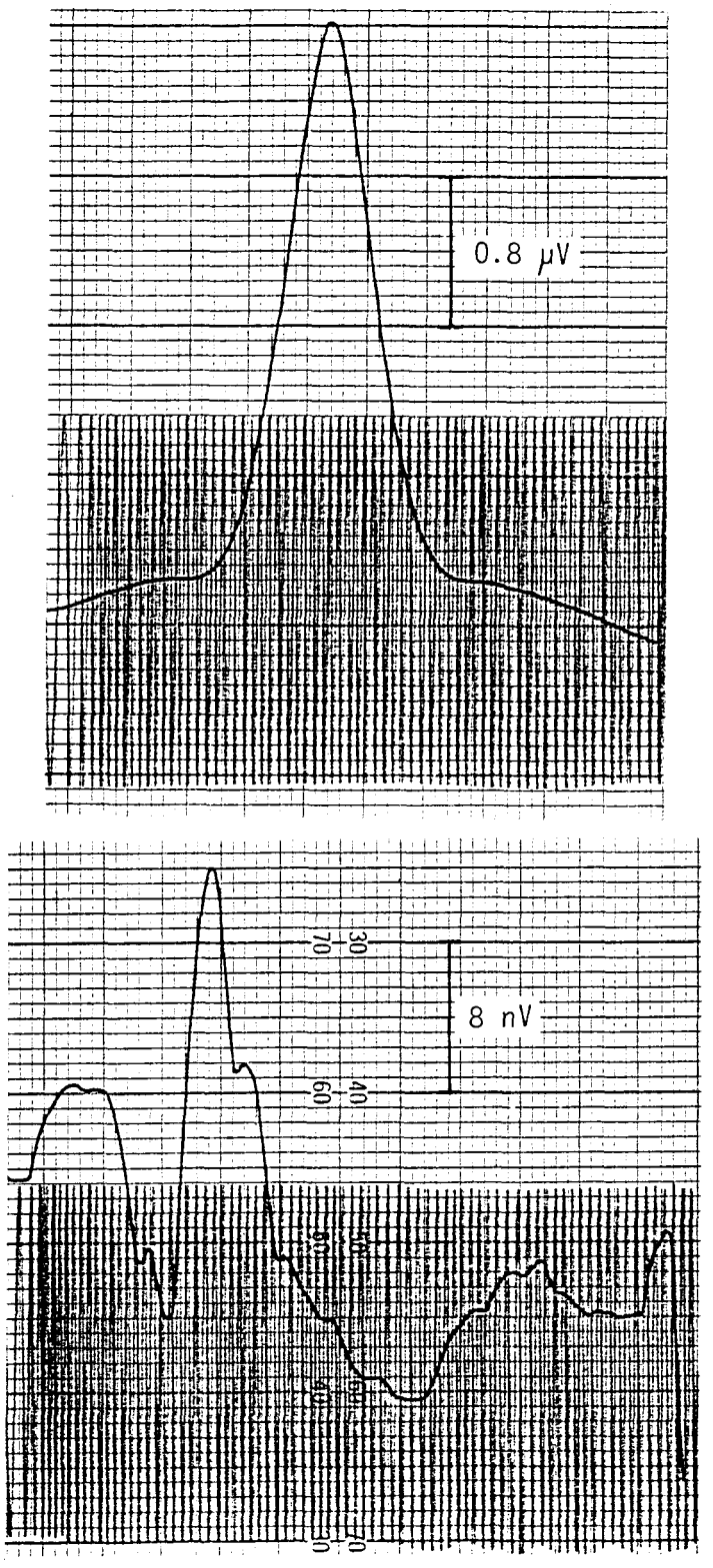

Fig. 40. Second harmonic data for a Cybernex head displayed below first harmonic data. Notice the different scales for the two plots. An EMF of 100 mVRMS at a frequency of 10 kHz was applied to the lower head.

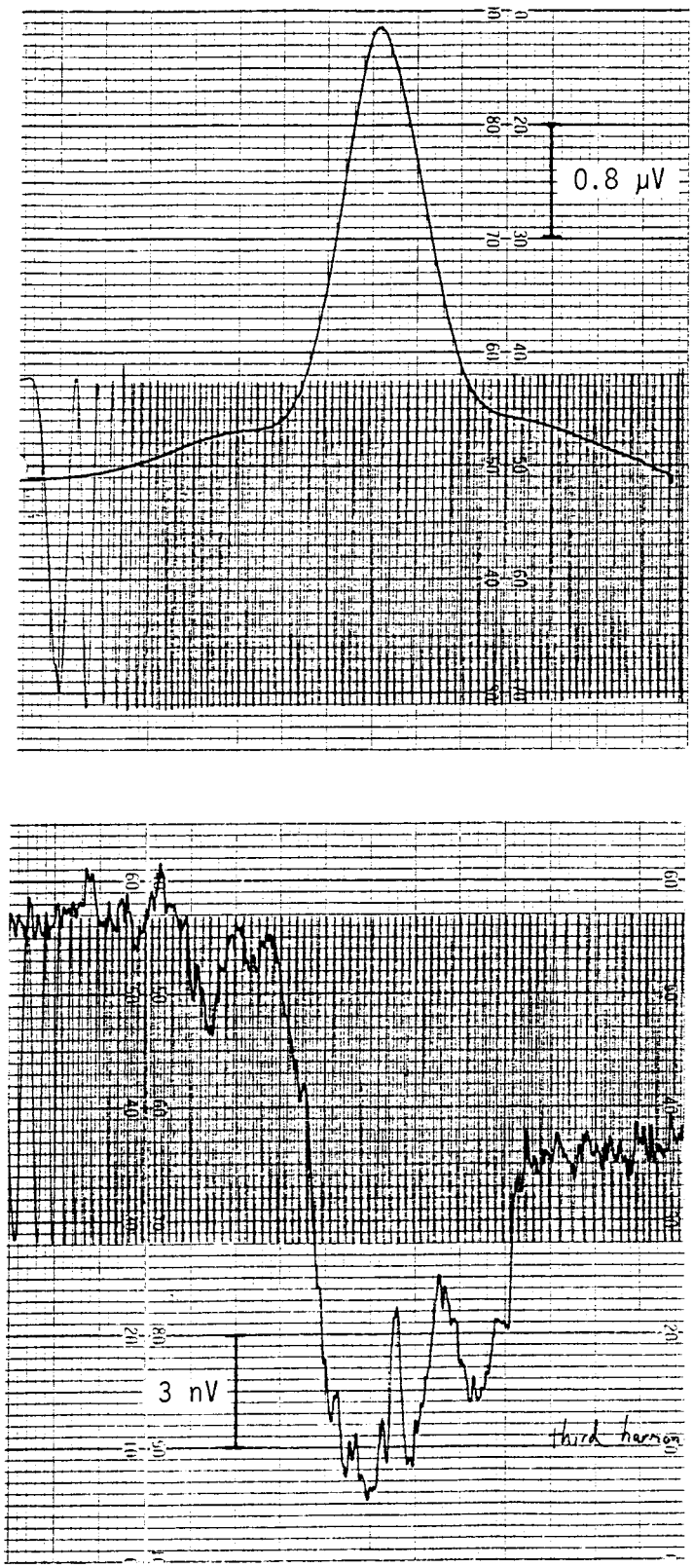

Fig. 41. Third harmonic data for a Cybernex head displayed below first harmonic data. Notice again the two different scales. An EMF of 50 mVRMS at a frequency of 10 kHz was applied to the lower head.

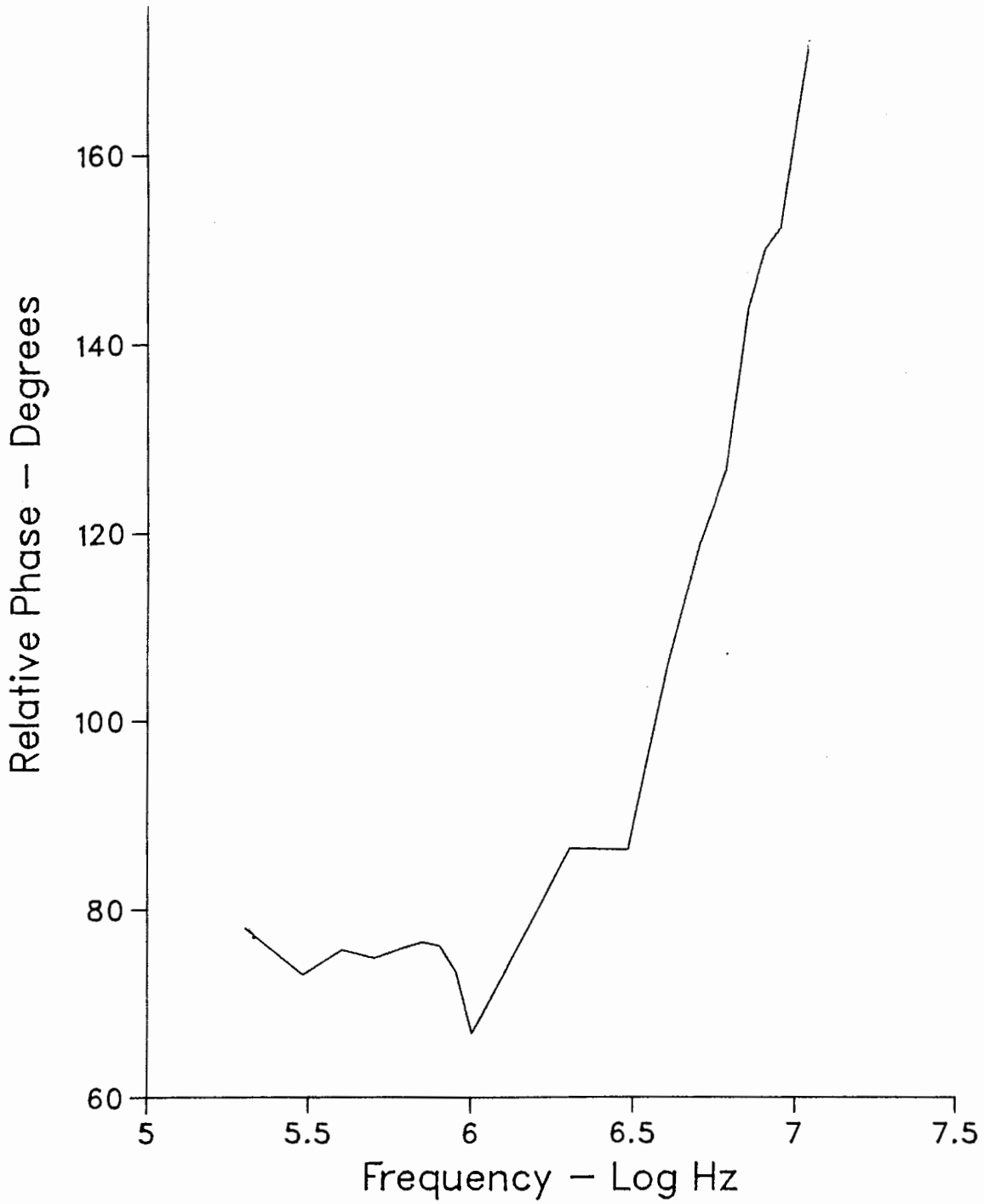

Fig. 42. Preliminary phase shift vs. frequency data for an IBM head.

capacitance per unit length. This was replaced with a ordinary coaxial cable. The various pieces of instrumentation were moved close to the experiment and the interconnecting leads made as short as possible.

The result of this effort was rather disappointing, in the sense that large (≥90 degree) phase shifts were no longer observed, up to a frequency of 50 MHz. The phase seemed to change over a range of several tens of degrees as a function of frequency (see Fig. 43), but it seems likely that this can be attributed to the instrumentation rather than the head. For example, it was observed that meter readings on the lock-in amplifier would change if it was touched, or even approached. The situation improved when a wooden dowel was fabricated which made it possible to turn the phase selection knob on the amplifier without actually touching it. The lock in amplifier itself had a large absolute phase error (± 15°), and a comparatively large relative phase error (± 5°). Using the in-phase and quadrature outputs of the amplifier to calculate the phase might have yielded more reliable results, but no attempt was made to use this method.

Clearly this result, that the phase does not shift by 90°, is inconsistent with the one published by Re and Kryder. Their data seems to indicate that, not only does the phase shift by 90° at a frequency of 8 MHz, but that it will probably be shifted by a substantially larger amount at higher frequencies. Their measurements were made on two different parts of the head, for which they obtained different results.

In the experiment performed by Re and Kryder, the reference signal for the lock-in amplifier was provided by a device known as a current probe. This is a form of transformer which measures the current passing through a wire by sensing the accompanying magnetic field. The main advantage of using a current probe over measuring the voltage drop across a resistor is that it does not put a large load on the test circuit. The typical insertion impedance for the device is on the order of a few tenths of an ohm at a frequency of several MHz.

It appeared as if the presence of a direct electrical connection between the lock-in amplifier and the driving circuit for the head might have been producing the unusual phase behavior. With this in mind, a current probe (a Tektronix P6042) and its accompanying amplifier were acquired and used to synchronize the lock-in amplifier. The phase shift curve for this arrangement is shown in Fig. 44. The upper diagram indicates that a substantial phase shift takes place with the heads in the circuit. However, according to the lower diagram, which represents the phase shift which occurs when the synthesizer is connected directly to the lock-in amplifier, an even larger phase shift can occur without the heads in place. Despite the presence of large frequency dependent phase shifts in the data, the curves do look smooth and reasonably well behaved. Consequently, the data can probably be trusted, although it may be hard to interpret.

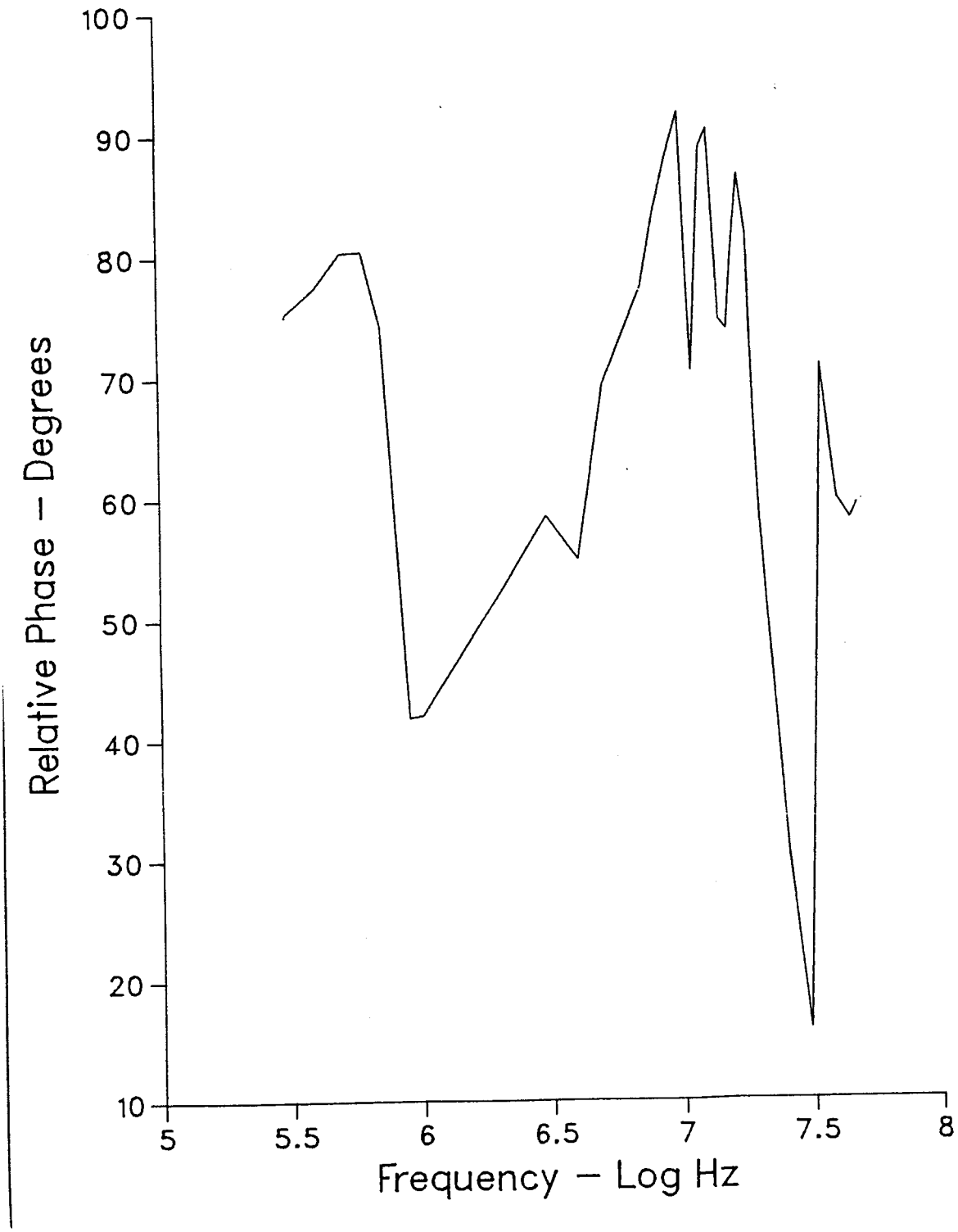

Fig. 43. Phase shift vs. frequency data after the substitution of low capacitance coaxial cables for the twisted lead low noise variety.

Fig. 44. Phase shift vs. frequency data obtained using a current probe as the phase reference. The curve on the left indicates the phase shift which took place with the heads in the circuit. The curve on the right represents the phase shift which occured when the synthesizer was connected directly to the lock-in amplifier.

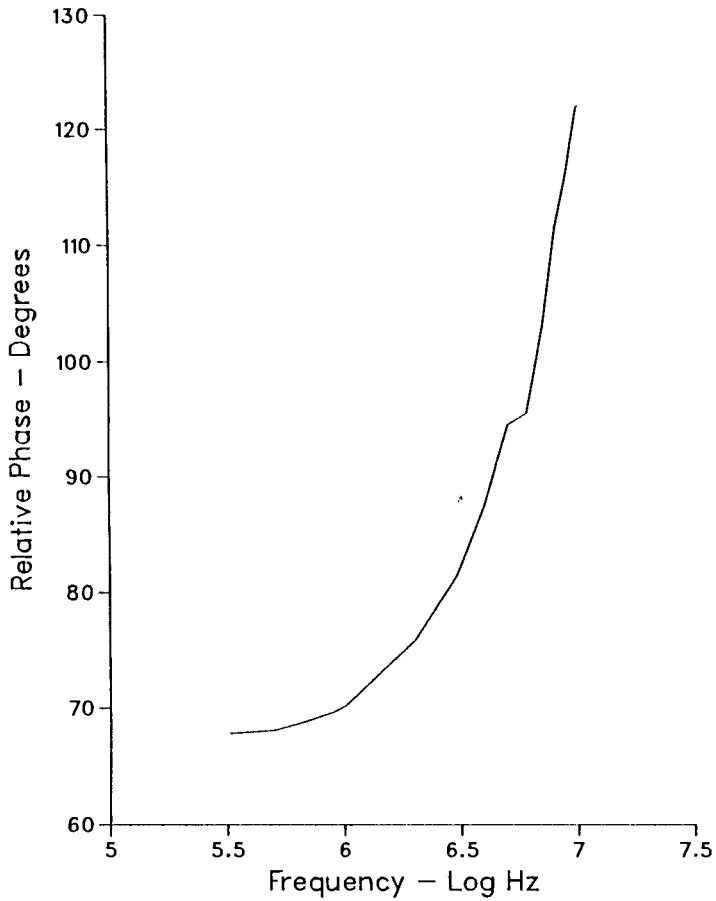
Relative Phase – Degrees
130
120
110
100
90
80
70
60
5
5.5
6
6.5
7
7.5
Frequency – Log Hz

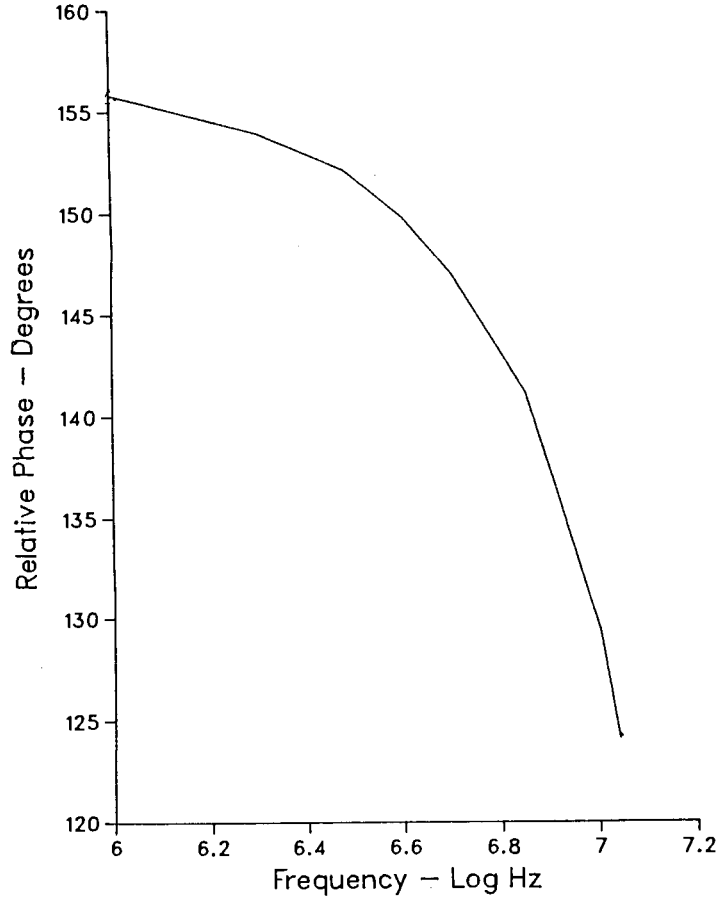
Relative Phase – Degrees
160
155
150
145
140
135
130
125
120
6
6.2
6.4
6.6
6.8
7
7.2
Frequency – Log Hz

The amplitude of the IBM (and Cybernex) head response was also measured as a function of frequency. It was found that the response (i.e. (head coil voltage)/frequency) decreases only slightly (by about 4% in the case of an IBM head) at a frequency of 1 MHz. It then slowly falls off to about 87% of its original value, in the case of an IBM head, at 3 MHz. Note that, according the the results of Hoyt[26], this decrease is too large. Beyond this frequency, the results become very uncertain because of the high frequency effects just discussed.

4.4) Effects Caused by External Applied Fields

One possible application for thin film heads involves using them to detect fields emanating from iron whiskers exposed to changing magnetic fields. The magnetic fields would be used to shift the position of domain walls inside the whiskers. This brings up the question of how changing magnetic fields affect the heads. In order to investigate this, experiments were carried out to determine the response of the heads during exposure to uniform magnetic fields.

Before making the measurements, two heads were paired and aligned using the positioning apparatus. As usual, the lower head was energized with an ac signal. This usually had a frequency of 10 kHz, although 50 kHz and 150 kHz were also used in order to reveal frequency dependencies. The main solenoids could produce (with the available power supply) a horizontal 80 G field in a direction perpendicular to a plane containing the head coils. To produce fields in other directions, a set of auxiliary coils were wound. These made it possible to produce a vertical or horizontal 20 G field within a plane containing the head coils.

Initially, the signal emerging from the lock-in amplifier was applied to the y axis input of an x-y chart recorder, while the voltage across the solenoids was applied to the x axis input. As the solenoid field was swept, the chart recorder would plot a curve representing the susceptibility of the heads as a function of field. Repeated sweeps produced the kind of curves seen in Fig. 45. It is clear from this data that what ever happens to the heads during a given sweep is not identical to the behavior during other sweeps. The general shape of the curves, on the other hand, appear to be the same.

The next question one might ask is whether the structure appearing in a given curve is random noise, or whether it is correlated with the structure appearing in other curves. If the structure is noise, then one should be able to use signal averaging to remove it. This would make the iron whisker experiments easier, unless attention was being paid to the behavior of similar noise in the whiskers. If the structure is not noise, some features should remain after summing the data obtained in successive sweeps.

Fig. 45. Signal coupled between two Cybernex heads as the current passing through the main solenoids is swept at a frequency of 2 mHz. An EMF of 50 mVRMS at a frequency of 10 kHz was applied to the lower head.

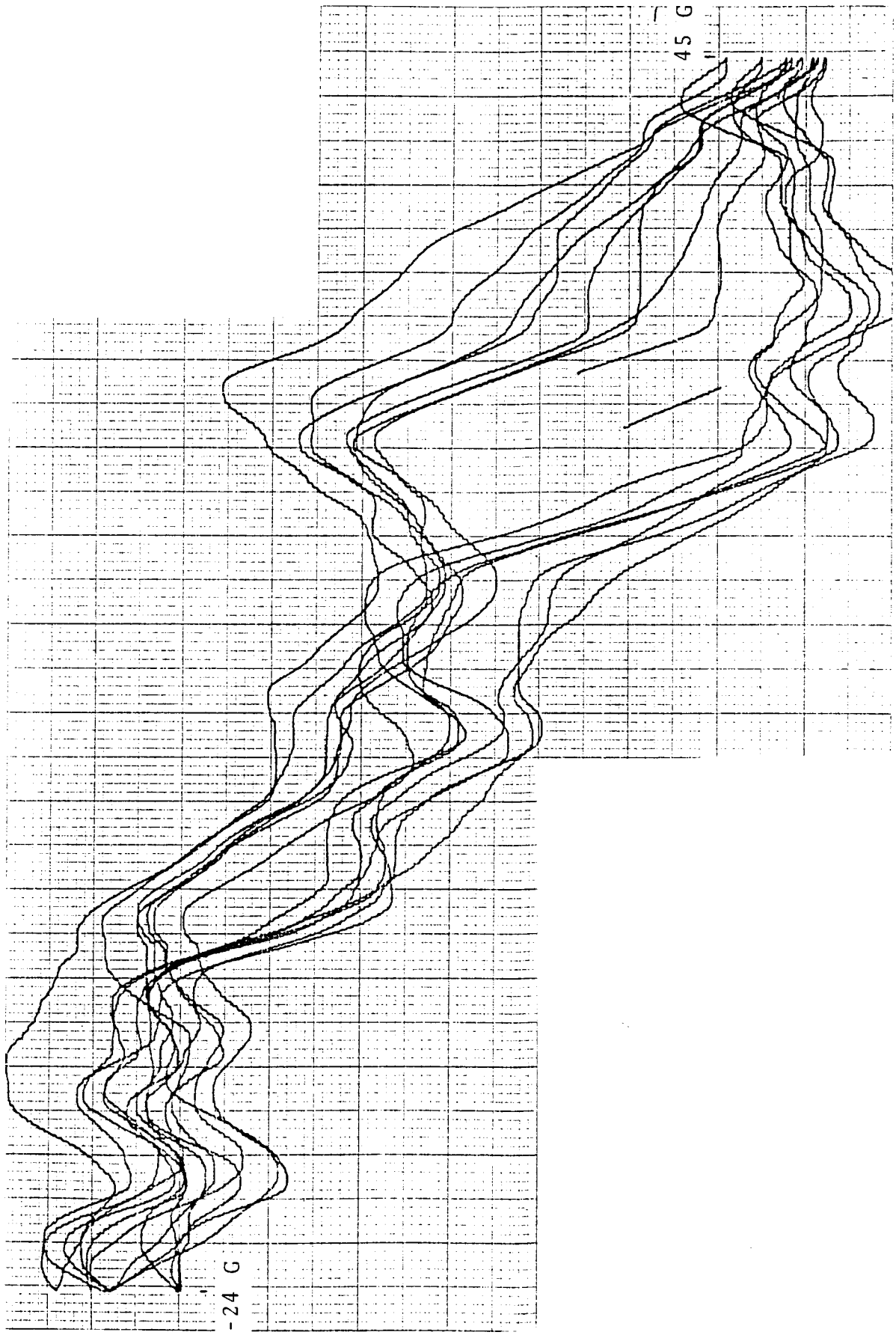
45 G
-24 G

Data recorded using a signal averager is shown in Fig. 46. As with the previous data, this was obtained using the main horizontal field coils. The plots in Fig. 46 are the sum of the data obtained in 512 separate sweeps. What this means in terms of the variation in the total signal level is illustrated in the lower plot, which represents the time variation of the signal for the duration of the experiment. Since any structure in the plot resulting from purely stochastic processes would be reduced by a factor of 23 in the averaging, it is fairly clear that the behavior which is producing these effects is not random.

Since the field source holder was offset from the symmetry axis of the main coils, it is possible that the effects seen in Figs 45 and 46 are due to components of the field which are orthogonal to this direction. From a micromagnetic point of view, it is not easy to see how a field which is oriented in the direction of the symmetry axis could alter the domain structure of the permalloy in the head. It is conceivable that the field affects that part of the head in which the two layers of permalloy are connected.

The first explanation seems more likely, however, when one considers the data displayed in Fig. 47. In this case, the auxiliary coils were used to produce a much smaller horizontal field in a direction perpendicular to the axis of the main coils. The magnetic field is aligned along the easy axis of magnetization of the head, so that one expects changes to take place. Two separate runs of 512 sweeps, which were obtained under identical conditions, are displayed in the diagram. Aside from small differences in the relative heights of the peaks, a one to one correspondence can be made between the features in the two graphs. Output from the strip chart recorder indicates that the relative change in the amplitude of the signal is comparable to the changes observed with the previous arrangement.

A somewhat different curve is obtained when a vertical field is applied to the heads (see Fig 48). In this case the applied field is aligned along the hard axis, which is the direction in which the heads are magnetized by the 10 kHz signal (except, perhaps, for that region where the two permalloy layers join). It appears to be possible to switch the heads off almost completely by applying a relatively weak field. Once again, graphs representing two separate runs (of 256 sweeps each) are plotted in order to show the repoducibility obtainable by signal averaging.

The reproducibility obtained when the field is swept over a relatively large range diminishes greatly when the field sweep range is reduced (see Fig. 49). As usual, the graphs shown each represent the sum of a large number of sweeps taken under identical conditions. In this case, however, the features in two successive runs can appear quite different. Notice also that much more structure appears in these plots than previous ones. Smoothed plots, in which adjacent data points have been averaged, are also presented so that their major features can be compared. It

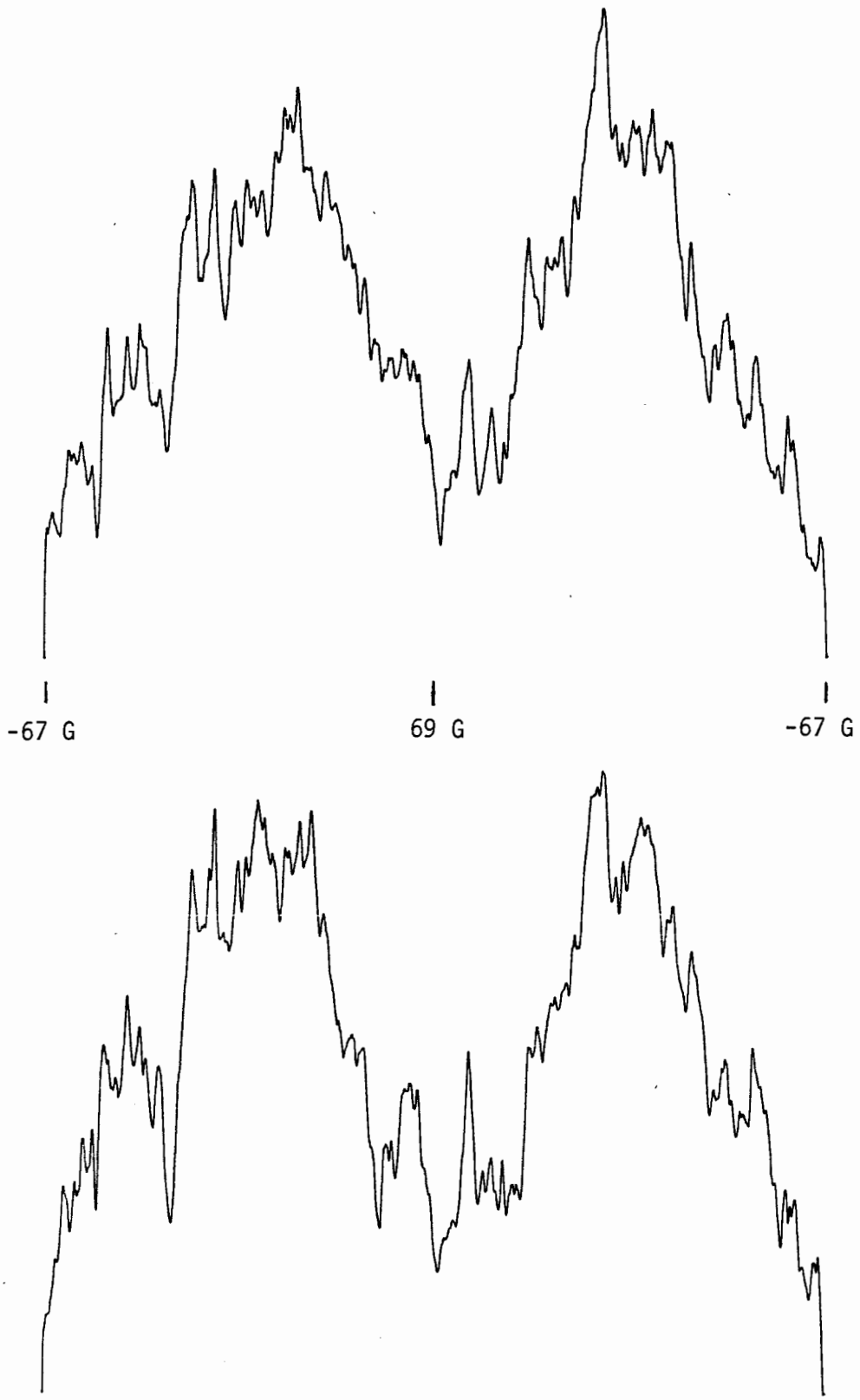

Fig. 46. Plots of the signal coupled between two Cybernex heads averaged over 512 sweeps of the solenoid current for a sweep frequency of 130 mHz. An EMF of 300 mVRMS at a frequency of 50 kHz was applied to the lower head.

Fig. 47. Plots of the signal coupled between two Cybernex heads (averaged over 512 sweeps at a frequency of 130 mHz) for the case in which auxiliary solenoids are producing a horizontal field. An EMF of 50 mVRMS at a frequency of 10 kHz was applied to the lower head. These changes represent a maximum of about 7% of the signal level in the absence of a field.

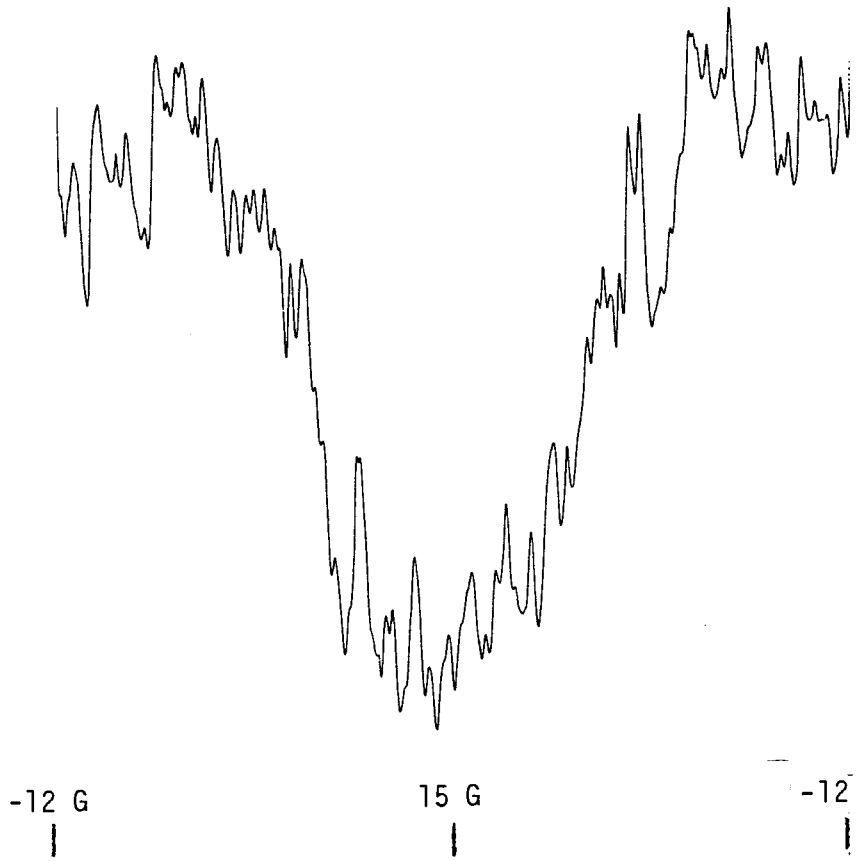
-12 G
15 G
-12 G

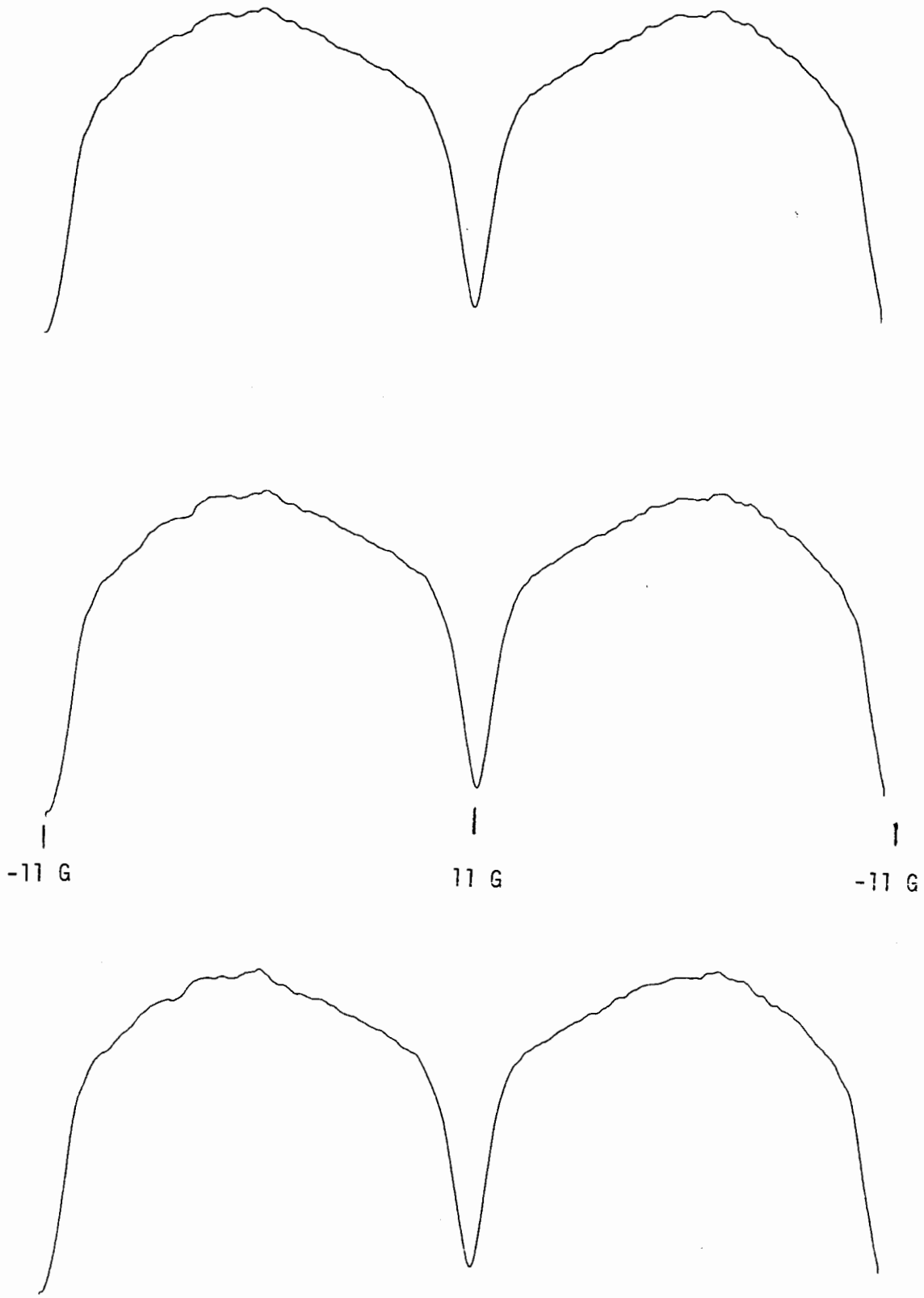

Fig. 48. Plots of the signal coupled between two Cybernex heads (averaged over 256 sweeps at a frequency of 130 mHz) for the case in which auxiliary solenoids are producing a vertical field. An EMF of 50 mVRMS at a frequency of 10 kHz was applied to the lower head. These changes represent a maximum of about 75% of the signal level in the absence of a field.

Fig. 49. Plots of the signal coupled between two Cybernex heads (averaged over 256 sweeps) as the current passing through the main solenoids is swept over a small range.An EMF of 50 mVRMS at a frequency of 10 kHz was applied to the lower head. These changes represent a maximum of about 2% of the signal level in the absence of a field.

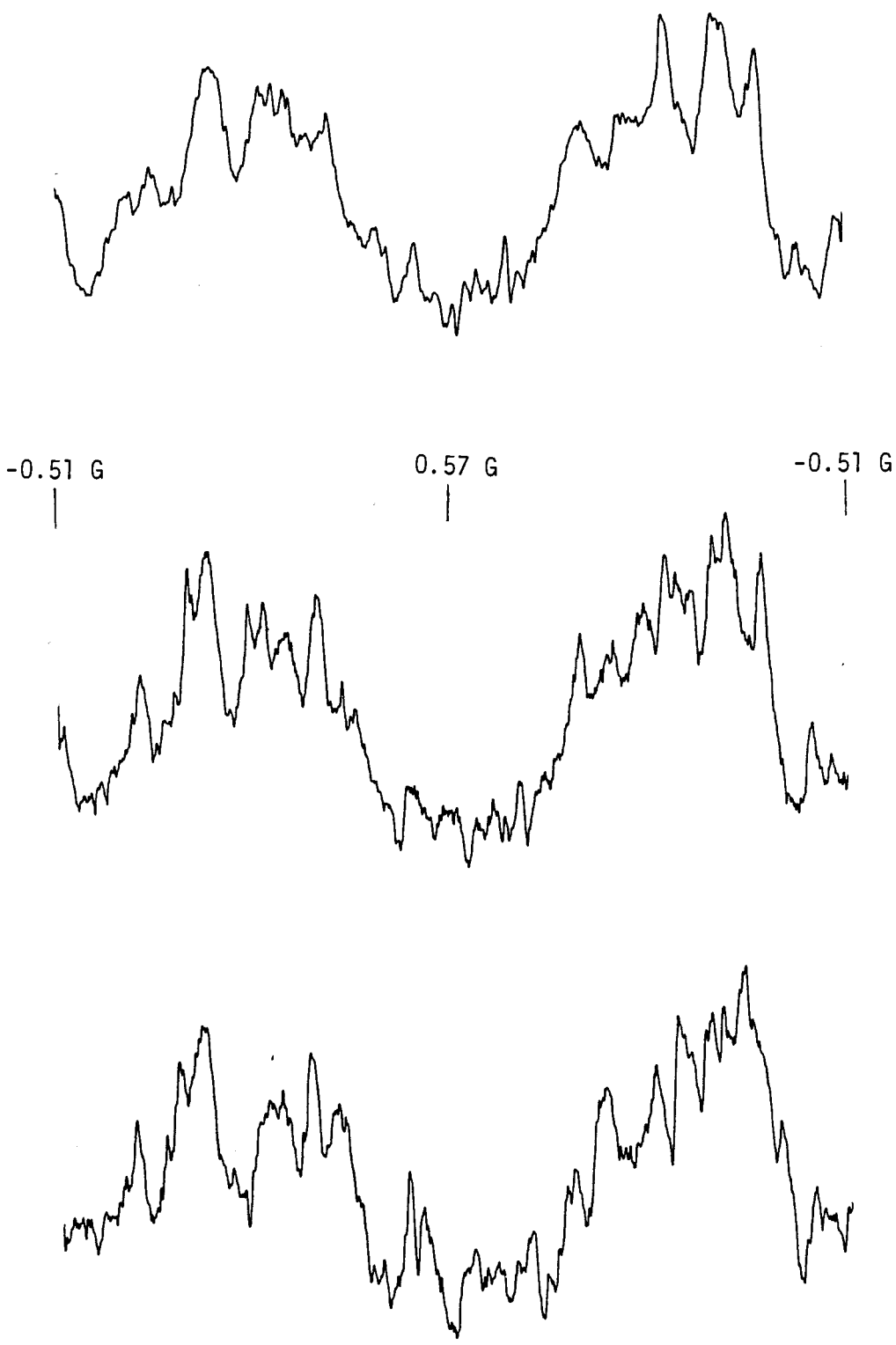
-0.51 G
0.57 G
-0.51 G

can be seen that only the very large scale structures are reproduced faithfully from one run to the next.

Most of the variable field measurements were carried out at a single frequency. Since it seemed plausible that the structures might have some kind of frequency dependence, a few measurements were made at other frequencies as well. Data from these experiments are shown in Fig. 50 for horizontal fields applied along the easy axis of magnetization. Apparently any frequency dependence, at least for the frequency range from 10 kHz to 150 kHz, must be fairly small.

If the thin film heads are used in micromagnetic studies, it is to be expected that they will be exposed to large magnetic fields. In fact, they may be exposed to much larger magnetic fields than the ones produced by the main field coils. In order to see if any lasting effects might result from the application of such fields, strong permanent magnets were brought up to the heads before the beginning of an experiment. Using this method, it was possible to apply uniform fields of several kilogauss to the permalloy.

The most noticeable result of this procedure was the production of bizarre intermittent response functions when two heads were passed across each other (see Fig. 51). Once a strong field had been applied, striking alterations in the shape of the usual curve appeared in a quasireproducible fashion - appearing and disappearing in an unpredictable way. Some of the distortions appeared in the same places in successive runs, while other distortions changed their shape, or vanished altogether. It seems unlikely that these effects could be caused by defects in the lock-in amplifier, such as the magnetization of the input transformer, since several functional preamplifiers were installed and produced the same results. However, it was observed that the phenomenon presented itself only when the head signals were detected using the low impedance (transformer) input of the lock-in preamplifier. This may not be significant, since one could never count on the appearance of the distortions in a given run anyway. The changes induced by the application of a magnetic field did not appear to be permanent, since after a certain length of time the distortions no longer recurred.

As might be expected, changes in the curves generated by field sweeping could be produced by the temporary application of a large field. An example of such an effect can be seen in Fig. 52. In this case, a series of sweeps was made with a horizontal field applied along the hard axis. The series was repeated in order to determine what reproducibility one could expect, and a 1 kG vertical field was applied using a permanent magnet. A repetition of the sweep series reveals an apparently irreversible change in the the behavior of the heads. Every new application of the field resulted in a slightly different curve. (It should be pointed out that it was not possible to apply exactly the same field every time, as the permanent magnets were handheld). It was not

Fig. 50. Plots of the signal coupled between two Cybernex heads (averaged over 256 sweeps), at three different frequencies, for the case in which auxiliary solenoids are producing a horizontal field. An EMF of 50 mVRMS was applied to the lower head. These changes represent a maximum of about 5% of the signal level in the absence of a field.

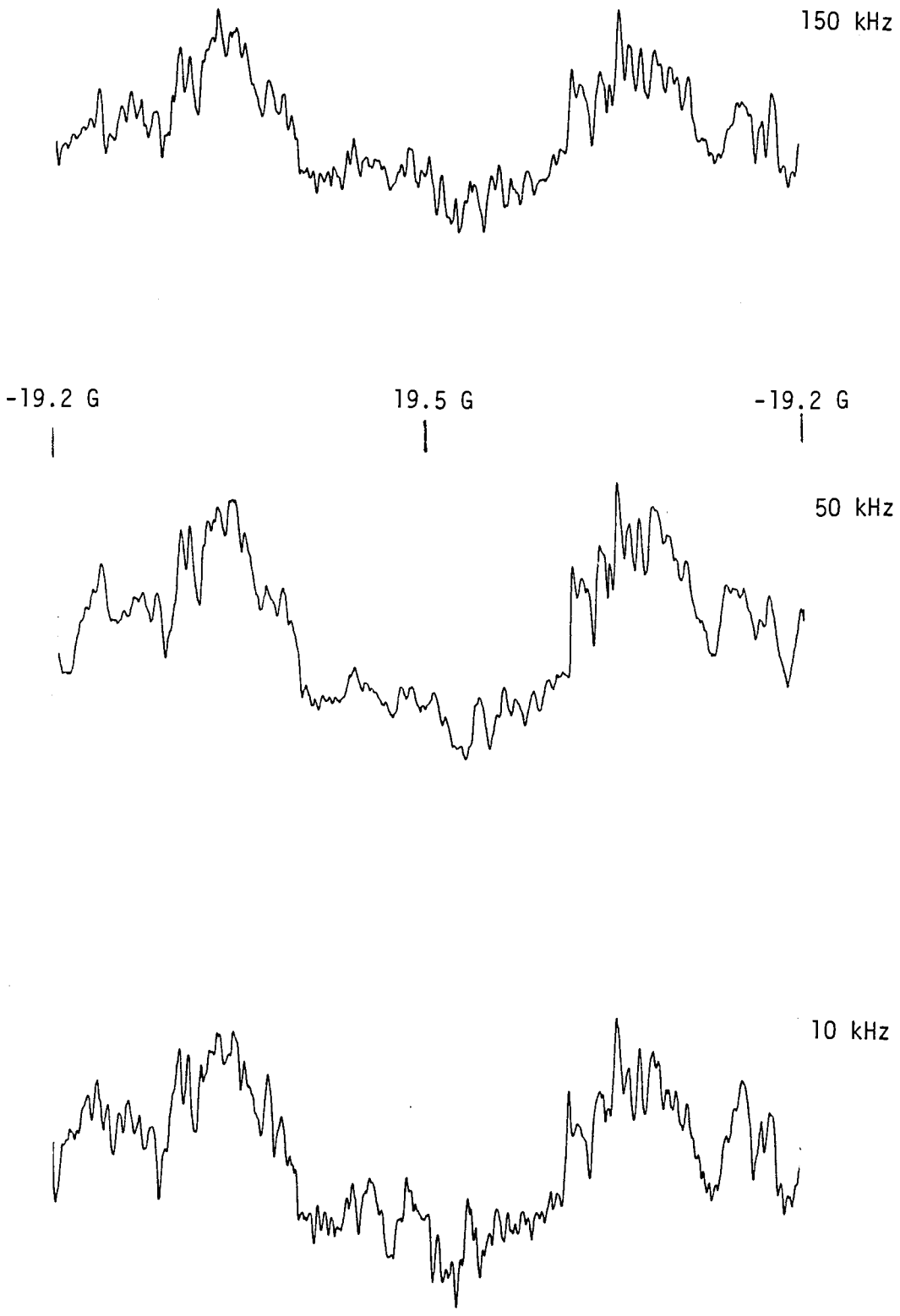
150 kHz
-19.2 G
19.5 G
-19.2 G
50 kHz
10 kHz

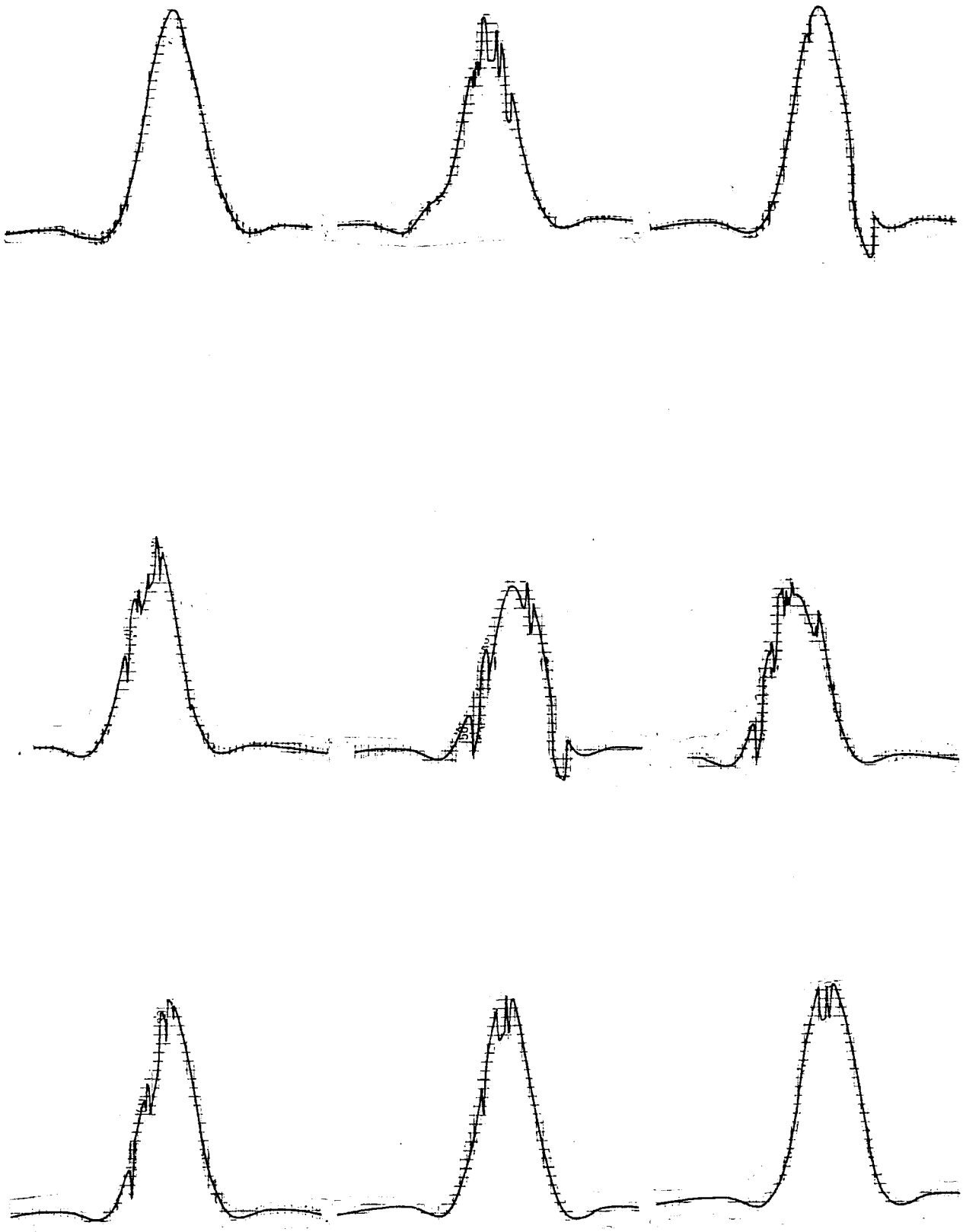

Fig. 51. Series of response functions produced after Cybernex heads were temporarily exposed to a strong (2 kG) vertical magnetic field. An EMF of 50 mVRMS at a frequency of 10 kHz was applied to the lower head.

Fig. 52. Curves representing the signal coupled between two Cybernex heads (averaged over as a function of field (produced in a horizontal direction using the auxiliary field coils) modified by applications of a 300 G vertical field.An EMF of 300 mVRMS at a frequency of 10 kHz was applied to the lower head. These changes represent a maximum of about 7% of the signal level in the absence of a field.

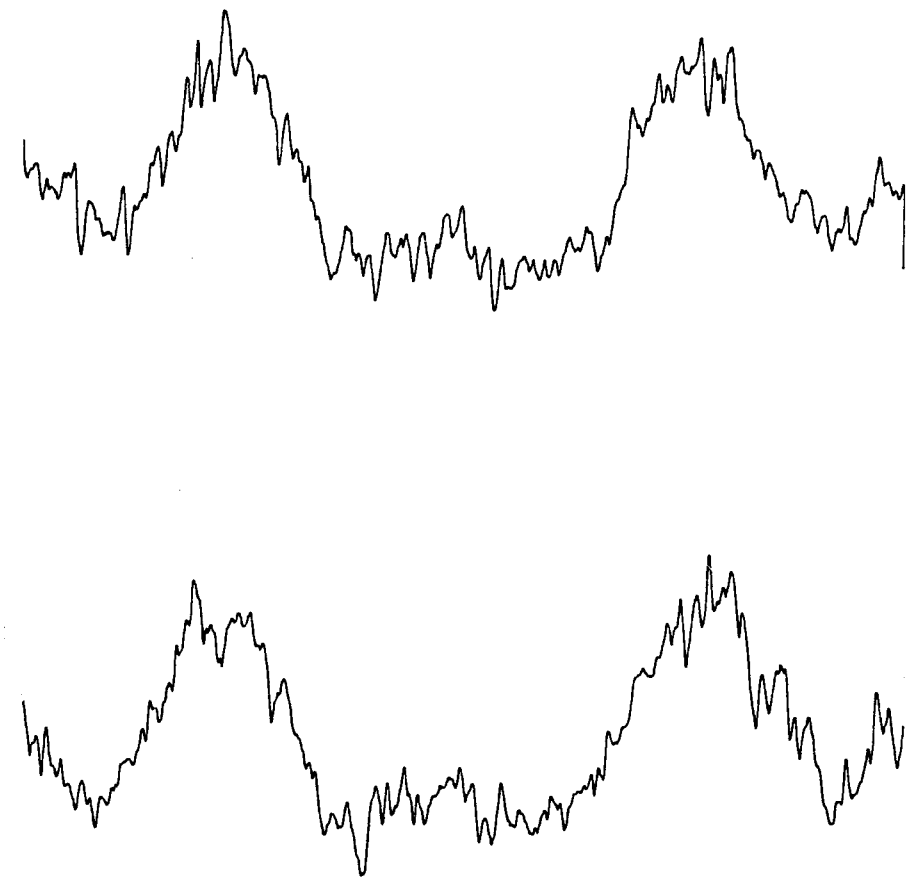

necessary to apply a kilogauss in order to produce the changes. The application of 300 G fields resulted in similar effects.

While the previous discussions have dealt with the effect of magnetic fields on Cybernex heads, similar experiments were carried out on IBM heads. The results of these measurements indicate that IBM heads display the same kinds of field-dependent structure as the Cybernex ones (see Figs. 53 - 55). Experiments were not carried out to determine the effects of temporary large magnetic fields on the IBM heads, but it is probably safe to assume that similar phenomena would be observed. The most noticeable difference between the behavior of the two heads is that the field dependent structures produced by the IBM heads are not as reproducible as those produced by the Cybernex ones.

4.5) The Efficiency of the Head

Thin film heads (and, in fact, all heads) sense fields by picking up magnetic flux in one region of space, and transferring it to another region, where it can be detected. When one considers this system, a natural question to ask is that of how efficient the transfer process is. Various authors have published calculations in which the efficiency of heads is determined on theoretical grounds. Hoyt et. al. have used small wire loops to determine experimentally the efficiency with which flux is transferred from the coils to the pole tips in (what are probably) IBM heads. Since the Cybernex heads looked like promising candidates for micromagnetics experiments, and since it appeared as if nobody had done any kind of investigation to determine their efficiency, experiments were carried out to measure it.

For these experiments, it was necessary to use field sources which would make it possible to determine the magnetic fields by calculation. This was the reason for the construction of the wire arrays described in an earlier chapter. Most of the field sources had resistivities on the order of 12 kΩ. In order to improve the signal to noise ratio (which was anticipated to be low), a source was chosen for the experiment which had a short (caused by an unetched section of metal) in the middle of the array. Calculations had already indicated that this would not appreciably affect the exponential character of the field. The resistance of the source was measured to be 6.12 kΩ.

An EMF of 10 V RMS at a frequency of 10 kHz was applied to the field source. When a Cybernex head was moved over the active portion of the source, the graph shown in Fig. 56 was generated. The cause of the slope in the plot is unknown. It may be caused by the pickup of stray fields by the parts of the head other than the pole tips (since the field source is finite and

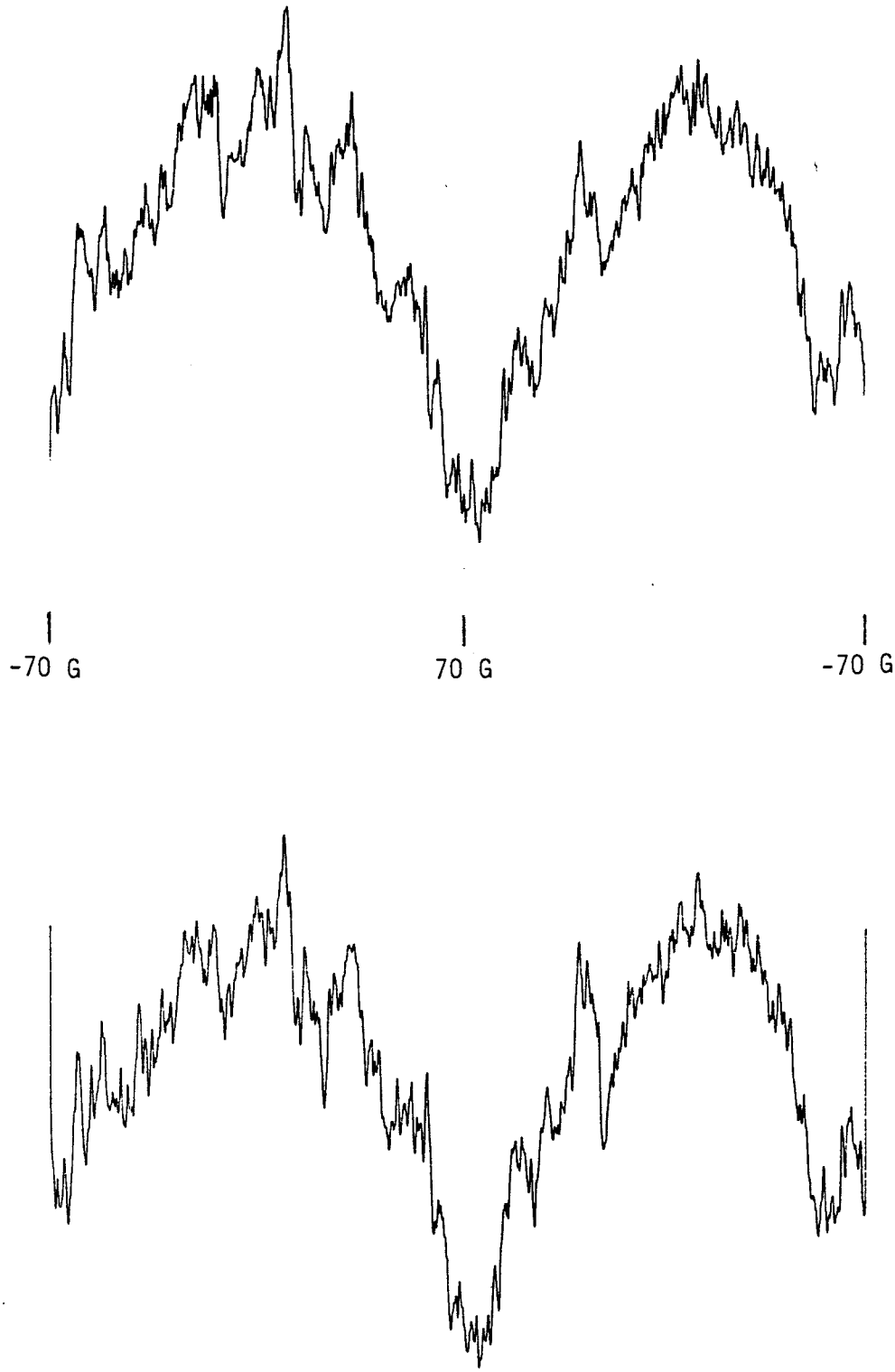

Fig. 53. Plots of the signal coupled between two IBM heads averaged over 256 sweeps of the solenoid current.An EMF of 300 mVRMS at a frequency of 10 kHz was applied to the lower head. These changes represent a maximum of about 5% of the signal level in the absence of a field.

Fig. 54. Plots of the signal coupled between two IBM heads (averaged over 256 sweeps) for the case in which auxiliary solenoids are producing a horizontal field. An EMF of 300 mVRMS at a frequency of 50 kHz was applied to the lower head. These changes represent a maximum of about 9% of the signal level in the absence of a field.


-20 G
20 G
-20 G

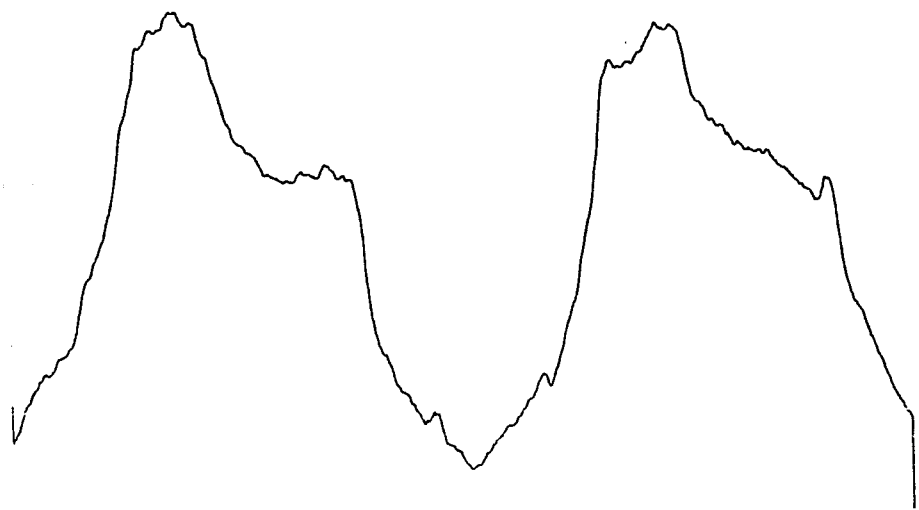

Fig. 55. Plots of the signal coupled between two IBM heads (averaged over 256 sweeps) for the case in which auxiliary solenoids are producing a vertical field. An EMF of 300 mVRMS at a frequency of 50 kHz was applied to the lower head. These changes represent a maximum of about 73% of the signal level in the absence of a field.

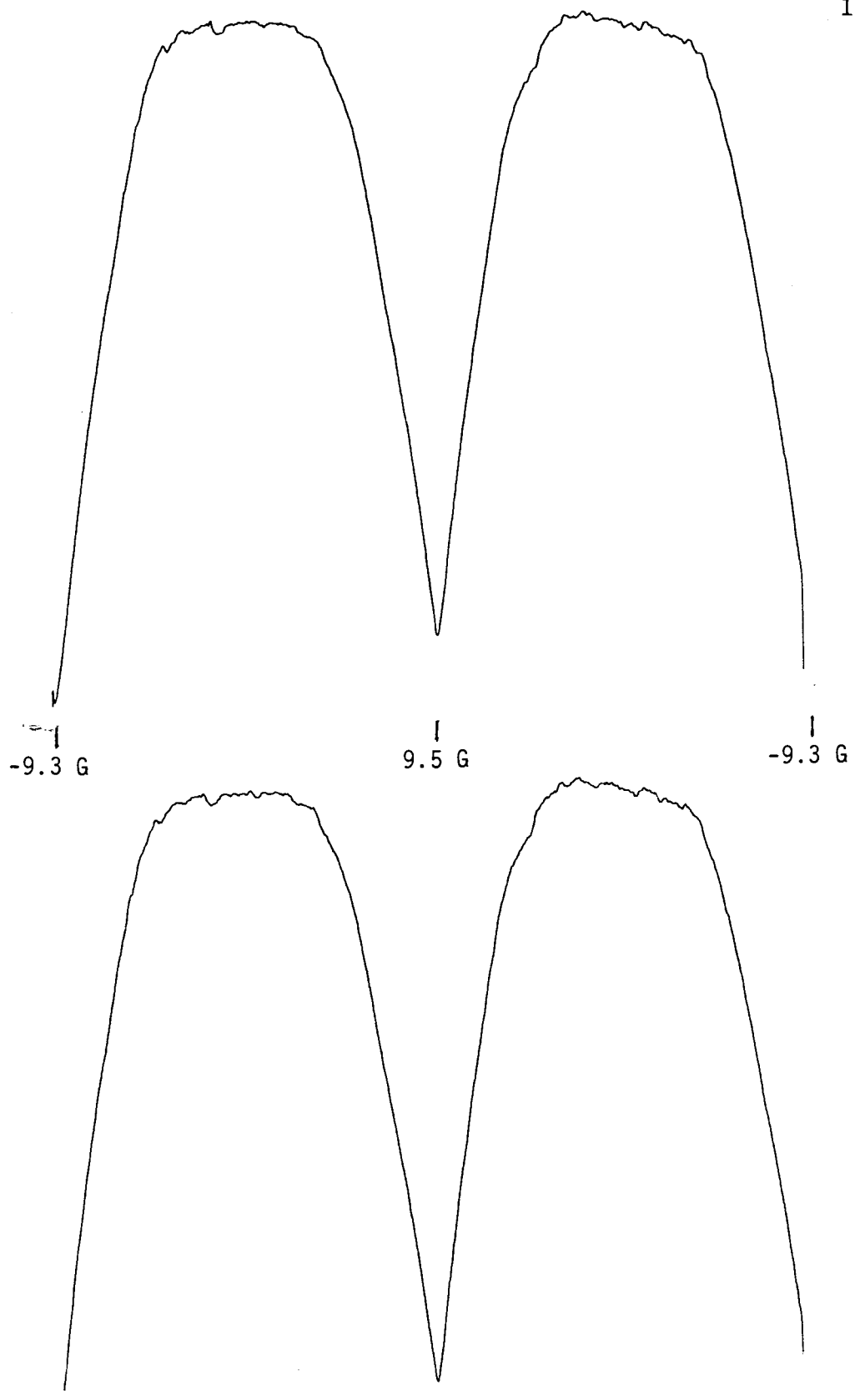
-9.3 G
9.5 G
-9.3 G

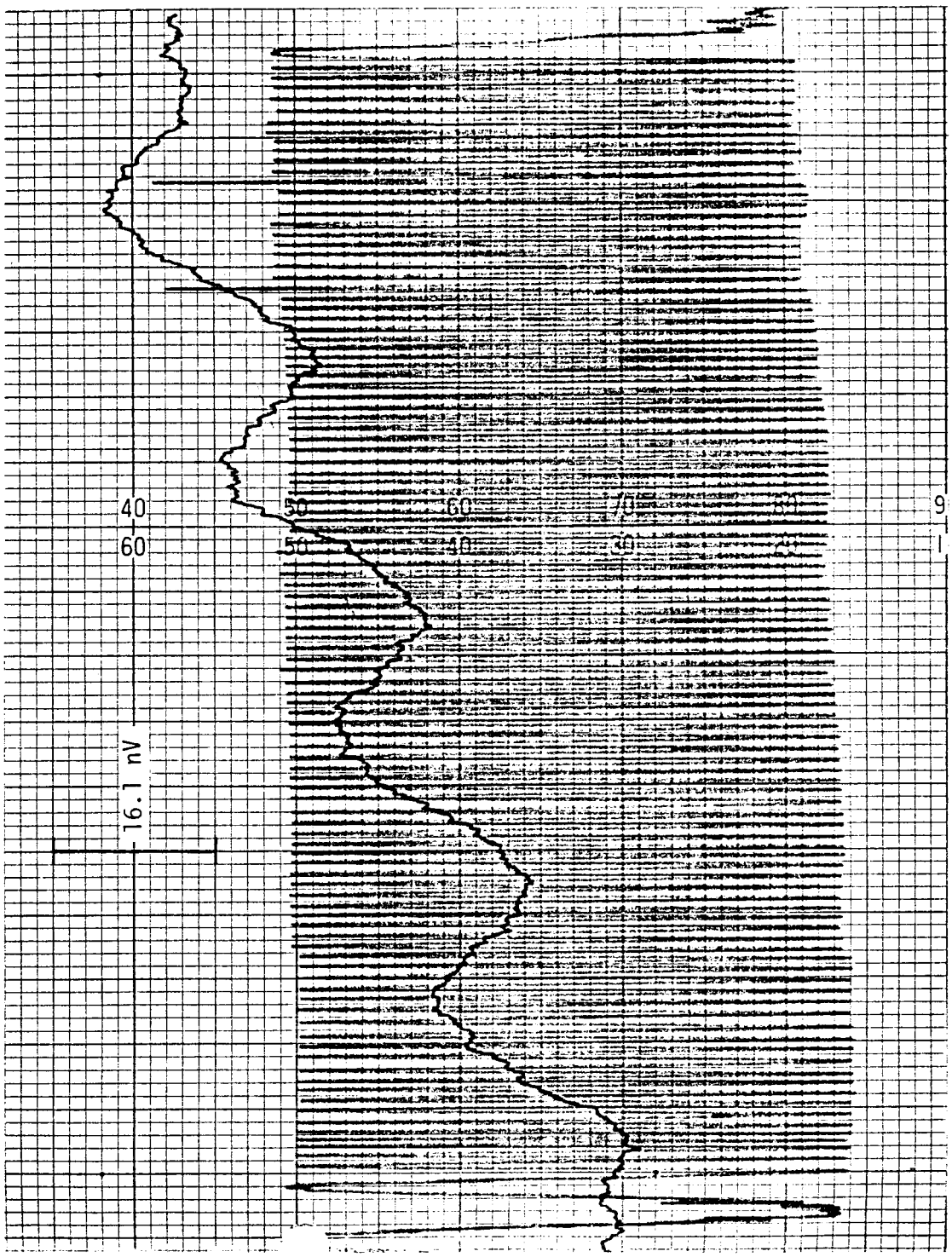

Fig. 56. Voltage generated in a Cybernex head as it moves 1.06 μm above a field source which is carrying a current of 1.63 mA RMS at a frequency of 10 kHz.

cannot produce a true short range field). It can be seen that the periodicity of the oscillations is 8 μm, which is what one would expect on the basis of a 4 μm center to center wire spacing. The amplitude of the variations can be determined by passing a straight line through the middle of the plot. After taking into account the step-up ratio of the lock-in preamplifier transformer, which is a function both of frequency and of source impedance, the amplitude is found to be (7.4 ± 0.5) nV RMS.

In order to determine the head efficiency, we must be able to calculate what the output voltage of the head should be on the basis of the amount of flux which it picks up from the source wires. The methods which were used to determine this flux are described in the last chapter. The calculations required a knowledge of a number of parameters which could not be determined by any means other than direct measurement. These were: the dimensions and separation of the source wires, the thickness of the quartz support layer, and the dimensions and separation of the pole tips. The values of these parameters, and the methods by which they were obtained, are listed in the following table.

Parameter	Value (μm)	Measurement Method
source wire width	1.77 ± 0.06	scanning electron microscopy
source wire separation	2.23 ± 0.06	"
periodicity of array	3.97 ± 0.01	optical diffraction
source wire thickness	0.415 ± 0.008	diamond stylus profilometry
quartz support thickness	1.06 ± 0.01	"
1st pole tip width	1.63 ± 0.08	scanning electron microscopy
2nd pole tip width	2.78 ± 0.08	"
1st pole tip length	20.8 ± 0.5	"
2nd pole tip length	17.1 ± 0.5	"
pole tip separation	0.65 ± 0.04	"

The calculated curve representing flux as a function of position is shown in Fig. 34 for a source driving current of 1.63 mA RMS. The amplitude of the variations has a value of (43.4 ± 1.9) G μm^2 . When account is taken of the driving frequency and the number of turns (24) in the coil of the head, this corresponds to an output EMF of (10.7 ± 0.5) nV RMS. Hence, the efficiency of the head, as defined in the last chapter, is (69 ± 6) %. Although this measurement was made at 10 kHz, the frequency response data indicates that the value remains fairly constant (to a few percent) up to at least 1 MHz. The number obtained by Hoyt et. al. for the low frequency efficiency of an IBM head is (at 76%) somewhat higher than this value. This

discrepancy could be caused by several factors, including experimental error, differences in the definition of "efficiency", and the fact that the Cybernex head has a longer flux path.

4.6) Using the Head as a Probe of Other Systems

Since thin film heads are being investigated primarily for the purpose of using them as micromagnetic probes, a few cursory investigations were made in order to determine how they could measure the magnetic properties of other systems. One such experiment made use of the fact that the coils in the Cybernex heads were provided with a centertap. Andre had previously investigated the possibility of exploiting this feature to measure the susceptibility of magnetic substances. His idea was to energize half the coil with an ac current, and measure the voltage across the other half. Changing the susceptibility of the gap between the pole tips could be expected to result in a change in the induced voltage. Although the early application of this approach was not very successful, it seemed worthwhile to reconsider it in light of the availability of better apparatus and experimental methods.

An easy way of testing the method consists of moving the energized head across another, disconnected, head. It is to be expected that the amplitude of the voltage across the active head will change as its pole tips become aligned with those in the passive one. Some experimentation revealed that high frequency signals produce the best results. Measurements from a run carried out at a frequency of 10 MHz (and with a longer time constant) can be seen in Fig. 57. It can be seen that the signal level drops (by about 35%) as the two heads become aligned. It is possible that this drop is caused a phase shift. Obviously, measurements of this kind are limited to heads which have centertaps. This consideration rules out the use of IBM heads.

Another experiment was performed in order to determine whether it was possible to use thin film heads to detect changes in the magnetic properties of iron whiskers as a magnetic field was applied to them. In this case, an iron whisker was placed on top of an upwards facing thin film head with its long axis pointing along the symmetry axis of the main solenoids. A horizontal ac field was then applied to both the whisker and the head using the main solenoids. The output from the head was sent into the transformer input of the PAR 124 lock-in amplifier, which in this case functioned merely as a low frequency ac amplifier. The signal monitor output of the lock-in was connected to the input of the Nicolet instrument computer, where the usual signal averaging procedure was carried out. The result of this experiment can be seen in Fig. 58. The spikes which appear at each end of the sweep suggest that the amplifier is responding to the sudden change in the polarity of the voltage which is applied to its input. In other words, the second

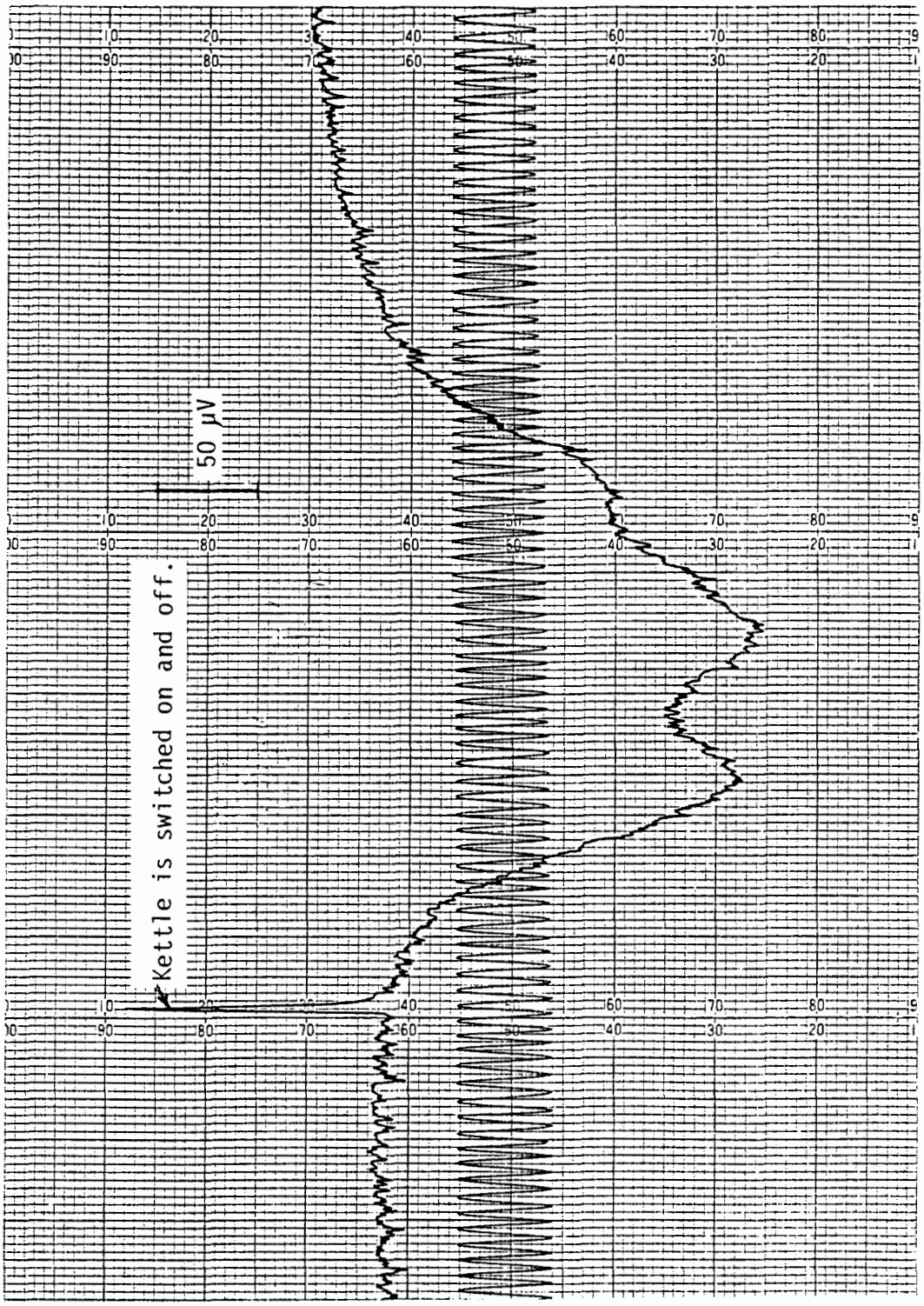

Fig. 57. Voltage produced across one half of a coil in a Cybernex head as it moves across another, disconnected, head. The other half of the coil was supplied with a current at a frequency of 10 MHz. The spike on the left hand side of the graph appeared as a result of the insertion and removal of an electric kettle from the power circuit which supplied the lock-in amplifier. The maximum drop in the signal level is about 35%.

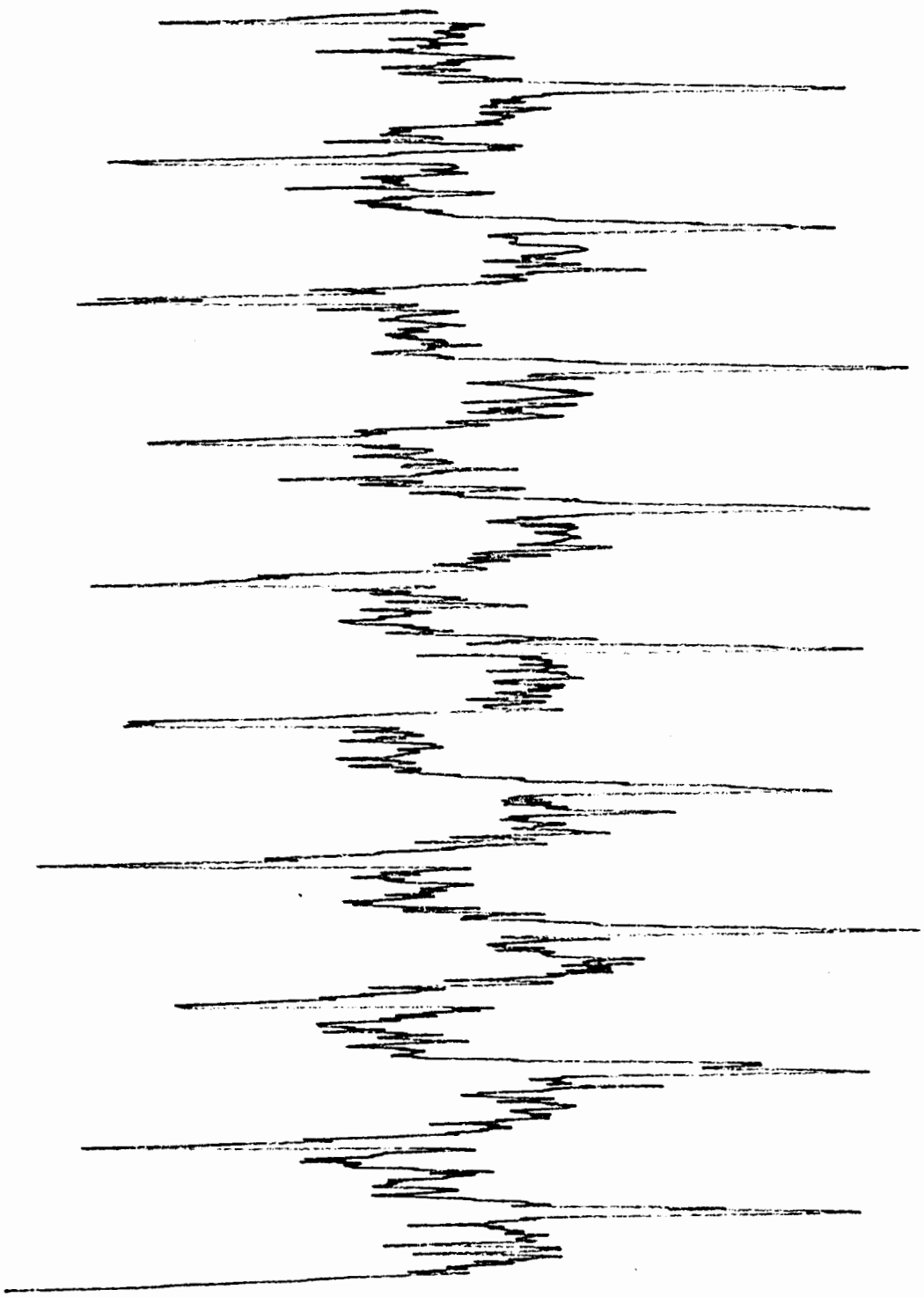

Fig. 58. Signal produced by a thin film head in contact with an iron whisker as the current passing through the main solenoids is swept at a frequency of 1 Hz (using a triangular waveform). The signal has been averaged over 64 sweeps.

derivative of the magnetization of the whisker is nonzero only at the ends of the sweep. In this case the transformer formed by the two heads takes the first derivative of the magnetization, while the transformer in the input stage of the amplifier takes the second. These patterns did not appear when the whisker was moved away from the head. Although it seems likely that this effect could be used to detect the presence of domain walls in the whisker, no effort was made to use it for this purpose.

The last experiment in this category made use of the same centertapped coil arrangement which was used in the first one. In this case, however, a head was used to detect the changes taking place in an iron whisker, rather than another head. An iron whisker was positioned (as before) atop an inverted head which was driven at a frequency of 10 MHz. The undriven side of the head coil supplied a signal to the input of the PAR 5202 lock-in amplifier, which was phase locked to the 10 MHz signal from the synthesizer. The output of the amplifier's phase sensitive detector provided the input for the signal averager, which was triggered in the usual way. The whisker and head were then exposed to an ac magnetic field from the main solenoids. The results of this measurement are shown in Fig. 59 for the case in which the whisker is present, and the case in which it is not. It is clear from these diagrams that the whisker is largely responsible for the peculiar shape of the first curve. The reason for the shape is unknown, but it apparently bears a strong resemblance to the shape of the curve representing the dc susceptibility of an iron whisker.

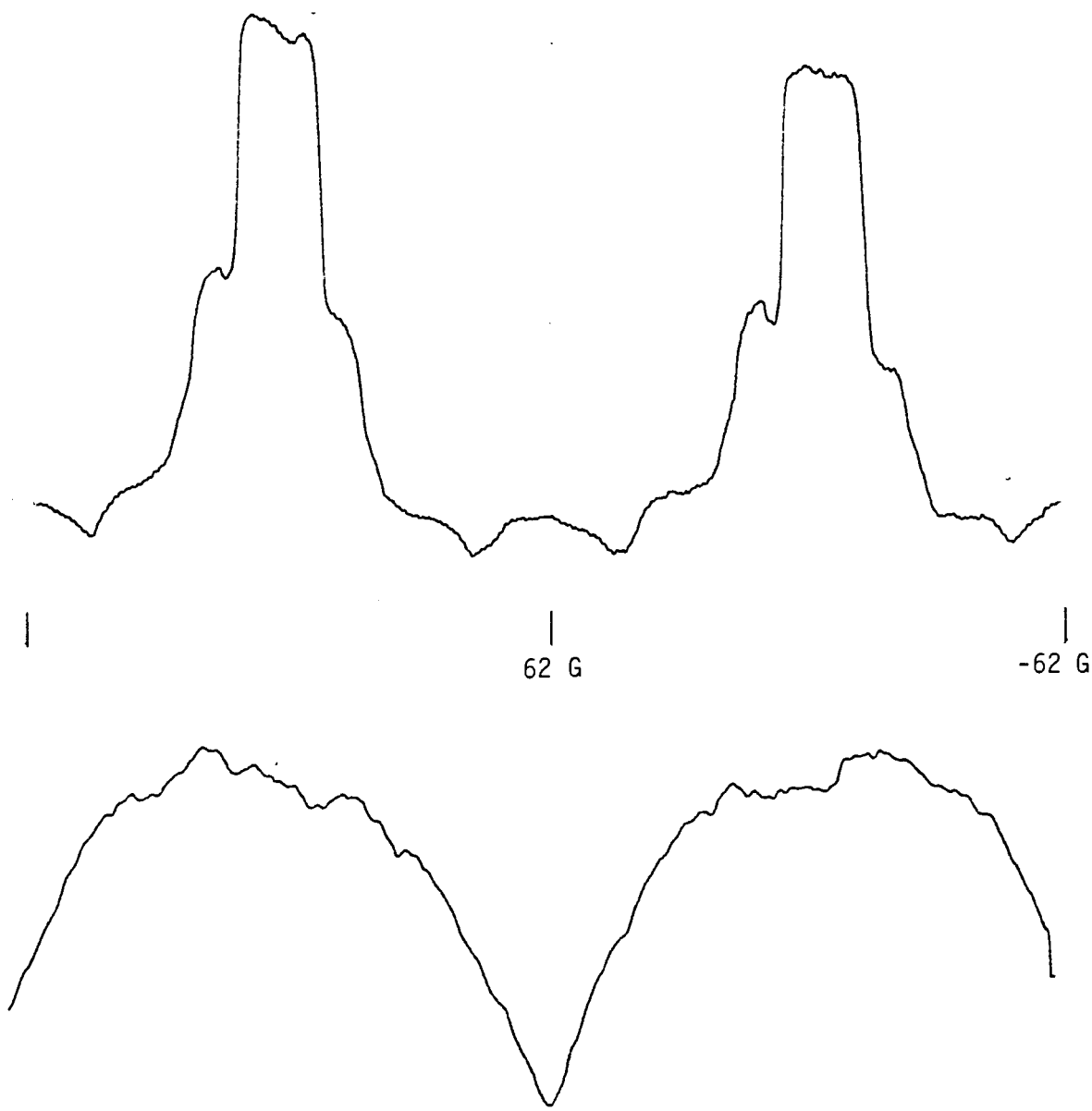

Fig. 59. Voltage produced across one half of a coil in a Cybernex head as the main solenoid current is swept. The signal has been averaged over 64 sweeps. An EMF of 50 mVRMS at a frequency of 10 MHz was produced across the other half of the coil. The upper diagram represents the case in which a whisker is present. The lower diagram represents the case in which it is not.

Chapter 5. Conclusions

This last chapter will conclude the thesis by: 1) Discussing the properties investigated in this research, 2) Comparing thin film heads with other micromagnetic probes, and 3) Making recommendations for future work.

5.1) Summary of Some Properties of Thin Film Heads

It was found that thin film heads are capable of detecting the presence of isolated magnetic structures with a resolution on the order of several microns. This discovery relieved early concerns about the possibility that heads can resolve small structures only under special conditions (i.e. if the structures are situated among other structures in such a way that long range fields are small). Furthermore, it was found that a relatively simple model of the fields produced by these heads is capable of explaining the features observed when one head is used to detect the field produced by another head.

As long as a given thin film head has not recently been exposed to a large external magnetic field, and assuming that it is not being driven into saturation, such a head will show a linear response to fields applied at the pole tips. Paired head measurements made with low (several mA) driving currents at a frequency of 10 kHz revealed that if any second or third harmonics are produced by the heads, they must be at least 50 dB below the fundamental. If the output voltage of the head is plotted against the input voltage, the resulting graph is found to be straight, up to the level at which saturation starts to occur.

Thin film heads which are exposed to external magnetic fields display effects which appear to be very similar to Barkhausen noise. Experiments in which paired heads were exposed to varying magnetic fields revealed that the strength of the signal, representing the susceptibility of the core material, varied in an unpredictable way as the strength of the field was changed. The variations seemed to have a hysteretic nature, since the pattern of the variations depended on the direction in which the field was swept. Although the variations were irreproducible from one field sweep to the next, their average over many field sweeps was reproducible. It was found that the behavior of Cybernex heads is more reproducible than that of the IBM ones in this sense.

Persistent, but probably not permanent, changes in the behavior of Cybernex heads were observed to take place following exposure to large external magnetic fields. After the application

of fields of up to several kilogauss, erratic (but sometimes reproducible) changes in the coupling between two heads could be seen as one was moved across the other. These changes were seen only when the heads were driving the lock-in amplifier through the low impedance transformer input. What role the transformer had to play in the production of these effects is not clear. It could be that they were not seen without the transformer just because of chance. Persistent changes were also observed in the field vs. susceptibility curve of the heads following exposure to external fields.

The efficiency of a Cybernex thin film head was measured using the field produced by a grid of very fine wires. For the purposes of this experiment, the efficiency is defined as follows. It is the ratio of the voltage which is actually induced in the coils of the head by flux entering the pole tips to the voltage which one expects to measure based on the frequency and magnitude of the field applied to the pole tips. According to this definition, the efficiency was found to be 0.66 at a frequency of 10 kHz. This number is comparable to, although somewhat lower than, the low frequency efficiency determined by Hoyt et. al. for what was probably an IBM head. In that case, the efficiency measured the ability of the head to take flux produced by the coils and carry it to the pole tips (rather than the other way around).

If a thin film head is equipped with a centertap, it is a relatively straightforward matter to use it as a susceptibility measuring device. Cybernex heads (but not IBM ones) can be used for this purpose. Experiments were carried out in which a suitably wired Cybernex head was used to detect the presence of another (disconnected) Cybernex head passing underneath. Another experiment was performed in which a Cybernex head was used to measure the field dependent susceptibility of an iron whisker. It was found that the use of a high frequency (several MHz) in the susceptibility measurements is necessary in order to obtain a high signal-to-noise ratio.

5.2) The Use of Thin Film Heads as Micromagnetic Probes

With the behavior of the heads under various conditions reasonably well understood, it is possible to make a sensible prediction about how they could be used as micromagnetic probes. We know, for example, that they are capable of sensing the presence of small isolated magnetic structures with a resolution of several microns. This by itself is a necessary, but insufficient condition, for their successful application to the study of micromagnetics. This section of the chapter will examine various aspects of thin film head behavior in connection with that application, and conclude with a comparison of thin film heads with other micromagnetic probes.

A desirable characteristic of any kind of sensor is linearity, unless some specific property of the sensor (such as sensitivity or dynamic range) is enhanced by a nonlinear response. From this point of view, thin film heads can make good field sensors, unless they are in a changing magnetic field or have been exposed to a large magnetic field sometime during their existence. Unfortunately, these conditions can arise in a number of situations. Consider the following. Since thin film sensors rely on Faraday induction to detect a signal, they will only operate if their pole tips are presented with a changing magnetic field. One method of changing the strength of the magnetic field emerging from a sample and entering the thin film head is to apply a changing magnetic field to the sample itself. For example, this is how one might move a domain wall inside an iron whisker. Although it is conceivable that a field could be applied to the sample without also applying it to the head, the most straightforward arrangement would have both the head and the sample exposed to a field. Another example of such a situation arises when the field dependent susceptibility of some material is to be measured. Once again it might be necessary to expose the entire head to a magnetic field.

As we have seen, changing magnetic fields are capable of producing noise in thin film heads, even for fields as small as a few Gauss. Although these effects will not necessarily overwhelm the signal produced by a sample, their existence must be taken into consideration during any experiment in which such fields are used. It is also necessary to recognize that, since the noise is not stochastic, it cannot be removed by signal averaging. On the other hand, since the strength of the noise is dependent on the orientation of the field with respect to the head (having a minimum when the field is perpendicular to both the hard and easy axes of magnetization of the permalloy in the head), it can be reduced by using the appropriate experimental arrangement.

Another possible way of producing a time varying flux in the pole tips of a thin film head involves moving the head back and forth very rapidly across the structure of interest. Although the head appears to be quite efficient at transferring flux from the pole tips to the detection coils, the extremely small area available for flux collection means that the signal produced by the head using this method will always be very small. Recall that the voltage induced in the head by a field of about 2 Gauss oscillating at a frequency of 10 kHz (produced by the fine wire array) was on the order of 7 nV. If we consider a situation in which a head is moving at a frequency of 1kHz above a sample producing stray fields with a strength of about 1 kG, we can expect to detect an EMF of a few hundred nV across the head coils. Now 1 kHz is a rather high frequency of vibration for an object as large as a head, yet it would probably still be necessary to use some kind of signal processor, such as a boxcar integrator, in order to separate the information representing the field from the background noise.

Compare the preceding example to the situation in which a thin film head is reading information from a magnetic disc. Assume that a 24 turn head with an efficiency of 0.5 is located 0.2 m away from the center of a disc which is rotating at 3000 RPM. In addition, suppose that bits written on the disc have a length of 4 μm, a width of 18 μm, and produce stray fields with a strength of around 500 G. Under these conditions, it can be seen that the signal induced in the head would have a value of about 500 μV. Clearly, in attempting to apply thin film heads to the measurement of micromagnetic stray fields, we are pushing them to do things for which they were not designed.

In addition to the problems associated with low signal levels, a vibrating head arrangement also presents mechanical difficulties. One of these has to do with the fact that the slider is mounted at the end of a flexible cantilevered suspension. We would like the head to move back and forth at a fairly high frequency, in order to maximize the signal level and minimize the amount of signal averaging required. It would also be desirable for the motion to be controllable in amplitude and direction. This may be difficult, however, if the motion is to be transmitted through a flexible arm.

There is also another difficulty, which concerns friction. Thin film heads are not designed to move backwards. The leading edge of a rigid disk recording head is canted slightly to allow a fluid layer to form between the head and the disk. This layer will not form if the head is not moving in the proper direction. Consequently, the lubricating film required for high speed motion will be absent. The presence of such a film was not required for the investigations described in this thesis, since movement was relatively slow. Under these conditions (involving static, rather than dynamic lubrication), the presence of a few monolayers of oil was sufficient to allow freedom of motion. However, it is likely that a considerable amount of friction and wear would take place if a vibrating head arrangement were used to sense magnetic fields.

When one compares the problems associated with using thin film heads to detect small, localized, magnetic fields, to the problems associated with the use of other micromagnetic probes for the same purpose, it is evident that the heads are really not very good. The only advantage which they may have over other probes is their ability to generate magnetic fields. Their capacity to produce relatively strong (1 kG) fields in very small regions appears to be a unique ability which might make thin film heads useful in the study of micromagnetics. For example, we have seen that it is possible to detect the presence of the pole tips of a dormant head by using another head to measure susceptibility. Admittedly, this is a somewhat artificial situation, but it shows that flux producing heads are capable of distinguishing structures by measuring their high frequency magnetic properties.

Another application along these lines might make use of two heads. One head could act as a transmitter, to set up magnetic disturbances in a sample, while the other acted as a receiver. The fact that sliders are normally provided with two heads might be useful in this regard, as it would allow the transmitter and receiver to be oriented very accurately along a line. Although such an arrangement would require attaching new wires to a slider, the experience with the IBM heads shows that this is not a difficult task. All of these applications could involve high frequency signals, so that it would not be necessary to move the heads rapidly in order to detect a voltage.

Two final comments should be made about the use of thin film heads in micromagnetic measurements. Firstly, the sliders in thin film heads are opaque, so that it is not easy to determine by observation where the pole tips of the head are in relation to the sample. This is not the situation with most other probes. Secondly, thin film heads are under development which combine two components for the production and detection of magnetic flux. These devices contain a coil and permalloy core for generating magnetic flux, and a magnetoresistive strip, placed in series with the permalloy flux path, for sensing flux[39]. The motive behind this arrangement is the move to higher bit densities in the magnetic recording industry, with attendant reductions in the level of the playback signal in conventional inductive heads. If magnetoresistive heads are sold commercially, they could potentially be very useful micromagnetic probes, since they could detect dc fields without the use of awkward techniques to generate a changing flux.

A comparison of the abilities of various micromagnetic probes is shown in the table below. Speculative methods, such as magnetic versions of scanning tunnelling microscopes, have not been included.

Method	Resolution	Sensitivity	Frequency response	Linearity	Imaging
TFH	≈ 3 μm	(see note 1)	(see note 1)	good	no
MHP	≈ 3 μm	≈ 3 G	dc to 3 MHz	good	"
MMP	≈ 3 μm	?	dc to (?)	nonlinear	"
KE	≈ 0.5 μm	?	dc to 50 MHz	-	yes
LM	(see note 2)	(see note 2)	(see note 3)	-	"
EBH	(see note 4)	?	"	-	"
SEMPA	≈ 60 Å	(see note 5)	"	-	"

TFH: thin film head; MHP: miniature Hall probe; MMP: miniature magnetoresistive probe; KE: magneto-optic Kerr effect; LM: Lorentz microscopy; EBH: electron beam holography; SEMPA: scanning electron microscopy with polarization analysis

Note 1: The sensitivity of a thin film head to magnetic fields depends on the size of the

pole tips and the rate at which the field changes. For the Cybernex heads used in this experiment, a 2 G field oscillating at 10 kHz produced a voltage of 7 nV across the head windings. Thin film heads can sense fields at frequencies of up to at least least 50 MHz.

Note 2: In Lorentz microscopy, the lower limit on the field which can be detected depends on the amount of flux enclosed by neighboring parts of the electron beam. The lower limit on the flux is set by the flux quantum (4×10^{-7} G cm^2) . This means that the sensitivity depends on the size of the magnetic structures which are being examined.

Note 3: In the case of electron beam methods, the frequency response is set by the speed of the scanning and detection electronics.

Note 4: The smallest features which I have seen published have micron dimensions. However, I know of no reason why, in principle, features of much smaller size (on the order of angstroms) could not be observed.

Note 5: The notion of sensitivity is not really applicable in the case of SEMPA, because the method is used to detect electron spin orientation, not magnetic fields.

5.3) Recommendations for Future Work

It seems clear that the only sensible reason for conducting micromagnetic studies with thin film heads, in their present form, is in order to make use of their capacity to generate localized magnetic fields. There are two things which should be kept in mind if such studies are carried out.

The first point is that the way in which samples must be prepared is extremely important. The head should be in intimate contact with the sample. If the slider is not resting on a surface which is microscopically smooth, flat, and free of particulate contamination, then the resolution which might otherwise be achieved will be lost. This requirement poses special problems for iron whiskers. Although they are microscopically smooth, and flat, their dimensions are small compared with those of a slider. It might be appropriate, in this case, to move whiskers over a head, rather than the opposite.

The second point is simply this. The apparatus which was used for this work may not necessarily be appropriate for actual micromagnetic studies. If it appears that a different experimental configuration would be better suited to the task at hand, then there should be no hesitation about modifying the apparatus, or even completely rebuilding it. It is much more efficient to spend time constructing equipment which is suited to the job than to force existing equipment to do things for which it was not designed.

Appendix

6.1) Program Used to Calculate the Fields Produced by the First Field Source

This program calculates the fields produced by the first field source by summing the contributions from each segment. In order to evaluate the last of the three integrals described in chapter 3, use is made of the function DQUANK, which is listed in section 6.6. The data resulting from this calculation (and most of the others) was plotted using a subroutine very similar to PLOT3D, which is listed in section 6.4.

```
      INTEGER I, J, K, M, N
      REAL*4 BXS, BYS, BZS
      REAL*8 CURENT, COEF, BX, BZ, BVL, EPS, OFFST1, OFFST2
      REAL*8 BYA(6500), BYB(6500)
      REAL*8 START1, END1, START2, END2, VAR1, VAR2, VAR3, X1, Y1, Z1
      REAL*8 XSTART(8), XEND(8), YSTART(8), YEND(8), B(8), DIR(8),
     1       DEPTH(8)
      COMMON START1, END1, START2, END2, VAR1, VAR2, VAR3
      COMMON XSTART, XEND, YSTART, YEND, B, DIR, DEPTH, EPS
      CURENT = 0.1
      DO 10 I = 1, 8
        READ (6,20) XSTART(I)
        READ (6,20) XEND(I)
        READ (6,20) YSTART(I)
        READ (6,20) YEND(I)
        READ (6,20) B(I)
        READ (6,20) DIR(I)
        READ (6,20) DEPTH(I)
   10 CONTINUE
   20 FORMAT (F6.2)
      COEF = (1000.) * CURENT
      K=50
      DO 90 I = 1817, 2415, 6
        EPS = 1.0E-7
        DO 40 J = 450, 550
          X1 = FLOAT(I)
          Y1 = FLOAT(J)
          Z1 = FLOAT(K)
          BX= XFIELD(X1, Y1, Z1)*COEF
```

```
          BYA(J)= YFIELD(X1, Y1, Z1)*COEF
          BZ= ZFIELD(X1, Y1, Z1)*COEF
          BXS=BX
          BZS=BZ
          EPS = (DSQRT(BX*BX + BYA(J)*BYA(J) + BZ*BZ)) / 10000.
          WRITE (5) BXS
          WRITE (3) BZS
   40   CONTINUE
C
C      The following part of the main program removes sudden offsets in the
C      data which appear to arise as a result of the use of a complex
logarithm.
C
        OFFST1=(YFIELD(X1,475.000001,Z1)-YFIELD(X1,474.999999,Z1))
        OFFST2=(YFIELD(X1,505.000001,Z1)-YFIELD(X1,504.999999,Z1))
        OFFST1=OFFST1*COEF
        OFFST2=OFFST2*COEF
        DO 80 J = 450, 550
          IF (I .GT. 2021) GO TO 60
          IF ((475 .GT. J) .OR. (J .GT. 495)) GO TO 50
          BYB(J) = BYA(J)-OFFST1
          GO TO 70
   50     IF ((505 .GT. J) .OR. (J .GT. 525)) GO TO 60
          BYB(J) = BYA(J)-OFFST2
          GO TO 70
   60     BYB(J) = BYA(J)
   70     IF (J.EQ.475.) BYB(J)=YFIELD(X1,474.999999,Z1)*COEF
          IF (J.EQ.495.) BYB(J)=YFIELD(X1,495.000001,Z1)*COEF
          IF (J.EQ.505.) BYB(J)=YFIELD(X1,504.999999,Z1)*COEF
          IF (J.EQ.525.) BYB(J)=YFIELD(X1,525.000001,Z1)*COEF
          BYS=BYB(J)
          WRITE(4) BYS
   80   CONTINUE
   90 CONTINUE
      STOP
      END
C
C
      REAL FUNCTION XFIELD(X1, Y1, Z1)
      EXTERNAL F
      REAL*8 EPS, TOL, FIFTH, ANS, START3, END3,BX
      REAL*8 START1, END1, START2, END2, VAR1, VAR2, VAR3, X1, Y1, Z1
```

```
      REAL*8 XSTART(8), XEND(8), YSTART(8), YEND(8), B(8), DIR(8),
     1       DEPTH(8)
      COMMON START1, END1, START2, END2, VAR1, VAR2, VAR3
      COMMON XSTART, XEND, YSTART, YEND, B, DIR, DEPTH, EPS
      INTEGER M, N, MS, MF
      BX = 0.
      DO 20 N = 1, 6, 5
        MS = (0 + N)
        MF = (2 + N)
        DO 10 M = MS, MF, 2
          START1 = XSTART(M)
          END1 = XEND(M)
          START2 = YSTART(M)
          END2 = YEND(M)
          BVL = B(M)
          START3 = DEPTH(M)
          A=0.64
          IF (DEPTH(M).EQ.0.) THEN A=0.68
          END3 = DEPTH(M) + A
          VAR1 = X1
          VAR2 = Y1
          VAR3 = Z1
          ANS = DQUANK(F,START3,END3,EPS,TOL,FIFTH) / (A*BVL)
          BX = BX + ANS
   10   CONTINUE
   20 CONTINUE
      XFIELD=BX
      RETURN
      END
C
C
      REAL FUNCTION YFIELD(X1, Y1, Z1)
      EXTERNAL F
      INTEGER M, N, MS, MF
      REAL*8 EPS, TOL, FIFTH, ANS, START3, END3, BY
      REAL*8 START1, END1, START2, END2, VAR1, VAR2, VAR3, X1, Y1, Z1
      REAL*8 XSTART(8), XEND(8), YSTART(8), YEND(8), B(8), DIR(8),
     1       DEPTH(8)
      COMMON START1, END1, START2, END2, VAR1, VAR2, VAR3
      COMMON XSTART, XEND, YSTART, YEND, B, DIR, DEPTH, EPS
      BY = 0.
      DO 20 N = 1, 4, 3
```

```
      MS = (1 + N)
      MF = (3 + N)
      DO 10 M = MS, MF, 2
        START1 = XSTART(M)
        END1 = XEND(M)
        START2 = YSTART(M)
        END2 = YEND(M)
        BVL = B(M)
        START3 = DEPTH(M)
        A=0.64
        IF (DEPTH(M).EQ.0.) THEN A=0.68
        END3 = DEPTH(M) + A
        VAR1 = X1
        VAR2 = Y1
        VAR3 = Z1
        ANS = DQUANK(F,START3,END3,EPS,TOL,FIFTH) / (A*BVL)
        BY = BY + ANS
   10   CONTINUE
   20 CONTINUE
      YFIELD=BY
      RETURN
      END
C
C
      REAL FUNCTION ZFIELD(X1, Y1, Z1)
      EXTERNAL F
      REAL*8 EPS, TOL, FIFTH, ANS, START3, END3, BZ
      REAL*8 START1, END1, START2, END2, VAR1, VAR2, VAR3, X1, Y1, Z1
      REAL*8 XSTART(8), XEND(8), YSTART(8), YEND(8), B(8), DIR(8),
     1       DEPTH(8)
      COMMON START1, END1, START2, END2, VAR1, VAR2, VAR3
      COMMON XSTART, XEND, YSTART, YEND, B, DIR, DEPTH, EPS
      INTEGER M, N, MS, MF
      BZ = 0.
      DO 20 N = 1, 6, 5
        MS = (0 + N)
        MF = (2 + N)
        DO 10 M = MS, MF, 2
          START1 = YSTART(M)
          END1 = YEND(M)
          START2 = DEPTH(M)
          A=0.64
```

```
          IF (DEPTH(M).EQ.0.) THEN A=0.68
          END2 = DEPTH(M) + A
          BVL = B(M)
          START3 = XSTART(M)
          END3 = XEND(M)
          VAR1 = Y1
          VAR2 = Z1
          VAR3 = X1
          ANS = DQUANK(F,START3,END3,EPS,TOL,FIFTH) / (A*BVL)
          BZ = BZ + ANS
   10   CONTINUE
   20 CONTINUE
      DO 40 N = 1, 4, 3
        MS = (1 + N)
        MF = (3 + N)
        DO 30 M = MS, MF, 2
          START1 = DEPTH(M)
          A=0.64
          IF (DEPTH(M).EQ.0.) THEN A=0.68
          END1 = DEPTH(M) + A
          START2 = XSTART(M)
          END2 = XEND(M)
          BVL = B(M)
          START3 = YSTART(M)
          END3 = YEND(M)
          VAR1 = Z1
          VAR2 = X1
          VAR3 = Y1
          ANS = DQUANK(F,START3,END3,EPS,TOL,FIFTH) / (A*BVL)
          BZ = BZ + ANS
   30   CONTINUE
   40 CONTINUE
      ZFIELD=BZ
      RETURN
      END
C
C
      REAL FUNCTION F(X)
      REAL*8 C11, C12, C21, C22, X
      REAL*8 START1, END1, START2, END2, VAR1, VAR2, VAR3, X1, Y1, Z1
      REAL*8 XSTART(8), XEND(8), YSTART(8), YEND(8), B(8), DIR(8),
     1       DEPTH(8)
```

```
      COMMON START1, END1, START2, END2, VAR1, VAR2, VAR3
      COMMON XSTART, XEND, YSTART, YEND, B, DIR, DEPTH
      C11 = (START1 - VAR1)
      C12 = (END1 - VAR1)
      C21 = (START2 - VAR2)
      C22 = (END2 - VAR2)
      F = ((FUN(C12,C22,X) - FUN(C11,C22,X)) - (FUN(C12,C21,X) - FUN(
     1C11,C21,X)))
      RETURN
      END
C
C
      REAL FUNCTION FUN(C1,C2,X)
      REAL*8 C1, C2, X, R, REST
      REAL*8 START1, END1, START2, END2, VAR1, VAR2, VAR3, X1, Y1, Z1
      REAL*8 XSTART(8), XEND(8), YSTART(8), YEND(8), B(8), DIR(8),
     1       DEPTH(8)
      COMMON START1, END1, START2, END2, VAR1, VAR2, VAR3
      COMMON XSTART, XEND, YSTART, YEND, B, DIR, DEPTH
      COMPLEX*16 CN1, CN2, CN3, CN4
      CN1 = DCMPLX(C2,-(X - VAR3))
      CN2 = DCMPLX(C2,(X - VAR3))
      R = DSQRT(C1*C1 + C2*C2 + (X - VAR3)*(X - VAR3))
      REST = ((X - VAR3)) * (C2*C2 + (X - VAR3)*(X - VAR3))
      CN3 = (R + C1) * C1 * CN2
      CN3 = CN3 + (0.,1.) * (REST)
      CN4 = (R + C1) * C1 * CN1
      CN4 = CN4 - (0.,1.) * (REST)
      FUN = DREAL((0.,0.5)*CDLOG(CN3/CN4))
      RETURN
      END
```

6.2) Program Used to Calculate the Fields Produced by the Second Field Source

This program is a modified version of the one listed in section 6.1. It calculates the field produced by the second field source by summing the contributions of the segments, but makes use of the periodicity of the array to simplify the specification of the segment positions. The fields produced by wires oriented in the y direction have been ignored for the purpose of

simplicity, since they make only a small contribution to the total field near the center of the array. The contributions of wires near the bonding pads have also been ignored.

```
      INTEGER I, J, K, M, N
      REAL*8 BXA, BZS
      REAL*8 CURENT, COEF, COEF1, BX, BZ, BVL, EPS, OFFST1, OFFST2
      REAL*8 BYS(6500), BYB(6500)
      REAL*8 START1, END1, START2, END2, VAR1, VAR2, VAR3, X1, Y1, Z1
      REAL*8 XSTART(8), XEND(8), YSTART(8), YEND(8), B(8), DIR(8),
     1       DEPTH(8)
      COMMON START1, END1, START2, END2, VAR1, VAR2, VAR3
      COMMON XSTART, XEND, YSTART, YEND, B, DIR, DEPTH, EPS
      CURENT = 0.1
      DO 10 I = 1, 8
        READ (6,20) XSTART(I)
        READ (6,20) XEND(I)
        READ (6,20) YSTART(I)
        READ (6,20) YEND(I)
        READ (6,20) B(I)
        READ (6,20) DIR(I)
        READ (6,20) DEPTH(I)
   10 CONTINUE
   20 FORMAT (F6.2)
      COEF = (1000.) * CURENT
      DO 97 K=4,15.4, 2
      DO 90 I = 1, 250, 2
        EPS = 1.0E-7
        BYS(I)=0.
        BZS = 0.
        COEF1=1
        DO 40 J = 1, 1021, 4
          X1 = 2000.
          Y1 = FLOAT(J)+FLOAT(I)/10.
          Z1 = FLOAT(K)/10.
          COEF1=-1*COEF1
          BY= YFIELD(X1, Y1, Z1)*COEF
C
C       The following part of the main program removes sudden offsets in the
C       data which appear to arise as a result of the use of a complex
logarithm.
C
          IF((509..LE.Y1).AND.(511..GE.Y1)) BY=(BY-314.15972)
```

```
        BZ= ZFIELD(X1, Y1, Z1)*COEF
        EPS = (DSQRT(BY*BY + BZ*BZ)) / 10000.
        BYS(I)=BYS(I)+BY*COEF1
        BZS=BZS+BZ*COEF1
 40   CONTINUE
      CONTINUE
      WRITE(3,95) BZS
 95   FORMAT(F12.6)
 90 CONTINUE
      DO 94 J=1,250, 2
      BYA=BYS(J)
      IF ((MOD(J,20)).EQ.0) BYA=(BYS(J+2)+BYS(J-2))/2.
      BYA=1.63*BYA
      WRITE(4,95) BYA
 94   CONTINUE
 97 CONTINUE
    STOP
    END
C
    REAL FUNCTION YFIELD(X1, Y1, Z1)
    EXTERNAL F
    INTEGER M, N, MS, MF
    REAL*8 EPS, TOL, FIFTH, ANS, START3, END3, BY
    REAL*8 START1, END1, START2, END2, VAR1, VAR2, VAR3, X1, Y1, Z1
    REAL*8 XSTART(8), XEND(8), YSTART(8), YEND(8), B(8), DIR(8),
   1       DEPTH(8)
    COMMON START1, END1, START2, END2, VAR1, VAR2, VAR3
    COMMON XSTART, XEND, YSTART, YEND, B, DIR, DEPTH, EPS
    BY = 0.
    DO 20 N = 1, 1
      MS = 4
      MF = 4
      DO 10 M = MS, MF
        START1 = XSTART(M)
        END1 = XEND(M)
        START2 = YSTART(M)
        END2 = YEND(M)
        BVL = B(M)
        START3 = DEPTH(M)
        END3 = DEPTH(M) + 0.3
        VAR1 = X1
        VAR2 = Y1
```

```
          VAR3 = Z1
          ANS = DQUANK(F,START3,END3,EPS,TOL,FIFTH) / (0.3*BVL)
          BY = BY + ANS
   10   CONTINUE
   20 CONTINUE
      YFIELD=BY
      RETURN
      END
C
C
      REAL FUNCTION ZFIELD(X1, Y1, Z1)
      EXTERNAL F
      REAL*8 EPS, TOL, FIFTH, ANS, START3, END3, BZ
      REAL*8 START1, END1, START2, END2, VAR1, VAR2, VAR3, X1, Y1, Z1
      REAL*8 XSTART(8), XEND(8), YSTART(8), YEND(8), B(8), DIR(8),
     1       DEPTH(8)
      COMMON START1, END1, START2, END2, VAR1, VAR2, VAR3
      COMMON XSTART, XEND, YSTART, YEND, B, DIR, DEPTH, EPS
      INTEGER M, N, MS, MF
      BZ = 0.
      DO 40 N = 1, 1
        DO 30 M = 4, 4
          START1 = DEPTH(M)
          END1 = DEPTH(M) + 0.3
          START2 = XSTART(M)
          END2 = XEND(M)
          BVL = B(M)
          START3 = YSTART(M)
          END3 = YEND(M)
          VAR1 = Z1
          VAR2 = X1
          VAR3 = Y1
          ANS = DQUANK(F,START3,END3,EPS,TOL,FIFTH) / (0.3*BVL)
          BZ = BZ + ANS
   30   CONTINUE
   40 CONTINUE
      ZFIELD=BZ
      RETURN
      END
C
C
      REAL FUNCTION F(X)
```

```
      REAL*8 C11, C12, C21, C22, X
      REAL*8 START1, END1, START2, END2, VAR1, VAR2, VAR3, X1, Y1, Z1
      REAL*8 XSTART(8), XEND(8), YSTART(8), YEND(8), B(8), DIR(8),
     1       DEPTH(8)
      COMMON START1, END1, START2, END2, VAR1, VAR2, VAR3
      COMMON XSTART, XEND, YSTART, YEND, B, DIR, DEPTH
      C11 = (START1 - VAR1)
      C12 = (END1 - VAR1)
      C21 = (START2 - VAR2)
      C22 = (END2 - VAR2)
      F = ((FUN(C12,C22,X) - FUN(C11,C22,X)) - (FUN(C12,C21,X) - FUN(
     1C11,C21,X)))
      RETURN
      END
C
C
      REAL FUNCTION FUN(C1,C2,X)
      REAL*8 C1, C2, X, R, REST
      REAL*8 START1, END1, START2, END2, VAR1, VAR2, VAR3, X1, Y1, Z1
      REAL*8 XSTART(8), XEND(8), YSTART(8), YEND(8), B(8), DIR(8),
     1       DEPTH(8)
      COMMON START1, END1, START2, END2, VAR1, VAR2, VAR3
      COMMON XSTART, XEND, YSTART, YEND, B, DIR, DEPTH
      COMPLEX*16 CN1, CN2, CN3, CN4
      CN1 = DCMPLX(C2,-(X - VAR3))
      CN2 = DCMPLX(C2,(X - VAR3))
      R = DSQRT(C1*C1 + C2*C2 + (X - VAR3)*(X - VAR3))
      REST = ((X - VAR3)) * (C2*C2 + (X - VAR3)*(X - VAR3))
      CN3 = (R + C1) * C1 * CN2
      CN3 = CN3 + (0.,1.) * (REST)
      CN4 = (R + C1) * C1 * CN1
      CN4 = CN4 - (0.,1.) * (REST)
      FUN = DREAL((0.,0.5)*CDLOG(CN3/CN4))
      RETURN
      END
```

6.3) Program Used to Calculate the Flux Intercepted by a Cybernex Head as it Passes Over the Second Field Source

This program is a slightly modified version of the program listed in section 6.2. In the interest of speed, a Gaussian integration routine (function FGAU16 - see section 6.7) was used to calculate the flux coupled between the field source and the pole tips of the head. Only the field intercepting the pole tips in a vertical direction was used to determine the total flux.

```
      INTEGER I, J, K, M, N
      REAL*4 FLUX
      REAL*8 BXA, BZS
      REAL*8 CURENT, COEF, COEF1, BX, BZ, BVL, EPS, OFFST1, OFFST2
      REAL*8 BYS(6500), BYB(6500)
      REAL*8 START1, END1, START2, END2, VAR1, VAR2, VAR3, X1, Y1, Z1
      REAL*8 XSTART(8), XEND(8), YSTART(8), YEND(8), B(8), DIR(8),
     1       DEPTH(8)
      COMMON START1, END1, START2, END2, VAR1, VAR2, VAR3
      COMMON XSTART, XEND, YSTART, YEND, B, DIR, DEPTH
      EXTERNAL TZFILD
      DO 10 I = 1, 8
        READ (6,20) XSTART(I)
        READ (6,20) XEND(I)
        READ (6,20) YSTART(I)
        READ (6,20) YEND(I)
        READ (6,20) B(I)
        READ (6,20) DIR(I)
        READ (6,20) DEPTH(I)
   10 CONTINUE
   20 FORMAT (F6.2)
      EPS=1.E-4
      DO 5 I=1,250
      WIDTH1=20.8
      WIDTH2=17.2
      P1=1.79
      P2=2.24
      G=0.60
      POLE1L=FLOAT(I)/10.
      POLE1U=FLOAT(I)/10.+P1
      POLE2L=FLOAT(I)/10.+P1+G
      POLE2U=FLOAT(I)/10.+P1+G+P2
      FLUX=(WIDTH1*FGAU16(POLE1L,POLE1U,TZFILD)-
```

```
     1  WIDTH2*FGAU16(POLE2L,POLE2U,TZFILD))/2.
C      EPS=FLUX/1.E2
       WRITE(3,4) FLUX
       WRITE(4,4) FLUX
    4  FORMAT(F12.6)
    5  CONTINUE
       STOP
       END
C
C
C
       REAL FUNCTION TZFILD(Y)
       REAL*8 X1,Y1,Z1,COEF,COEF1,BZS,BZ,EPS,CURENT,EPS
       CURENT=0.001
       COEF=(1000.)*CURENT
         EPS = 1.0E-6
         BZS = 0.
         COEF1=1
         DO 40 J = 256,765,4
           X1 = 2000.
           Y1 = FLOAT(J)+Y
           Z1 = 1.06
           COEF1=-1*COEF1
           BZ= ZFIELD(X1, Y1, Z1, EPS)*COEF
           BZS=BZS+BZ*COEF1
    40   CONTINUE
         WRITE(2,6) BZS
         TZFILD=BZS
     6   FORMAT(F12.6)
       RETURN
       END
C
C
       REAL FUNCTION ZFIELD(X1, Y1, Z1, EPS)
       EXTERNAL F
       REAL*8 EPS, TOL, FIFTH, ANS, START3, END3, BZ
       REAL*8 START1, END1, START2, END2, VAR1, VAR2, VAR3, X1, Y1, Z1
       REAL*8 XSTART(8), XEND(8), YSTART(8), YEND(8), B(8), DIR(8),
      1       DEPTH(8)
       COMMON START1, END1, START2, END2, VAR1, VAR2, VAR3
       COMMON XSTART, XEND, YSTART, YEND, B, DIR, DEPTH
       INTEGER M, N, MS, MF
```

```
      BZ = 0.
      DO 40 N = 1, 1
        DO 30 M = 4, 4
          START1 = DEPTH(M)
          END1 = DEPTH(M) + 0.415
          START2 = XSTART(M)
          END2 = XEND(M)
          BVL = B(M)
          START3 = YSTART(M)
          END3 = YEND(M)
          VAR1 = Z1
          VAR2 = X1
          VAR3 = Y1
          ANS = DQUANK(F,START3,END3,EPS,TOL,FIFTH) / (0.415*BVL)
          BZ = BZ + ANS
   30   CONTINUE
   40 CONTINUE
      ZFIELD=BZ
      RETURN
      END
C
C
      REAL FUNCTION F(X)
      REAL*8 C11, C12, C21, C22, X
      REAL*8 START1, END1, START2, END2, VAR1, VAR2, VAR3, X1, Y1, Z1
      REAL*8 XSTART(8), XEND(8), YSTART(8), YEND(8), B(8), DIR(8),
     1       DEPTH(8)
      COMMON START1, END1, START2, END2, VAR1, VAR2, VAR3
      COMMON XSTART, XEND, YSTART, YEND, B, DIR, DEPTH
      C11 = (START1 - VAR1)
      C12 = (END1 - VAR1)
      C21 = (START2 - VAR2)
      C22 = (END2 - VAR2)
      F = ((FUN(C12,C22,X) - FUN(C11,C22,X)) - (FUN(C12,C21,X) - FUN(
     1C11,C21,X)))
      RETURN
      END
C
C
      REAL FUNCTION FUN(C1,C2,X)
      REAL*8 C1, C2, X, R, REST
      REAL*8 START1, END1, START2, END2, VAR1, VAR2, VAR3, X1, Y1, Z1
```

```
      REAL*8 XSTART(8), XEND(8), YSTART(8), YEND(8), B(8), DIR(8),
     1       DEPTH(8)
      COMMON START1, END1, START2, END2, VAR1, VAR2, VAR3
      COMMON XSTART, XEND, YSTART, YEND, B, DIR, DEPTH
      COMPLEX*16 CN1, CN2, CN3, CN4
      CN1 = DCMPLX(C2,-(X - VAR3))
      CN2 = DCMPLX(C2,(X - VAR3))
      R = DSQRT(C1*C1 + C2*C2 + (X - VAR3)*(X - VAR3))
      REST = ((X - VAR3)) * (C2*C2 + (X - VAR3)*(X - VAR3))
      CN3 = (R + C1) * C1 * CN2
      CN3 = CN3 + (0.,1.) * (REST)
      CN4 = (R + C1) * C1 * CN1
      CN4 = CN4 - (0.,1.) * (REST)
      FUN = DREAL((0.,0.5)*CDLOG(CN3/CN4))
      RETURN
      END
```

6.4) Program Used to Calculate and Plot the Fields Produced by a Thin Film Head

This program makes use of the approximate closed form expressions for the fields produced by the pole tips of a thin film head (see section 3.3). Note that factors of (I/8π) and (I/16π) in the cases of H_x and H_y, respectively, have been left out of the listing. The results of the calculation are plotted with the aid of PLOT3D, which uses DISSPLA® subroutines to create a plot file. This subroutine was also used to display the results of calculations carried out by other programs in the appendix.

```
      REAL ZDAT(101,100)
      DO 20 I = 1,100
        DO 10 J=1,101
          K=101-I
          ZDAT(J,I)=FIELD(J,K)
   10   CONTINUE
   20 CONTINUE
   30 FORMAT (F8.5)
      CALL PLOT3D(ZDAT)
      STOP
      END
C
```

```
C
      SUBROUTINE PLOT3D(ZDAT)
      DIMENSION ZDAT(101,100)
      COMMON WORK(6000)
      CALL DSPDEV('PLOT')
      CALL RESET('ALL')
      CALL PAGE(11., 8.5)
      CALL NOBRDR
      CALL INTAXS
      CALL ZAXANG(90.)
      CALL COMPLX
      CALL BASALF('L/CST')
      CALL MIXALF('STAND')
      CALL AREA2D(9.5,6.5)
      CALL HEADIN(' ', 1, 3, 3)
      CALL HEADIN(' ', 1, 3, 3)
      CALL RESET('HEIGHT')
      CALL X3NAME('(X) (A)XIS - um$', 100)
      CALL Y3NAME('(Y) (A)XIS - um$', 100)
      CALL Z3NAME('(Y) (F)IELD$', 100)
      CALL VOLM3D(10., 10., 8.)
      CALL GRAF3D(-5., 'SCALE', 5., 2., 'SCALE', 0., -30.,
     1     'SCALE',30.)
      CALL BLSUR
      CALL SURMAT(ZDAT, 1, 101, 1, 100, 0)
      CALL GRFITI(0., 0., 0.0, 1., 0., 0.0, 0., 1., 0.)
      CALL INTAXS
      CALL AREA2D(10., 10.)
      CALL GRAF(-5., 'SCALE', 5., 2., 'SCALE', 0.)
      CALL BCOMON(6000)
      CALL CONMAK(ZDAT, 101, 100, 'SCALE')
      CALL CONLIN(4, 'SOLID', 'LABELS', 2, 10)
      CALL CONANG(90.)
      CALL FRAME
      CALL HEIGHT(.3)
      CALL CONTUR(5, 'LABELS', 'DRAW')
      CALL END3GR(0)
      CALL ENDPL(0)
      RETURN
      END
C
C
```

```
      REAL FUNCTION FIELD(I,J)
      REAL HX,HY,PI,G,P1,P2,X,Y
      INTEGER I,J
      PI=3.1415927
      G=0.75
      P1=1.75
      P2=2.2
      Y=(FLOAT(J))/50.
      X=(FLOAT(I-50))/10.
      HX=G*X*Y*(2*P2+G)*ALOG((2*P2+G)**2/(4*(X+P2+G/2)**2+4*Y**2))
      HX=HX-G*X*Y*(2*P1+G)*ALOG((2*P1+G)**2/(4*(X-P1-G/2)**2+4*Y**2))
      HX=HX+8*(X**2+Y**2)**2*(ATAN((2*X-G)/(2*Y))-ATAN((2*X+G)/(2*Y)))
      HX=HX+G*(2*P1+G)*(X**2-Y**2)*ATAN((2*X-2*P1-G)/(2*Y))
      HX=HX-G*(2*P2+G)*(X**2-Y**2)*ATAN((2*X+2*P2+G)/(2*Y))
      HX=HX+X**2*G*(4*Y+PI*(P1+P2+G))
      HX=HX+Y**2*G*(4*Y-PI*(P1+P2+G))
      HX=-HX/(G*(X**2+Y**2)**2)
      HY=(2*P2*G+G**2)*(X**2-Y**2)*ALOG((4*(X+P2+G/2)**2+4*Y**2)
     1  /(2*P2+G)**2)
      HY=HY+(2*P1*G+G**2)*(Y**2-X**2)*ALOG((4*(X-P1-G/2)**2+4*Y**2)
     1  /(2*P1+G)**2)
      HY=HY+8*(X**2+Y**2)**2*ALOG((4*(X+G/2)**2+4*Y**2)/(4*(X-G/2)**2
     1  +4*Y**2))
      HY=HY+4*X*Y*G*((2*P1+G)*ATAN((2*X-2*P1-G)/(2*Y))-(2*P2+G)*
     1  ATAN((2*X+2*P2+G)/(2*Y)))
      HY=HY-4*X*G*(2*(X**2+Y**2)-PI*Y*(P1+P2+G))
      HY=-HY/(G*(X**2+Y**2)**2)
      FIELD=HX
      RETURN
      END
```

6.5) Subroutine Used to Fit Experimental Two Head Data to the Model

This subroutine, which was used in conjunction with MINUIT, calculates the square of the difference between the data representing the signal coupled between two thin film heads and that predicted by the model (i.e. χ^2). The model makes use of the reciprocity theorem (described in section 4.1) and the approximate closed form expression for the field produced by a thin film head (see section 3.3). Note that factors of $(I/8\pi)$ and $(I/16\pi)$ in the cases of H_x and H_y, respectively, have been left out of the listing. The subroutine also contains commands for setting

up the version of minuit (SFU Surface Science MINUIT / Version 1.0) which was used to carry out the fit.

```
      SUBROUTINE FCN(NPAR,G,CHISQR,PAR,IFLAG)
      COMMON /UNIT/   SYSIN, SYSOUT, SYSLOG, SYSPAR, SYSINC,
     .                SYSDAT, CONIN, CONOUT
      COMMON /CTRL/   LDDATA, LDPARM
C
      INTEGER*4    SYSIN, SYSOUT, SYSLOG, SYSPAR, SYSINC,
     .             SYSDAT, CONIN, CONOUT
      LOGICAL*4    LDDATA, LDPARM
C
      REAL*8 X,Y,PHI,SIG,PI,GAP,P1,P2,W,I,B,T,XPR,YPR
      REAL*8 UPER1X,LOWR1X,UPERY,LOWRY,UPER2X,LOWR2X
      REAL*8 EPS,TOL,FIFTH,M
      REAL*8 DATAX(700),DATAY(700),G(60),PAR(60),CHISQR
      INTEGER J,K,NDATA
      COMMON PI,GAP,P1,P2,UPERY,LOWRY
      EXTERNAL F
      NDATA=127
      SIGMA=1.
      IF (IFLAG.NE.1) GOTO 6
      DO 4 J=1,NDATA
      READ(SYSDAT,5) DATAX(J),DATAY(J)
    5 FORMAT (F12.4,F12.4)
    4 CONTINUE
      LDDATA=.TRUE.
      I=1.
      PI=3.14159265
      W=15.
      EPS=0.0001
    6 CONTINUE
      CHISQR=0.
      M=PAR(1)
      B=PAR(2)
      T= 5.0
      QC1=PAR(4)
      QC2=PAR(5)
      P1=PAR(6)
      P2=PAR(7)
      GAP=PAR(8)
C     WRITE(4,17) M,B,T,QC1,QC2
```

```
   17 FORMAT (F12.6,F12.6,F12.6,F12.6,F12.6)
   18 FORMAT (F12.6)
      DO 10 J=1, NDATA
      X=DATAX(J)
C     WRITE(4,18) X
      UPER1X=(X-GAP/2.)
      LOWR1X=(X-GAP/2.-P2)
      UPERY=B+T
      LOWRY=B
      UPER2X=X+GAP/2.+P1
      LOWR2X=X+GAP/2.
      SIG=-DQUANK(F,LOWR1X,UPER1X,EPS,TOL,FIFTH)
      SIG=SIG+(P2/P1)*DQUANK(F,LOWR2X,UPER2X,EPS,TOL,FIFTH)
      SIG=-4*PI*W*M*SIG+QC1*X**2+QC2
      CHISQR=CHISQR+(DATAY(J)-SIG)**2/SIGMA**2
   10 CONTINUE
      RETURN
      END
C
C
      FUNCTION F(X)
      REAL*8 PI,GAP,P1,P2,FLUX,X,F,UPERY,LOWRY
      COMMON PI,GAP,P1,P2,UPERY,LOWRY
      F=(PHI(X,UPERY)-PHI(X,LOWRY))
      RETURN
      END
C
C
      FUNCTION PHI(X,Y)
      REAL*8 PHI,X,Y,GAP,P1,P2,PI,ANS3,ANS2,ANS1
      COMMON PI,GAP,P1,P2,UPERY,LOWRY
      ANS3=-DLOG(DABS((4*X**2-8*X*P1-4*X*GAP+4*Y**2+4*P1**2+4*P1
     . *GAP+GAP**2)/4))*Y*GAP**2-8.*DLOG(DABS((4*X**2-4*X*GAP+4*Y
     . **2+GAP**2)/4))*X**2*Y-8.*DLOG(DABS((4*X**2-4*X*GAP+4*Y**2
     . +GAP**2)/4))*Y**3+2.*DLOG(DABS((4*X**2+8*X*P2+4*X*GAP+4*Y
     . **2+4*P2**2+4*P2*GAP+GAP**2)/4))*Y*P2*GAP+DLOG(DABS((4*X**
     . 2+8*X*P2+4*X*GAP+4*Y**2+4*P2**2+4*P2*GAP+GAP**2)/4))*Y*GAP
     . **2+8.*DLOG(DABS((4*X**2+4*X*GAP+4*Y**2+GAP**2)/4))*X**2*Y
     . +8.*DLOG(DABS((4*X**2+4*X*GAP+4*Y**2+GAP**2)/4))*Y**3+4.*
     . DLOG(DABS((2*P1+GAP)/2))*Y*P1*GAP+2.*DLOG(DABS((2*P1+GAP)/
     . 2))*Y*GAP**2-2.*X*PI*P2*GAP-2.*X*PI*P1*GAP-2.*X*PI*GAP**2
      ANS2=4.*DATAN((2*X-2*P1-GAP)/(2*Y))*X**2*GAP-4.*DATAN((2*X-2
```

```
     . *P1-GAP)/(2*Y))*X*P1*GAP-2.*DATAN((2*X-2*P1-GAP)/(2*Y))*X*
     . GAP**2+4.*DATAN((2*X-2*P1-GAP)/(2*Y))*Y**2*GAP+16.*DATAN((2
     . *X-GAP)/(2*Y))*X**3-8.*DATAN((2*X-GAP)/(2*Y))*X**2*GAP+16.
     . *DATAN((2*X-GAP)/(2*Y))*X*Y**2-8.*DATAN((2*X-GAP)/(2*Y))*Y
     . **2*GAP+4.*DATAN((2*X+2*P2+GAP)/(2*Y))*X**2*GAP+4.*DATAN((2
     . *X+2*P2+GAP)/(2*Y))*X*P2*GAP+2.*DATAN((2*X+2*P2+GAP)/(2*Y)
     . )*X*GAP**2+4.*DATAN((2*X+2*P2+GAP)/(2*Y))*Y**2*GAP-16.*
     . DATAN((2*X+GAP)/(2*Y))*X**3-8.*DATAN((2*X+GAP)/(2*Y))*X**2*
     . GAP-16.*DATAN((2*X+GAP)/(2*Y))*X*Y**2-8.*DATAN((2*X+GAP)/(2
     . *Y))*Y**2*GAP-4.*DLOG(DABS((-2*P2-GAP)/2))*Y*P2*GAP-2.*
     . DLOG(DABS((-2*P2-GAP)/2))*Y*GAP**2-2.*DLOG(DABS((4*X**2-8*
     . X*P1-4*X*GAP+4*Y**2+4*P1**2+4*P1*GAP+GAP**2)/4))*Y*P1*GAP+
     . ANS3
      PHI=ANS2/(16.*PI*GAP*(X**2+Y**2))
      RETURN
      END
```

6.6) Integration Function DQUANK

This function (and the following one, FGAU16) were given to me by Tom Nicol of the University of British Columbia Computing Center.

```
      FUNCTION DQUANK(FUN,A,BIG,ERROR,RUM,FIFTH)
C     CONVERTED TO DOUBLE PRECISION BY PETER MADDEROM NOVEMBER 1976
      IMPLICIT REAL*8 (A-H,O-Z)
C ACM ALGORITHM NUMBER 379, APRIL 1970.
C SQUANK= SIMPSON:QUADRATURE:USED:ADAPTIVELY::NOISE:KILLED.
C CALLING PROGRAM REQUIRES:
C       (1) EXTERNAL FUN...THIS IS THE FUNCTION TO BE INTEGRATED.
C       (2) A.............LOWER LIMIT OF INTEGRATION.
C       (3) BIG...........UPPER LIMIT.
C       (4) ERROR.........REQUIRED ABSOLUTE ERROR.
C OUTPUT FROM THIS SUBPROGRAM INCLUDES:
C       (1) SQUANK.........THE FIFTH ORDER RESULT.
C       (2) RUM...........CLAIMED TOLERANCE (ADJUSTED FOR ROUNDOFF ERROR)
C       (3) FIFTH.........THE FIFTH ORDER ADJUSTMENT TERM.
C
C
C
      DIMENSION FX3ST(30),X3ST(30),ESTST(30),FX5ST(30),X5ST(30)
```

```
      DIMENSION PREDIF(30)
      DOUBLE PRECISION SUM,SIM
      EPMACH=0.75D-14
C
C          ****    STAGE ONE    ****
C     INITIALISE ALL QUANTITIES REQUIRED FOR CENTRAL CALCULATION (STAGE
C
      SUM = 0.0D0
      SIM = 0.0D0
      CEPSF = 180.0D0*ERROR/(BIG - A)
      CEPS = CEPSF
      ADIFF = 0.0D0
      LEVTAG = -1
      FACERR = 1.0D0
      XZERO = A
      EFACT = 0.0D0
      NIM = 1
      LEV = 0
C     FIRST INTERVAL
      X1 = A
      X5 = BIG
      X3 = 0.5D0*(A+BIG)
      FX1= FUN(X1)
      FX3= FUN(X3)
      FX5= FUN(X5)
      EST = FX1 + FX5 + 4.0D0*FX3
C
C          ****    STAGE TWO    ****
C     SET A STARTING VALUE FOR TOLERANCE IN CASE THAT CEPSF = 0.0
C
      IF(CEPSF) 295,205,295
205   LEVTAG = 0
      FACERR = 15.0D0
      CEPS = EPMACH*DABS (FX1)
      IF(FX1) 295,210,295
210   CEPS = EPMACH*DABS (FX3)
      LEVTAG = 3
      IF(FX3) 295,215,295
215   CEPS = EPMACH*DABS (FX5)
      IF(FX5) 295,220,295
220   CEPS = EPMACH
295   QCEPS = 0.25D0*CEPS
```

```
C     INITIALISING COMPLETE
C
C          ****     STAGE THREE     ****
C     CENTRAL CALCULATION.
C                    REQUIRES X1,X3,X5,FX1,FX3,FX5,EST,ADIFF.
C
300   CONTINUE
      X2 = 0.5D0*(X1 + X3)
      X4 = 0.5D0*(X3 + X5)
      FX2= FUN(X2)
      FX4= FUN(X4)
      EST1 = FX1 + 4.0D0*FX2 + FX3
      EST2 = FX3 + 4.0D0*FX4 + FX5
      ADIFF1 = ADIFF
      DIFF = EST + EST - EST1 - EST2
      IF(LEV - 30) 305,800,800
305   ADIFF= DABS (DIFF)
      CRIT = ADIFF - CEPS
      IF(CRIT)  700,700,400
C     END OF CENTRAL LOOP
C
C          ****     STAGE FOUR     ****
C      NO NATURAL CONVERGENCE.  A COMPLEX SEQUENCE OF INSTRUCTIONS
C      FOLLOWS WHICH ASSIGNS CONVERGENCE AND / OR ALTERS TOLERANCE
C      LEVEL IN UPWARD DIRECTION IF THERE ARE INDICATIONS OF ROUND OFF
C      ERROR.
C
400   CONTINUE
      IF(ADIFF1 - ADIFF)  410,410,500
C      IN A NORMAL RUN WITH NO ROUND OFF ERROR PROBLEM,  ADIFF1  IS GREA
C      ADIFF AND THE REST OF STAGE FOUR IS OMITTED.
410   IF(LEV - 5) 500,415,415
415   EFACT = EFACT + CEPS *(X1 - XZERO)*FACERR
      XZERO = X1
      FACERR = 15.0D0
C      THE REST OF STAGE FOUR DEALS WITH UPWARD ADJUSTMENT OF TOLERANCE
C       BECAUSE OF SUSPECTED ROUND OFF ERROR TROUBLE.
      IF(ADIFF-2.0D0*CEPS)  420,420,425
C      SMALL JUMP IN CEPS. ASSIGN CONVERGENCE
420   CEPS =     ADIFF
      LEVTAG = 0
      GO TO 780
```

```
425   IF( ADIFF1 - ADIFF)  435,430,435
C      LARGE JUMP IN CEPS
430   CEPS = ADIFF
      GO TO 445
C      FACTOR TWO  JUMP IN CEPS
435   CEPS = 2.0D0*CEPS
      IF(LEVTAG - 3) 440,445,445
440   LEVTAG = 2
445   QCEPS = 0.25D0*CEPS
C
C          ****    STAGE FIVE    ****
C       NO ACTUAL CONVERGENCE.
C     STORE RIGHT HAND ELEMENTS
C
500   CONTINUE
      NIM = 2*NIM
      LEV = LEV + 1
      ESTST(LEV) = EST2
      X3ST(LEV)= X4
      X5ST(LEV)= X5
      FX3ST(LEV)=FX4
      FX5ST(LEV)=FX5
      PREDIF(LEV) = ADIFF
C
C          ****    STAGE SIX    ****
C      SET UP QUANTITIES FOR CENTRAL CALCULATION.
C
C     READY TO GO AHEAD AT LEVEL LOWER WITH LEFT HAND ELEMENTS
C     X1 AND FX1 ARE THE SAME AS BEFORE
      X5 = X3
      X3 = X2
      FX5 = FX3
      FX3 = FX2
      EST = EST1
      GO TO 300
C
C          ****    STAGE SEVEN    ****
C      NATURAL CONVERGENCE IN PREVIOUS INTERVAL. THE FOLLOWING COMPLEX S
C      CHECKS PRIMARILY THAT TOLERANCE LEVEL IS NOT TOO HIGH. UNDER CERT
C      CIRCUMSTANCES NON CONVERGENCE IS ASSIGNED AND / OR TOLERANCE LEVE
C      IS RE-SET.
C
```

```
700   CONTINUE
C     CHECK THAT IT WAS NOT LEVEL ZERO INTERVAL.IF SO ASSIGN NOW CONVERG
      IF( LEV ) 400,400, 705
C
C      LEVTAG =-1   CEPS = CEPSF, ITS ORIGINAL VALUE.
C      LEVTAG = 0   CEPS IS GREATER THANCEPSF. REGULAR SITUATION.
C      LEVTAG = 2   CEPS IS GREATER THANCEPSF.CEPS PREVIOUSLY ASKED FOR
C                           JUMP, BUT DID NOT GET ONE.
C      LEVTAG = 3   CEPS IS GREATER THANCEPSF.CEPS PREVIOUSLY HAD A BIG
C
705   IF(LEVTAG) 800,710,710
C      IN A NORMAL RUN WITH NO ROUND OFF ERROR PROBLEM,  LEVTAG = -1 AND
C      REST OF STAGE SEVEN IS OMITTED.
710   CEPST = 15.0D0*CEPS
C      CEPST HERE IS FACERR*CURRENT VALUE OF CEPS
      IF(CRIT) 715,800,800
715   IF(LEVTAG - 2)  720,740,750
C      LEVTAG = 0
720   IF(ADIFF) 800,800,725
725   IF(ADIFF - QCEPS) 730,800,800
730   IF(ADIFF - CEPSF) 770,770,735
735   LEVTAG = 0
      CEPS = ADIFF
      EFACT = EFACT + CEPST*(X1 - XZERO)
      XZERO = X1
      GO TO 445
C      LEVTAG = 2
740   LEVTAG = 0
      IF(ADIFF) 765,765,725
C      LEVTAG = 3
750   LEVTAG = 0
      IF(ADIFF) 775,775,730
765   CEPS = ADIFF1
      GO TO 775
770   LEVTAG = -1
      FACERR = 1.0D0
      CEPS = CEPSF
775   EFACT = EFACT + CEPST*(X1 - XZERO)
      XZERO = X1
780   CONTINUE
      QCEPS = 0.25D0*CEPS
C          ****    STAGE EIGHT    ****
```

```
C       ACTUAL CONVERGENCE IN PREVIOUS INTERVAL.  INCREMENTS ADDED INTO
C       RUNNING SUMS
C
C      ADD INTO SUM AND SIM
800    CONTINUE
       SUM = SUM +(EST1+EST2)*(X5-X1)
       IF(LEVTAG) 805,810,810
C       WE ADD INTO SIM ONLY IF WE ARE CLEAR OF ROUND OFF LEVEL.
805    SIM = SIM + DIFF*(X5-X1)
810    CONTINUE
C
C           ****     STAGE NINE     ****
C       SORT OUT WHICH LEVEL TO GO TO.  THIS INVOLVES NIM NUMBERING SYSTE
C       DESCRIBED BEFORE STAGE ONE.
C
905    NUM = NIM/2
       NOM = NIM - 2*NUM
       IF(NOM) 910,915,910
910    NIM = NUM
       LEV = LEV - 1
       GO TO 905
915    NIM = NIM + 1
C      NEW LEVEL IS SET. IF LEV=0 WE HAVE FINISHED
       IF( LEV ) 1100,1100,1000
C
C           ****     STAGE TEN     ****
C       SET UP QUANTITIES FOR CENTRAL CALCULATION.
C
1000   CONTINUE
       X1 = X5
       FX1= FX5
       X3 = X3ST(LEV)
       X5 = X5ST(LEV)
       FX3= FX3ST(LEV)
       FX5= FX5ST(LEV)
       EST= ESTST(LEV)
       ADIFF = PREDIF(LEV)
       GO TO 300
C
C           ****     STAGE ELEVEN     ****
C       CALCULATION NOW COMPLETE. FINALISE.
C
```

```
1100  CONTINUE
      EFACT=EFACT+CEPS*(BIG-XZERO)*FACERR
      RUM      = EFACT/180.0D0
      THIRD= SUM/12.0D0
      FIFTH =-SIM/180.0D0
      DQUANK   = THIRD + FIFTH
      RETURN
      END
```

6.7) Integration Function DGAU16

This function uses Gaussian quadrature to integrate a function (AUX) over an interval (A,B). The chief virtue of Gaussian quadrature is its speed in integrating functions which can be closely approximated by a polynomial (i.e. smooth functions).[40]

```
      FUNCTION DGAU16(A,B,AUX)
      IMPLICIT REAL*8(A-H,O-Z)
      DIMENSION AX(8), H(8)
      DATA AX/0.989400934991650,0.944575023073233,0.865631202387832,
     $0.755404408355003,0.617876244402644,0.458016777657227,
     $0.281603550779259,0.095012509837637/
      DATA H/0.027152459411754,0.062253523938648,0.095158511682493,
     $0.124628971255534,0.149595988816577,0.169156519395003,
     $0.182603415044924,0.189450610455069/
      P = (B+A)*0.5
      Q = (B-A)*0.5
      SUM = 0.0
      DO 30 J = 1,8
      R = AX(J)*Q
      X = P+R
      Y=AUX(X)
      Z = Y
      X = P-R
      Y=AUX(X)
30    SUM = SUM + H(J)*(Z+Y)
      DGAU16=Q*SUM
      RETURN
      END
```

References

1. R.M. Bozorth: *Ferromagnetism* (D. Van Nostrand Co., Princeton, N.J., 1951).
2. F. Bitter, *Phys. Rev.* **38**, 1903 (1931).
3. H.J. Williams, R.M. Bozorth and W. Shockley, *Phys. Rev.* **75**, 155 (1949).
4. E.E. Huber, D.O. Smith and J.B. Goodenough, *J. Appl. Phys.* **29**, 294 (1958).
5. C.D. Lustig, A.W. Baird, W.F. Chaurette, H. Minden, W.T. Maloney and A.J. Kurtzig, *Rev. Sci.Instrum.* **50**, 321 (1979).
6. J.P.J. Groenland and J.H.J. Fluitman, *J. Phys. E* **14**, 503 (1981).
7. M.E. Re, R.R. Katti, S.L. Zeder and M.H. Kryder, *IEEE Trans. Magn.* **MAG-22**, 840 (1986). For a recent discussion of Kerr effect imaging methods, see: B.E. Argyle, B. Petek and D.A. Herman, Jr., *J. Appl. Phys.* **61**, 4303 (1987).
8. S. Chikazumi: *Physics of Magnetism* (John Wiley & Sons, New York, N.Y., 1964), pp. 405-407.
9. R.H. Wade, *IEEE Trans. Magn.* **MAG-12**, 34 (1976).
10. J.B. Elsbrock, W. Schroeder and E. Kubalek, *IEEE Trans. Magn.* **MAG-21**, 1593 (1985).
11. K. Yoshida, T. Okuwaki, N. Osakabe, H. Tanabe, Y. Horiuchi, T. Matsuda, K. Shinagawa, A.Tonomura and H. Fujiwara, *IEEE Trans. Magn.* **MAG-18**, 1600 (1983).
12. R.J. Celotta and D.T. Pierce, *Science* **234**, 333 (1986).
13. C. F. Quate, *Physics Today* **39**-8, 26 (1986).
14. A.S. Arrott, Personal communication (1987).
15. E.P. Valstyn and L.F. Shew, *IEEE Trans. Magn.* **MAG-9**, 317 (1973).
16. D.P. Gregg, "Deposited Film Transducing Apparatus and Method of Producing the Apparatus", U.S. Patent 3,344,237, September 26, 1967 (Filed April 19, 1961).
17. Y. Watanabe, S. Matsumoto and N. Najima, *IEEE Trans. Magn.* **MAG-5**, 918 (1969).
18. L.T. Romankiw, I.M. Croll and M. Hatzakis, *IEEE Trans. Magn.* **MAG-6**, 597 (1970).
19. A.D. Kaske, P.E. Oberg, M.C. Paul and G.F. Sauter, *IEEE Trans. Magn.* **MAG-7**, 675

(1971).

20. J.P. Lazzari and I. Melnick, *IEEE Trans. Magn.* **MAG-6**, 601 (1970).
21. Ref. 15 and: J.P. Lazzari, *IEEE Trans. Magn.* **MAG-9**, 322 (1973).
22. F. Jeffers, *Proc. IEEE* **74**, 1540 (1986).
23. R.W. Wood, *Proc. IEEE* **74**, 1557 (1986).
24. W. G. Jacobs, "Magnetic Head Slider Assembly", U.S. Patent 4,251,841, February 17, 1981 (Filed June 1, 1979).
25. R.F. Hoyt, *J. Appl. Phys.* **57**, 3947 (1985).
26. R.F. Hoyt, D.E. Heim, J.S. Best, C.T. Horng and D.E.Horne, *J. Appl. Phys.* **55**, 2241 (1984).
27. R.E. Jones, Jr., *IEEE Trans. Magn.* **MAG-15**, 1619 (1979).
28. W.F. Druyvesteyn, L. Postma and G. Somers, *IEEE Trans. Magn.* **MAG-15**, 1613 (1979).
29. M.E. Re and M.H. Kryder, *J. Appl. Phys.* **55**, 2245 (1984).
30. B.E. Argyle, B. Petek and D.A. Herman, Jr., *J. Appl. Phys.* **61**, 4303 (1987).
31. R.F. Soohoo, *IEEE Trans. Magn.* **MAG-18**, 1128 (1982).
32. T.L. Templeton, A.S. Arrott and A. Aharoni, *J. Appl. Phys.* **55**, 2189 (1984).
33. G.K. Wehner and G.S. Anderson, "The Nature of Physical Sputtering" in *Handbook of Thin Film Technology* , edited by L.I. Maissel and R. Glang (McGraw-Hill, New York, N.Y. 1970), pp. 3-8, 3-9.
34. R.I. Potter, *IEEE Trans. Magn.* **MAG-11**, 80 (1975).
35. R.M. White: *Introduction to Magnetic Recording* (IEEE Press, New York, N.Y.,1984).
36. J. Wessel-Berg and H.N. Bertram, *IEEE Trans. Magn.* **MAG-14**, 129 (1978).
37. R. Jones, *IEEE Trans. Magn.* **MAG-14**, 509 (1978).
38. K. Kanai, *IEEE Trans. Magn.* **MAG-15**, 1130 (1979).
39. See reference 22.
40. William H. Press, Brian P. Flannery, Saul A. Teukolsky and William T. Vetterling: *Numerical Recipes* (Cambridge University Press, Cambridge, 1986), pp. 121-126.

Index